Neutrino windows to new physics

Doctoral Thesis of

Julia Gehrlein

At the Instituto de Física Teórica UAM-CSIC

Supervisors: Dr. Enrique Fernández-Martinez, Dr. Mattias Blennow

Duration: September 2016 – May 2019

This thesis is based on the author's work [1–3] conducted from September 2016 until May 2019 at the IFT:

1. *"Dark Matter and the elusive Z' in a dynamical Inverse Seesaw scenario"*,
   V. De Romeri, E. Fernandez-Martinez, J. Gehrlein, P. A. N. Machado and V. Niro,
   JHEP **1710** (2017) 169
   arXiv:1707.08606 [hep-ph].

2. *"IceCube bounds on sterile neutrinos above 10 eV"*,
   M. Blennow, E. Fernandez-Martinez, J. Gehrlein, J. Hernandez-Garcia and J. Salvado,
   Eur. Phys. J. C **78**, no. 10, 807 (2018)
   arXiv:1803.02362 [hep-ph].

3. *"Natural and Dynamical Neutrino Mass Mechanism at the LHC"*,
   J. Gehrlein, D. Gonves, P. A. N. Machado and Y. F. Perez-Gonzalez,
   Phys. Rev. D **98**, no. 3, 035045 (2018)
   arXiv:1804.09184 [hep-ph].

Motivaciónes y objetivos

El modelo estándar de la física de partículas ha sido comprobado con gran precisión y describe con éxito las interacciones fuertes y electrodébiles de todas las partículas observadas actualmente. Con el descubrimiento del bosón de Higgs en el LHC en 2012, se ha encontrado la última pieza del modelo estándar. ¿Pero, está completa nuestra comprensión teórica de la naturaleza? De hecho, el modelo estándar solo no puede describir varias observaciones fenomenológicas, por ejemplo, la existencia de *materia oscura*. Solo un 5% de la energía del Universo está contenido en la materia visible descrita por el modelo estándar. Aproximadamente 25% del contenido de energía del Universo está compuesto por materia oscura.

Experimentalmente, solo hemos observado materia oscura gravitacionalmente, por lo que sabemos que la materia oscura debería ser eléctricamente neutra y solo debería tener un pequeño acoplamiento al modelo estándar. Se ha propuesto una gran cantidad de candidatos de materia oscura en nuevos modelos de física con masas de materia oscura que van desde 10^{-22} a 10^{18} GeV. Actualmente existe un amplio programa experimental para detectar materia oscura de varias maneras: detección directa (a través de la dispersión de nucleones con la materia oscura), detección indirecta (detección de los productos de aniquilación de la materia oscura) o en colisionadores (a través de la producción de partículas de materia oscura en colisiones de partículas del modelo estándar).

El 70 % restante del contenido de energía del Universo se atribuye a *energía oscura* que se necesita para explicar la aceleración observada en la expansion del Universo. La energía oscura podría ser la contribución de una constante cosmológica, sin embargo, el origen de esta constante es actualmente desconocido, o la energía oscura podría estar relacionada con la energía de vacío del modelo estándar. Sin embargo, una estimación de esta energía difiere alrededor de 50 órdenes de magnitud con respecto al valor experimental.

Otra pregunta abierta que surge debido al vacío del modelo estándar es el *problema CP fuerte* en QCD. Los efectos de QCD topológicos y las fases en la matriz de masa de quarks contribuyen a un término $\sim \theta G_{\mu\nu}\tilde{G}_{\mu\nu}$ en el Lagrangiano del modelo estándar. Experimentalmente, se ha determinado que θ es menor que 10^{-10}. Esta cancelación de dos contribuciones independientes provenientes de diferentes sectores (QCD en un lado, la rotura de CP electrodébil en el otro lado) requiere una explicación.

Además, surge la cuestión fundamental de la asimetría materia-antimateria. Si todos los procesos respetan la simetría entre partículas y antipartículas, no se puede explicar el hecho de que nuestro Universo está hecho principalmente de materia y no de antimateria. *Bariogenésis*, un mecanismo propuesto para generar la asimetría bariónica del Universo, afirma que los procesos en el Universo temprano favorecieron la creación de partículas con respecto a la creación de antipartículas a través de procesos que violan el número bariónico, una simetría global accidental del modelo estándar. A pesar de que el modelo estándar contiene todos los ingredientes para que tenga lugar la bariogénesis, no es capaz de explicar la asimetría observada.

El modelo estándar contiene otra simetría global accidental, el número leptónico. Además, en el límite de fermiones sin masa, el modelo estándar tiene una simetría de sabor global que solo se rompe con los acoplamientos de Yukawa de los fermiones. Los parámetros en el

modelo estándar que están relacionados con el sector del sabor, es decir, los acoplamientos de Yukawa y las mezclas de los fermiones, son parámetros ad hoc en el modelo estándar y sus valores numéricos deben introducirse a mano. Esto parece muy arbitrario y sería deseable tener una visíon más profunda sobre el origen de estos parámetros. Especialmente porque observamos una gran jerarquía entre las diferentes masas de fermiónes (empeoradas por la ligereza de las masas de neutrinos). También surgen preguntas como "¿por qué hay tres generaciones?" y "¿por qué la mezcla es en el sector leptónico tan grande cuando solo observamos pequeños ángulos de mezcla en el sector quark?". Todas estas preguntas constituyen el *puzzle del sabor* del modelo estándar. Sin embargo, muchas explicaciones del puzzle del sabor introducen nuevas partículas físicas que conducen al *problema del sabor*. El problema del sabor caracteriza el hecho de que los observables de sabor, especialmente los procesos que están muy suprimidos en el modelo estándar debido al mecanismo GIM, son muy sensibles a las contribuciones de la nueva física. En general, no se espera que el nuevo modelo de física muestre el mismo patrón de sabor que el modelo estándar. Sin embargo, aún no hemos visto ningún signo de nueva física en los observables de sabor.

Todas las preguntas abiertas descritas anteriormente requieren nueva física más allá del modelo estándar. Junto con el hecho de que el modelo estándar describe solo las interacciones fuertes y electrodébiles, pero no es capaz de incorporar de manera consistente una teoría cuántica de la gravedad, el SM puede considerarse como una teoría de baja energía. Sin embargo, la introducción de física más allá del modelo estándar a una escala más alta da lugar al *problema de la jerarquía*: El mecanismo de Higgs, necesario para introducir masas para los fermiones y los bosones gauge, también conduce a una partícula escalar de Higgs cuyo valor de esperado en el vacío establece la escala electrodébil. La masa del Higgs, por otra parte, no está protegida por ninguna simetría y recibiría grandes contribuciones de cualquier teoría más allá del modelo estándar. Por lo tanto, se requiere un significativo ajuste fino de los parámetros para estabilizar la masa a la escala electrodébil.

El sector de los neutrinos está abriendo precisamente una ventana a algunos de estos problemas y la física más allá del modelo estándar. Los experimentos de oscilación de neutrinos han demostrado que los neutrinos son masivos. Incluir un término de masa de neutrinos en el SM es, en si mismo, una evidencia de física nueva, ya que es necesario introducir nuevas partículas. Además, explicar las masas de neutrinos también tiene implicaciones en otras áreas de la física de partículas. Por ejemplo, cuando se introducen neutrinos pesados para explicar la ligereza de la masa de los neutrinos a través del mecanismo de seesaw, surgen nuevas fuentes de violacion de CP y del número de leptones que pueden permitir la bariogénesis a través del mecanismo de leptogénesis. La existencia de especies adicionales de neutrinos se predice in muchos modelos de nueva física. Buscar sus masas e interacciones es de gran interés para obtener información sobre posibles modelos de nueva física. Finalmente, comprender la mezcla y las masas en el sector de los neutrinos podría ayudar a obtener una comprensión más profunda del sector del sabor del modelo estándar.

Esta tesis explora modelos de masa de neutrinos que pueden servir como una ventana a la nueva física relacionando el problema de las masas de neutrinos con las otras preguntas abiertas del SM. El punto de partida común de los modelos presentados será la generación de masas de neutrinos. Después de presentar los conceptos básicos de la física necesaria en esta tesis en los capítulos 1 y 2, en el capítulo 3 se presentan las cotas experimentales a la mezcla de neutrinos adicionales con masas por encima de 10 eV. Para este objetivo, estudiamos por la primera vez los datos actuales y futuros de la desaparición de neutrinos atmosféricos del experimento IceCube. El capítulo 4 está dedicado a una realización dinámica de un mecanismo de masa de neutrinos. Para lograr tal modelo, se necesita un nuevo sector de física que contiene un candidato a DM. En el capítulo 5 introducimos un mecanismo de masa de neutrinos natural y dinámico que puede ser investigado en el LHC. Finalmente, concluimos en el capítulo 6.

Motivation and goals

The Standard Model of particle physics has been tested to great accuracy and it describes successfully the strong and electroweak interactions of all currently observed particles. With the discovery of the Higgs boson at the LHC in 2012, the last missing piece of the Standard Model has been found. But is our theoretical understanding of nature complete? In fact, the Standard Model alone cannot describe several phenomenological observations, for example the existence of *Dark Matter*. Only 5% of the energy of the Universe is contained in visible matter described by the Standard Model. Roughly 25% of the energy budget of the Universe is contained in Dark Matter. Experimentally, we have only observed Dark Matter gravitionally, hence we know that Dark Matter needs to be electrically neutral and should only have a small coupling to the Standard Model. The Standard Model alone lacks a Dark Matter candidate that can explain all observations. A plethora of Dark Matter candidates in new physics models have been proposed with masses ranging from 10^{-22} to 10^{18} GeV. A vast experimental program is conducted to detect Dark Matter in various ways: direct detection (via Dark Matter-nucleon scattering), indirect detection (detecting the annihilation products of Dark Matter) or at colliders (via the production of Dark Matter particles in collisions of Standard Model particles).

The remaining 70% of the energy budget of the Universe is attributed to *Dark Energy* which is needed to explain the observed accelerated expansion of the Universe. Dark Energy could be the contribution of a cosmological constant, however the origin of this constant is presently unknown, or Dark Energy could be related to the vacuum energy of the Standard Model. Nevertheless, a naive estimate of this energy differs around 50 orders of magnitude with respect to the experimental value.

Another open question which arises due to the vacuum of the Standard Model is the *strong CP problem* in QCD. Topological QCD effects and the phases in the quark mass matrix contribute to a term $\sim \theta G_{\mu\nu}\tilde{G}_{\mu\nu}$ in the Standard Model Lagrangian. Experimentally θ has been constraint to be smaller than 10^{-10}. This cancellation of two independent contributions coming from different sectors (QCD on one side, the electroweak CP violation on the other side) calls for explanation.

Moreover, the very fundamental question of the matter-antimatter asymmetry arises. If all processes respect the symmetry between particles and antiparticles, the fact that our Universe is mainly made of matter and not antimatter cannot be explained. *Baryogenesis*, a proposed mechanism to generate the baryon asymmetry of the Universe, states that processes in the early Universe favoured the creation of particles with respect to the creation of antiparticles through interactions which violate baryon number, an accidental global symmetry of the Standard Model. Even though the Standard Model contains all

the ingredients for baryogenesis to take place, it is not able to explain the size of the asymmetry observed.

The Standard Model contains another accidental global symmetry, lepton number. Furthermore, in the limit of massless fermions the Standard Model has a global flavour symmetry which is only broken by the Yukawa couplings of the fermions. The parameters in the Standard Model which are related to the flavour sector, i.e., the Yukawa couplings and mixings of the fermions, are ad hoc parameters in the Standard Model and their numerical values need to be introduced by hand. This seems very arbitrary and it would be desirable to have a deeper insight on the origin of these parameters. Especially because we observe a large hierarchy between the different fermion masses (worsened by the smallness of neutrino masses). Also questions like "why are there three generations?" and "why is the mixing in the lepton sector so large when we only observe small mixing angles in the quark sector?" arise. All these questions constitute the *flavour puzzle* of the Standard Model. However, many explanations of the flavour puzzle introduce new physics particles which leads to the *flavour problem*. The flavour problem refers to the issue that flavour observables, especially processes that are very suppressed in the Standard Model due to the GIM mechanism, are very sensitive to new physics contributions since one does not expect generally the new physics model to exhibit the same flavour pattern as the Standard Model. However, we did not see any sign of new physics in flavour observables yet.

All of the open questions described above call for new physics beyond the Standard Model. Together with the fact that the Standard Model describes only the strong and electroweak interactions but it is not able to incorporate in a consistent way a quantum theory of gravity, the Standard Model can be regarded as a low-energy theory. However, introducing a beyond the Standard Model theory at a higher scale gives rise to the *hierarchy problem*: The Higgs mechanism, needed to introduce masses for the fermions and gauge bosons, also leads to a scalar Higgs particle whose vacuum expectation value sets the electroweak scale. The mass of the Higgs on the other hand is not protected by any symmetry and would receive large contributions from any theory beyond the Standard Model proportional to that new scale. Hence a strong fine tuning of the parameters is required to stabilize the mass at the order of the electroweak scale.

The neutrino sector is precisely opening a window to some of these problem and physics beyond the Standard Model. Neutrino oscillation experiments have demonstrated that neutrinos are massive. Including a neutrino mass term in the Standard Model is evidence for new physics itself since new particles need to be introduced. Furthermore, explaining neutrino masses also has implications in other areas of particle physics. For example when heavy neutrinos are introduced to explain the smallness of neutrino mass via a seesaw mechanism, new sources of CP and lepton number violation arise which can enable the baryogenesis through leptogenesis mechanism. The existence of additional neutrino species is expected in many extensions accounting for neutrino masses. Probing their masses and interactions is of great interest to obtain insights in possible new physics models. Finally, understanding the mixing and masses in the neutrino sector could help to obtain a deeper understanding of the Standard Model flavour sector.

This thesis explores neutrino mass models which can serve as a window to new physics by relating the problem of non-vanishing neutrino masses to the other open questions of the Standard Model. The common starting point of the presented models will be the generation of neutrino masses. After introducing the basics of the physics needed in this thesis in chapters 1 and 2, constraints on the mixing of additional neutrinos with masses above 10 eV are presented in chapter 3. To this aim we studied for the first time present and future atmospheric neutrino disappearance data of the IceCube experiment assuming averaged out sterile neutrino oscillations. Chapter 4 is dedicated to a dynamical realisation of a neutrino mass mechanism. To achieve such a model a new physics sector needed to be introduced which contains a DM candidate. In chapter 5 we introduce a natural and

dynamical neutrino mass mechanism. All additional particles are found at the TeV scale which makes this model testable at the LHC. Finally, we conclude in chapter 6.

Contents

1. The Standard Model

Understanding the laws of nature has always been of great interest to humanity. The theories and discoveries of many physicists have emerged into the current understanding of the fundamental structure of matter: everything is made of building blocks called fundamental particles which interact via fundamental forces. The mathematical theory which describes the strong [4,5] and electroweak interactions [6–8] of all currently know particles is called the Standard Model (SM) of particle physics. In the following we will give a short overview of the basic ingredients of the SM.

1.1. Gauge structure and particle content

The SM is a renormalisable quantum field theory based on the gauge group $G_{SM} = SU(3)_C \times SU(2)_L \times U(1)_Y$. The strong interactions of quantum chromodynamics (QCD) are based on the $SU(3)_C$ symmetry and are mediated by eight massless vector gauge bosons associated to this symmetry while the electroweak interactions (EW) are mediated by the vector gauge bosons associated to $SU(2)_L \times U(1)_Y$. The eight generators of $SU(3)_C$ $T^i, i = 1, \dots 8$ and three generators of $SU(2)_L$ $\tau^j, j = 1, 2, 3$ are hermitian matrices that obey the commutation relations

$$[T^a, T^b] = \mathrm{i} f^{abc} T^c, \quad [\tau^a, \tau^b] = \mathrm{i}\epsilon^{ijk}\tau^k \ , \tag{1.1.1}$$

where f^{abc} and ϵ^{ijk} are the structure constants of the corresponding groups. The Lagrangian describing the pure gauge sector of the SM is

$$\mathcal{L}_{gauge} = -\frac{1}{4}\mathrm{Tr}\left(G_{\mu\nu}G^{\mu\nu}\right) - \frac{1}{4}\mathrm{Tr}\left(W_{\mu\nu}W^{\mu\nu}\right) - \frac{1}{4}B_{\mu\nu}B^{\mu\nu} \tag{1.1.2}$$

where $G_{\mu\nu}$, $W_{\mu\nu}$ and $B_{\mu\nu}$ are the field strength tensors of $SU(3)_C$, $SU(2)_L$ and $U(1)_Y$ respectively. They are given by

$$B_{\mu\nu} = \partial_\mu B_\nu - \partial_\nu B_\mu \ , \tag{1.1.3}$$

$$W^i_{\mu\nu} = \partial_\mu W^i_\nu - \partial_\nu W^j_\mu + g\epsilon^{ijk}W^k \ , \tag{1.1.4}$$

$$G^j_{\mu\nu} = \partial_\mu G^j_\nu - \partial_\nu G^l_\mu + g'' f^{jlm} G^m \ , \tag{1.1.5}$$

with the gauge couplings g and g'' of $SU(2)_L$ and $SU(3)_C$, respectively. The mediators of $SU(2)_L$ are the three weak isospin bosons W^i_μ, the gluons G^j_μ are the mediators of $SU(3)_C$, and B_μ is the hypercharge gauge boson of $U(1)_Y$. The field strength tensors for the non-abelian groups $SU(2)_L$ and $SU(3)_C$ contain self-interactions of the gauge bosons, this is not the case for the abelian group $U(1)_Y$.

Name	Particles	Quantum Numbers		
		$SU(3)_C$	$SU(2)_L$	$U(1)_Y$
Quarks	Q'_L	**3**	**2**	$\frac{1}{6}$
	u'_R	**3**	**1**	$\frac{2}{3}$
	d'_R	**3**	**1**	$-\frac{1}{3}$
Leptons	L'_L	**1**	**2**	$-\frac{1}{2}$
	e'_R	**1**	**1**	-1
Higgs Boson	Φ	**1**	**2**	$\frac{1}{2}$
Gluons	G	**8**	**1**	0
Weak gauge bosons	W	**1**	**3**	0
Hypercharge gauge boson	B	**1**	**1**	0

Table 1.1.: Quantum numbers of the fermions, the Higgs boson and the gauge bosons under the Standard model gauge group $SU(3)_C \times SU(2)_L \times U(1)_Y$.

Apart from the gauge bosons, the SM also contains fermions, i.e., quarks and leptons. Fermion fields can be written as gauge multiplets with certain transformation properties under $SU(3)_C$ and $SU(2)_L$ that define their representation under these symmetries. The transformation properties under $U(1)_Y$ are given by the hypercharge of the fermions. The full field content of the SM, including the gauge bosons and the fermions, is given in Tab. 1.1.

Notice that there is no right-handed neutrino in the SM. The fermions appear in three copies, called generations/families that have the same gauge charges and only differ by their masses, as we will see later. Explicitly,

$$\begin{aligned} Q'_L &= \left\{ \begin{pmatrix} u'_L \\ d'_L \end{pmatrix}, \begin{pmatrix} c'_L \\ s'_L \end{pmatrix}, \begin{pmatrix} t'_L \\ b'_L \end{pmatrix} \right\}, \; u'_R = \{u'_R,\; c'_R,\; t'_R\} \;, d'_R = \{d'_R,\; s'_R,\; b'_R\} \;, \\ L'_L &= \left\{ \begin{pmatrix} \nu'_{eL} \\ e'_L \end{pmatrix}, \begin{pmatrix} \nu'_{\mu L} \\ \mu'_L \end{pmatrix}, \begin{pmatrix} \nu'_{\tau L} \\ \tau'_L \end{pmatrix} \right\}, \; e'_R = \{e'_R,\; \mu'_R,\; \tau'_R\} \;. \end{aligned} \tag{1.1.6}$$

To ensure gauge invariance the covariant derivate needs to be introduced which couples the fermions Ψ to the gauge fields

$$\mathcal{L}_\Psi = \mathrm{i}\overline{\Psi} \not{D} \Psi \tag{1.1.7}$$

where

$$\not{D} = \not{\partial} - \mathrm{i}g' \not{B} \frac{Y}{2} - \mathrm{i}g \not{W}^i \tau^i - \mathrm{i}g'' \not{G}^j T^j \;, \tag{1.1.8}$$

where g' is the gauge coupling of $U(1)_Y$.

1.2. Higgs mechanism

In the Lagrangians of the previous subsection we have not introduced yet mass terms for neither the fermions nor for the gauge bosons. However, we experimentally observe that all fermions have mass [9] and that the weak interactions are mediated by massive gauge bosons [9, 10]. In fact, in an unbroken gauge theory the gauge bosons are strictly massless. Fermion masses also break the $SU(2)_L \times U(1)_Y$ gauge symmetry, since a mass term always couples left- to right-handed fields, which are in different representations of $SU(2)_L$ and have different hypercharge. To generate mass terms for the gauge bosons of

$SU(2)_L \times U(1)_Y$, this symmetry needs to be spontaneously broken down to the electromagnetic $U(1)_{\text{em}}$ symmetry [11–14]. To achieve this we introduce a complex $SU(2)_L$ scalar doublet Φ with hyercharge $Y = 1/2$ (see tab. 1.1)

$$\Phi = \begin{pmatrix} \phi^+ \\ \phi^0 \end{pmatrix} \tag{1.2.1}$$

with Lagrangian

$$\mathcal{L}_H = (D\Phi)^\dagger (D\Phi) - V(\Phi) \tag{1.2.2}$$

and potential

$$V(\Phi) = -\mu^2 \Phi^\dagger \Phi + \lambda (\Phi^\dagger \Phi)^2 \ . \tag{1.2.3}$$

This scalar field is known as the Higgs field. For $\mu > 0$ the minimum of the potential is not at $|\Phi| = 0$ but at $|\Phi| = \mu/\sqrt{2\lambda} \equiv v/\sqrt{2}$, where v is the vacuum expectation value (vev) of Φ. Since all field configurations with $|\Phi| = \mu/\sqrt{2\lambda} \equiv v/\sqrt{2}$ are equivalent, we have freedom in the choice of the vacuum. We choose our basis such that

$$\langle \Phi \rangle = \begin{pmatrix} 0 \\ v/\sqrt{2} \end{pmatrix} \ . \tag{1.2.4}$$

The unbroken generator is then $(\tau^3 + Y)\langle \Phi \rangle = 0$ and the electric charge Q of the unbroken group $U(1)_{\text{em}}$ is given by the Gell-Mann–Nishijima formula [15, 16]

$$Q = T_3 + Y \ , \tag{1.2.5}$$

where T_3 is the third component of the weak isospin. In this way we obtain massive weak gauge bosons but have a massless photon γ associated to the unbroken $U(1)_{\text{em}}$.

Expanding Φ around its minimum in eq. (1.2.2) we obtain the masses for the $W^\pm$ and Z gauge bosons. The $W^\pm$ bosons ($W^\pm = \frac{1}{\sqrt{2}}(W^1 \mp \mathrm{i} W^2)$) are electrically charged and have mass

$$m_W = \frac{gv}{2} \ . \tag{1.2.6}$$

The photon γ and the Z boson are linear combinations of W^3 and B

$$\begin{pmatrix} Z \\ \gamma \end{pmatrix} = \begin{pmatrix} \cos\theta_W & -\sin\theta_W \\ \sin\theta_W & \cos\theta_W \end{pmatrix} \begin{pmatrix} W^3 \\ B \end{pmatrix} \tag{1.2.7}$$

where the weak mixing angle θ_W is given by $\tan\theta_W = g'/g$ and the mass of the Z boson is $m_Z = gv/(2\cos\theta_W)$. The massless photon couples with the electric coupling $e = g\sin\theta_W = g'\cos\theta_W$.

From the measured gauge boson masses and couplings we determine the Higgs vev to be $v = 246$ GeV, which sets the electroweak scale. The second parameter λ in the potential can be determined from $\lambda = M_H^2/(2v^2)$ with the measured value of the Higgs mass $M_H = 125$ GeV [9] to be $\lambda \simeq 0.13$.

1.3. Flavour sector

The introduction of the Higgs field also allows to the introduction of fermion mass terms, which would otherwise break the electroweak symmetry. The Yukawa coupling terms of the Higgs to the fermions are given by

$$\mathcal{L}_Y = -y_d^{ij} \overline{Q_L'^i} \Phi d_R'^j - y_u^{ij} \overline{Q_L'^i} \Phi^c u_R'^j - y_l^{ij} \overline{L_L'^i} \Phi e_R'^j + \text{h.c.} \tag{1.3.1}$$

where y_f^{ij} are components of general complex Yukawa matrices and the charge conjugated Higgs doublet is $\Phi^c = \mathrm{i}\tau^2\Phi^*$. Once the Higgs field acquires its vev, mass terms for the fermions are generated with fermion mass matrices $m_f = y_f v/\sqrt{2}$.

We will first concentrate on the quark sector and treat the lepton sector later. Since every complex matrix can be diagonalised by a bi-unitary transformation, we can write

$$m_d = W_L m_d^{\mathrm{diag}} W_R^\dagger, \quad m_u = V_L m_u^{\mathrm{diag}} V_R^\dagger \,, \tag{1.3.2}$$

where W_L, W_R, V_L and V_R are unitary matrices and $m_{u/d}^{\mathrm{diag}}$ are real diagonal matrices. In order to go to the basis in which the mass matrices m_f are diagonal, we need to introduce the rotated fermion fields

$$d_R^i = W_{R,ij} d_R^{'j}, \quad d_L^i = W_{L,ij} d_L^{'j}, \quad u_R^i = V_{R,ij} u_R^{'j} \text{ and } u_L^i = V_{L,ij} u_L^{'j} \,, \tag{1.3.3}$$

and obtain

$$\mathcal{L}_{mass}^q = -m_d^{\mathrm{diag}} \overline{d}_L d_R - m_u^{\mathrm{diag}} \overline{u}_L u_R + \mathrm{h.c.} \,. \tag{1.3.4}$$

This basis is called the quark mass basis and in this basis the fermion fields d and u have definite masses.

On the other hand, the weak gauge bosons couple to the fermions in this basis as (from eq. (1.1.7))

$$\mathcal{L}_\Psi = \frac{g}{\sqrt{2}} W_\mu^+ \overline{u}_L^{'i} \gamma^\mu d_L^{'i} + \mathrm{h.c.} = \frac{g}{\sqrt{2}} W_\mu^+ \underbrace{(V_L W_L^\dagger)_{ij}}_{\equiv (V_{CKM})_{ij}} \overline{u}_L^i \gamma^\mu d_L^i + \mathrm{h.c.} \,, \tag{1.3.5}$$

where V_{CKM} is the Cabibbo–Kobayashi–Maskawa (CKM) matrix [17, 18], which relates the mass basis to the weak interaction basis. Since the neutral currents (NC) mediated by the Z boson couple the same components of the $SU(2)_L$ doublets (and $SU(2)_L$ singlets) the unitarity matrices $W_{L/R}$, $V_{L/R}$ cancel. The same argument applies to the coupling of the photon. Hence the Z boson and the photon couplings are flavour diagonal.

The CKM matrix is a unitary 3×3 matrix and can be parametrised with three angles θ_{12}, θ_{13} and θ_{23} and six phases. However, five phases can be removed by rephasing of the quark fields and hence only one phase is physical. In the standard parametrisation [9] the CKM matrix is given as

$$V_{\mathrm{CKM}} = \begin{pmatrix} c_{12}c_{13} & s_{12}c_{13} & s_{13}\mathrm{e}^{-\mathrm{i}\delta} \\ -s_{12}c_{23} - c_{12}s_{23}s_{13}\mathrm{e}^{\mathrm{i}\delta} & c_{12}c_{23} - s_{12}s_{23}s_{13}\mathrm{e}^{\mathrm{i}\delta} & s_{23}c_{13} \\ s_{12}s_{23} - c_{12}c_{23}s_{13}\mathrm{e}^{\mathrm{i}\delta} & -c_{12}s_{23} - s_{12}c_{23}s_{13}\mathrm{e}^{\mathrm{i}\delta} & c_{23}c_{13} \end{pmatrix} \,, \tag{1.3.6}$$

where $s_{ij} = \sin\theta_{ij}$, $c_{ij} = \cos\theta_{ij}$, and δ is the complex Dirac CP-phase. This phase is of special importance as it can induce CP violation, i.e., the violation of the symmetry between matter and antimatter. Experimentally, the absolute value of the elements of the CKM matrix are [9]

$$|V_{\mathrm{CKM}}^{\mathrm{exp}}| = \begin{pmatrix} 0.97446 \pm 0.00010 & 0.22452 \pm 0.00044 & 0.00365 \pm 0.00012 \\ 0.22438 \pm 0.00044 & 0.97359^{+0.00010}_{-0.00011} & 0.04214 \pm 0.00076 \\ 0.00896^{+0.00024}_{-0.00023} & 0.04133 \pm 0.00074 & 0.999105 \pm 0.000032 \end{pmatrix} \,. \tag{1.3.7}$$

Turning now to the lepton sector. Since there is no right-handed neutrino field in the SM, neutrinos are strictly massless and the only mass term in the lepton sector is the one for the charged leptons. Following the same approach as for the quarks we obtain for the mass term

$$\mathcal{L}_{\mathrm{mass}}^l = -m_l^{\mathrm{diag}} \overline{L}_L e_R + \mathrm{h.c.} \tag{1.3.8}$$

and the Lagrangian in the mass basis

$$\mathcal{L}_\Psi = \frac{g}{\sqrt{2}} W_\mu^+ (W_L^{l\dagger} V_L^\nu)_{ij} \overline{L}_L^i \gamma^\mu \nu_L^i + \text{h.c.} \tag{1.3.9}$$

for the charged current interaction. Since there is no neutrino mass matrix we can choose $V_L^\nu = W_L^l$ and hence the lepton mass basis then coincides with the weak interaction basis.

Apart from the gauge symmetry of the SM there are also two accidental global symmetries present in the SM. The SM Lagrangian is invariant under the transformation $\Psi \to \Psi \mathrm{e}^{\mathrm{i}\theta}$ of the fermion fields, which means the Lagrangian is invariant under global phase transformations. If the quark fields are transformed, the conserved charge associated to this global symmetry is baryon number B. Similar arguments apply to the leptons, where the conserved charge is lepton number L. In fact since there is no lepton mixing in the SM, the invariance of the Lagrangian under a rephasing of the different lepton families leads to three conserved charges which are the individual lepton numbers $L_e,\ L_\mu,\ L_\tau$. However, non-perturbative processes violate the combination $B+L$ while conserving $B-L$. We will come back to this issue in sec. 2.1.3.

2. Open questions in the Standard Model

Despite that the SM successfully describes most of the particle physics experimental results, there are several indications that it is incomplete. In the following we will discuss the open questions of the SM calling for new physics explanations related to this work, i.e., neutrino masses and mixings, the hierarchy problem and the flavour puzzle, and the need for a Dark Matter candidate.

2.1. Physics of massive neutrinos

The discovery of neutrino oscillations was a milestone for beyond the SM physics. It is the first laboratory based evidence for new physics, since the phenomenon of neutrino oscillations can only be explained with massive neutrinos whereas neutrinos are strictly massless in the SM. It is not possible to introduce a mass term for neutrinos as for the other fermions, since there are no right-handed neutrinos in the particle content of the SM (see tab. 1.1). In the following we will first describe the basics of lepton mixing and then discuss possible neutrino mass generation mechanisms in beyond the SM theories.

Another open question in the SM, the origin of the baryon asymmetry of the Universe, might be related to the neutrino mass generation mechanism. We introduce the leptogenesis mechanism and, finally, we discuss the current experimental status of searches for additional neutrino generations.

2.1.1. Lepton mixing

The first hints for neutrino oscillations came from observations of the solar neutrino flux with radiochemical experiments [19–22] and by the Kamiokande experiment [23–25]. These experiments showed for the first time that the Sun produces neutrinos however the measured flux was lower than theoretically expected from solar models [26, 27]. Evidence for neutrino oscillations came from the successor of the Kamiokande experiment, Super-Kamiokande, which measured the atmospheric neutrino flux.[1] A directional analysis of the neutrino flux showed that, while the electron neutrino flux was in agreement with the expected flux without oscillations, there was a deficit in the muon neutrino flux when the neutrinos had traveled through the Earth [29]. Together with the SNO experiment, which measured solar neutrinos [30], the Super-Kamiokande experiment was awarded the Nobel prize in 2015.

In the following we will first introduce the theoretical basis of neutrino oscillations before we give an overview of the measurements of the leptonic mixing parameters and

[1] Initially, this experiment was designed to discover proton decay, and provides the current best bound on the lifetime of the proton [28].

the physics involved. Finally, we describe the unknown parameters in the neutrino sector and experimental prospects.

2.1.1.1. Theoretical basics of neutrino oscillations

Neutrino oscillations describe the effect that, when a neutrino with a certain flavour is produced in a reaction involving a charged lepton of a given flavour, it might be detected via its interaction with a charged lepton of a different flavour. This means that the neutrino can change its flavour during the propagation from production to detection. The probability that describes the flavour change depends on the difference of the squares of the neutrino masses. Hence, if neutrino oscillations are observed neutrinos must be massive and the different neutrino generations must have three different masses. In other words, massless neutrinos as implemented in the SM, cannot account for the observed neutrino oscillations. The observation of neutrino oscillations therefore calls for beyond the SM (BSM) physics.

Taking that neutrinos are massive into account we cannot chose $V_L^\nu = W_L^l$ in eq. (1.3.9) anymore. This means that, also in the lepton sector, a unitary 3×3 matrix that relates the mass basis to the flavour basis arises. This matrix is called the Pontecorvo–Maki–Nakagawa–Sakata (PMNS) [31–34] matrix and, similarly to the CKM matrix, can be parametrised by three angles and at least one phase

$$U^{\text{PMNS}} = UP_0, \tag{2.1.1}$$

where U is a unitary matrix defined in the parametrisation of eq. (1.3.6) and $P_0 = \text{diag}(\text{e}^{-\text{i}\phi_1/2}, \text{e}^{-\text{i}\phi_2/2}, 1)$ is a diagonal matrix containing the two phases $\phi_{1,2}$. These are unphysical, i.e., can be rotated away, if neutrinos are Dirac particles. For this reason these phases do not appear in the quark sector.

A neutrino in the flavour eigenstate ν_α, $\alpha = e,\ \mu,\ \tau$, is related to the mass eigenstates ν_i, $i = 1, 2, 3$, with masses m_i, momentum p_i, and energy $E = \sqrt{m_i^2 + p_i^2}$ via the PMNS matrix as [2]

$$|\nu_\alpha\rangle = \sum_{i=1}^{3} U_{\alpha i}^* \, |\nu_i\rangle \ . \tag{2.1.2}$$

The amplitude of the flavour transition $\nu_\alpha \to \nu_\beta$ after distance L and time t is given by

$$A_{\nu_\alpha \to \nu_\beta} = \langle \nu_\beta | \nu_\alpha(t, L) \rangle = U_{\alpha i}^* T_i(t, L) U_{\beta i} \ , \tag{2.1.3}$$

where $T_i(t, L)$ describes the evolution of the mass eigenstate i. First, we will focus on vacuum oscillations. In this case $T_i(t, L)$ can be obtained from the Schrödinger equation for ν_i with mass m_i

$$\text{i}\frac{\text{d}}{\text{d}\tau} \, |\nu_i(\tau_i)\rangle = m_i \, |\nu_i(\tau_i)\rangle \ , \tag{2.1.4}$$

with τ_i the proper time of ν_i in its rest frame. The time evolution from eq. (2.1.4) for $|\nu_i\rangle$ is given by

$$|\nu_i(\tau_i)\rangle = \text{e}^{-\text{i}m_i\tau_i} \, |\nu_i(0)\rangle \ . \tag{2.1.5}$$

Thus $T_i(t, L)$ for the amplitude $\langle \nu_i(0) | \nu_i(\tau_i) \rangle$ is simply $T_i(t, L) = \text{e}^{-\text{i}m_i\tau_i}$. The expression for $m_i\tau_i$ is given in terms of the laboratory frame variables energy E_i, time t, distance L, and momentum p_i

$$m_i\tau_i = E_i t - p_i L \ . \tag{2.1.6}$$

[2] In this section we refer to the PMNS matrix simply as U instead of U^{PMNS}.

We assume that the initial flavour eigenstate is a mixture of mass eigenstates with sharp energy E and different momenta. Then the momentum p_i associated to mass eigenstate $|\nu_i\rangle$ with mass m_i and energy E is

$$p_i = \sqrt{E^2 - m_i^2} \approx E - \frac{m_i^2}{2E} \ . \tag{2.1.7}$$

Substituting this expression in eq. (2.1.6), we arrive at

$$m_i \tau_i \approx E(t - L) + \frac{m_i^2}{2E} L \ . \tag{2.1.8}$$

The factor $E(t-L)$ is an irrelevant phase factor in the time evolution and will cancel when calculating the oscillation probability by taking the modulus squared of the amplitude. The time evolution is then given by

$$T_i(L) = \exp(-\mathrm{i} m_i^2 \tfrac{L}{2E}) \ . \tag{2.1.9}$$

With this expression eq. (2.1.3) reads

$$A_{\nu_\alpha \to \nu_\beta} = U_{\alpha i}^* \mathrm{e}^{-\mathrm{i} m_i^2 \frac{L}{2E}} U_{\beta i} \ . \tag{2.1.10}$$

The final oscillation probability for ${}^{(-)}\nu_\alpha \to {}^{(-)}\nu_\beta$ is then given by

$$\begin{aligned} P_{\overset{(-)}{\nu}_\alpha \to \overset{(-)}{\nu}_\beta} = |A_{{}^{(-)}\nu_\alpha \to {}^{(-)}\nu_\beta}|^2 =& \delta_{\alpha\beta} - 4 \sum_{i>j} \mathrm{Re}\left(U_{\alpha i}^* U_{\beta i} U_{\alpha j} U_{\beta j}^*\right) \sin^2\left(\frac{\Delta m_{ij}^2}{4E} L\right) \\ & \pm 2 \sum_{i>j} \mathrm{Im}\left(U_{\alpha i}^* U_{\beta i} U_{\alpha j} U_{\beta j}^*\right) \sin\left(\frac{\Delta m_{ij}^2}{2E} L\right) \ , \end{aligned} \tag{2.1.11}$$

where $\Delta m_{ij}^2 = m_i^2 - m_j^2$ and the lower sign applies to antineutrinos. An important limiting case of eq. (2.1.11) to analyse neutrino oscillations is the two-flavour regime, where only two different neutrino generations play a role. In this case, the mixing matrix with mixing angle θ is given by

$$U = \begin{pmatrix} \cos\theta & \sin\theta \\ -\sin\theta & \cos\theta \end{pmatrix} \tag{2.1.12}$$

and the oscillation probability from eq. (2.1.11) reads

$$P_{\alpha\to\beta}^{2fl} = \sin^2(2\theta) \sin^2\left(\frac{\Delta m^2 L}{4E}\right) \ . \tag{2.1.13}$$

Notice that in the two flavour regime no CP violation is possible since the mixing matrix is real.

There are several important implications of eq. (2.1.11). First, notice that neutrino oscillation experiments are only sensitive to the mass squared differences but not to the absolute neutrino mass scale. Furthermore, it is useful to express the argument of the oscillatory term as

$$\frac{\Delta m_{ij}^2}{4E} L = 1.27 \Delta m_{ij}^2 \ (\mathrm{eV}) \frac{L \ (\mathrm{km})}{E \ (\mathrm{GeV})} \ , \tag{2.1.14}$$

then for oscillation experiments to be sensitive to the oscillatory term $\sin^2\left(\frac{\Delta m_{ij}^2}{4E} L\right)$ mass splittings need to satisfy

$$\Delta m^2 \ (\mathrm{eV}^2) \geq \frac{E \ (\mathrm{GeV})}{L \ (\mathrm{km})} \tag{2.1.15}$$

or the oscillatory term does not develop. If, on the other hand, $\Delta m^2 L/(4E) \gg 1$ the oscillatory behaviour will average out due to the finite energy resolution and only an average oscillation probability can be measured, which is independent of Δm^2.

$$P_{\alpha\beta} \simeq \frac{1}{2}\sin^2(2\theta) \ . \tag{2.1.16}$$

Since the PMNS matrix is complex, $P_{\nu_\alpha\to\nu_\beta}$ and $P_{\overline{\nu}_\alpha\to\overline{\nu}_\beta}$ are different. However, the survival probabilities for neutrinos and antineutrinos are equal

$$P_{\overline{\nu}_\alpha\to\overline{\nu}_\alpha} = P_{\nu_\alpha\to\nu_\alpha} \ , \tag{2.1.17}$$

since this channel is its own T conjugate. The unitarity of the U implies the probability conservation

$$P_{\nu_\alpha\to\nu_\alpha} = 1 - \sum_{\beta\neq\alpha} P_{\nu_\alpha\to\nu_\beta} \ . \tag{2.1.18}$$

An observation of $P_{\nu_\alpha\to\nu_\beta} \neq P_{\overline{\nu}_\alpha\to\overline{\nu}_\beta}$ in vacuum would demonstrate CP violation in the lepton sector.[3] The measure for CP violation in the mixing matrix is the Jarlskog invariant [35]

$$J = \sin\theta_{12}\cos\theta_{12}\sin\theta_{23}\cos\theta_{23}\cos^2\theta_{13}\sin\theta_{13}\sin\delta \ , \tag{2.1.19}$$

which is only non-zero if all mixing angles, and the CP phase δ is non-zero.

Finally, the oscillation probability is also invariant under a transformation with diagonal and real phase matrices ϕ and Φ

$$U \to \mathrm{e}^{-\mathrm{i}\phi} U \mathrm{e}^{\mathrm{i}\Phi} \ . \tag{2.1.20}$$

The phase matrix ϕ can be absorbed in a field redefinition of L_L^i. This field redefinition is unphysical since in the Dirac mass term for charged leptons (see eq. (1.3.8)) we can choose the right-handed charged lepton field to have the same phase such that the phase vanishes in the mass term. The phase matrix Φ can be absorbed in a field redefinition of ν_L^i. Similar as for the charged leptons this phase redefinition is unphysical if a Dirac mass term for the neutrinos is introduced. Is, however, a Majorana mass term for the neutrinos introduced which couples $\overline{\nu_L}^c\nu_L$ the phases in ϕ are physical and they are called Majorana phases (see the phases ϕ_1, ϕ_2 introduced in eq. (2.1.1)). Since neutrino oscillations experiments are not sensitive to Majorana phases we cannot distinguish Dirac from Majorana neutrinos from the observation of oscillations alone.

The mixing angles θ_{ij} in the 3-flavour regime are well determined by now. In Tab. 2.1 we have collected the global fit results that we will use in this work. In the following we will describe the measurements of the individual mixing parameters in more detail.

2.1.1.2. Solar neutrinos

The solar parameters θ_{12} and Δm^2_{21} have been determined from the measurement of solar neutrinos originating from fusion processes in the Sun, and from reactor experiments. Solar neutrino energies are few MeV and the distance travelled to the detector is around 10^8 km. These values suggest sensitivity to a mass splitting of $\Delta m^2_{21} \sim 10^{-10}$ eV^2. However, for neutrinos travelling through the Sun, matter effects have to be taken into account. In the previous section we derived the oscillation probability only in vacuum. In the case of oscillations in matter the Schrödinger equation in the flavour basis can be written in matrix form as (we consider the two flavour case $\Psi_\nu = (\nu_e, \nu_\alpha)^T$, $\alpha = \mu$ or τ)

$$\mathrm{i}\frac{\mathrm{d}}{\mathrm{d}t}\Psi_\nu = H\Psi_\nu \tag{2.1.21}$$

[3] Notice that these relations only hold in vacuum, matter effects violate CP and CPT because the matter background is not CP symmetric.

Parameter	best-fit ($\pm1\sigma$)	3σ range
θ_{12} [°]	$33.63^{+0.78}_{-0.75}$	$31.44 \to 36.07$
θ_{13} [°]	$8.52^{+0.15}_{-0.15} \oplus 8.55^{+0.14}_{-0.14}$	$8.07 \to 8.98$
θ_{23} [°]	$48.7^{+1.4}_{-6.9} \oplus 49.1^{+1.2}_{-1.6}$	$39.3 \to 52.4$
δ [°]	$228^{+51}_{-33} \oplus 281^{+30}_{-33}$	$128 \to 390$
Δm^2_{21} [10^{-5} eV^2]	$7.40^{+0.21}_{-0.20}$	$6.80 \to 8.02$
Δm^2_{31} [10^{-3} eV^2] (NO)	$2.515^{+0.035}_{-0.035}$	$2.408 \to 2.621$
Δm^2_{32} [10^{-3} eV^2] (IO)	$-2.483^{+0.034}_{-0.035}$	$-2.580 \to -2.389$

Table 2.1.: The best-fit values and the 3σ ranges for the mixing and mass parameters taken from ref. [36]. There are two minima for θ_{13}, θ_{23} and δ. The first one corresponds to the normal mass ordering whereas the second one corresponds to the inverted mass ordering. The 3σ ranges are given for either ordering.

and the Hamiltonian is

$$H = U \begin{pmatrix} \frac{m_1^2}{2E} & 0 \\ 0 & \frac{m_2^2}{2E} \end{pmatrix} U^\dagger \ . \tag{2.1.22}$$

With this Hamiltonian the neutrino evolution is given by the S-matrix

$$S = \mathrm{e}^{-\mathrm{i}HL} = U \begin{pmatrix} \mathrm{e}^{-\mathrm{i}(m_1^2 L/(2E))} & 0 \\ 0 & \mathrm{e}^{-\mathrm{i}(m_2^2 L/(2E))} \end{pmatrix} U^\dagger \ , \tag{2.1.23}$$

and the oscillation probability is $P_{\alpha\to\beta} = |S_{\alpha\beta}|^2$.

In matter a potential V for the neutrinos is generated. It needs to be taken into account as an additional term in the Schrödinger equation

$$\mathrm{i}\frac{\mathrm{d}}{\mathrm{d}t}\Psi_\nu = (H + V)\Psi_\nu \ . \tag{2.1.24}$$

The potential arises from the coherent neutral current (NC) interactions for all neutrino flavours which interact with the Z boson, and just for the electron neutrinos an additional potential from the charged current (CC) interactions needs to be taken into account. The CC interactions for energies below the W mass are described by

$$\mathcal{H}^{\mathrm{CC}}_{\mathrm{eff}} = \frac{G_F}{\sqrt{2}}\left[\bar{e}\gamma_\mu(1-\gamma_5)e\right]\left[\bar{\nu}_e\gamma^\mu(1-\gamma_5)\nu_e\right] \ , \tag{2.1.25}$$

where G_F is the Fermi constant $G_F = \sqrt{2}g^2/(8m_W^2)$. The electron bilinear needs to be averaged over the background, since the electrons in the medium have some distribution associated to some temperature. For a medium at rest ($\langle v_i \rangle = 0$) composed by non-relativistic, non-polarized electrons and no positrons

$$\langle \bar{e}\gamma^\mu P_L e\rangle = \frac{N_e}{2}(1,0,0,0)^\mu \tag{2.1.26}$$

and

$$\langle \mathcal{H}^{\mathrm{CC}}_{\mathrm{eff}}\rangle = G_F\sqrt{2}N_e\bar{\nu}_e\gamma_0 P_L\nu_e \ , \tag{2.1.27}$$

with the electron density N_e. Hence an effective potential $V_{\mathrm{CC}} = G_F N_e \sqrt{2}$ is generated for electron neutrinos. The NC interactions can be calculated in a similar way

$$\langle \mathcal{H}_{\mathrm{eff}}^{\mathrm{NC}} \rangle = -\frac{G_F}{\sqrt{2}} N_n \sum_{\alpha} \bar{\nu}_\alpha \gamma_0 P_L \nu_\alpha \ , \tag{2.1.28}$$

with the neutron density N_n with the resulting potential $V_{\mathrm{NC}} = -\frac{1}{2} G_F N_n$.

Including these potentials in the Hamiltonian from eq. (2.1.22) leads to

$$H = U \begin{pmatrix} 0 & 0 \\ 0 & \frac{\Delta m^2}{2E} \end{pmatrix} U^\dagger + \begin{pmatrix} V_{\mathrm{NC}} + V_{\mathrm{CC}} & 0 \\ 0 & V_{\mathrm{NC}} \end{pmatrix} \ , \tag{2.1.29}$$

where we defined $\Delta m^2 = m_2^2 - m_1^2$. The contribution from V_{NC} only leads to a phase in the S-matrix which is irrelevant for neutrino oscillations. Combining both matrices the Hamiltonian reads

$$H = \frac{\Delta m^2}{4E} \begin{pmatrix} -\cos 2\theta + A & \sin 2\theta \\ \sin 2\theta & \cos 2\theta - A \end{pmatrix} \tag{2.1.30}$$

with

$$A = \pm \frac{2\sqrt{2} G_F N_e E}{\Delta m^2} \ , \tag{2.1.31}$$

where the plus sign is for neutrinos and the minus sign for antineutrinos. The dimensionless parameter A describes the importance of matter effects. The relation between the flavour eigenstates and the matter eigenstates ν_{im} is

$$\begin{pmatrix} \nu_e \\ \nu_\alpha \end{pmatrix} = \begin{pmatrix} \cos\theta_m & \sin\theta_m \\ -\sin\theta_m & \cos\theta_m \end{pmatrix} \begin{pmatrix} \nu_{1m} \\ \nu_{2m} \end{pmatrix} \ . \tag{2.1.32}$$

The effective mixing parameters in matter are

$$\Delta m_m^2 = C \Delta m^2 \ , \tag{2.1.33}$$

$$\sin 2\theta_m = \sin 2\theta / C, \tag{2.1.34}$$

$$C = \sqrt{(\cos 2\theta - A)^2 + \sin^2 2\theta} \ . \tag{2.1.35}$$

The resulting oscillation probability for electron neutrinos is

$$P(\nu_e \to \nu_\mu) = \sin^2\theta_m \sin^2\left(\frac{\Delta m_m^2 L}{4E}\right) \ . \tag{2.1.36}$$

If $\cos 2\theta = A$ the oscillation probability can be resonantly enhanced. Depending on the sign of Δm^2 the resonance occurs for neutrinos if $\Delta m^2 > 0$ or antineutrinos where $V_{CC} < 0$ if $\Delta m^2 < 0$. This resonance condition is known as the Mikheyev-Smirnov-Wolfenstein (MSW) [37–40] resonance. The matter resonance happening in the Sun made it possible to determine the sign of the mass splitting Δm_{21}^2.

Experiments like Super-Kamiokande [41] and SNO [42], which measured the solar neutrino flux, determined the solar parameters to a high accuracy. Measuring these mixing parameters with terrestrial neutrino sources requires energies of a few MeV and baselines around 100 km. These are the energies and baselines characterising the KamLand experiment [43], which uses anti-electron neutrinos coming from surrounding reactors to measure anti-electron neutrino disappearance.

For the KamLand experiment matter effects do not play a role hence the determined parameters correspond to their values in vacuum. The results from KamLand confirm the results from the solar experiments.

2.1.1.3. Atmospheric neutrinos

Turning now to the atmospheric parameters θ_{23} and Δm^2_{32}, where the sign of the mass splitting is currently unknown. These parameters have been determined using atmospheric neutrinos. Atmospheric neutrinos originate from cosmic ray interactions with the atmosphere which produce a cascade of mesons, mainly pions and kaons. The mesons in turn decay to muons and electrons

$$\pi^{\pm} \to \mu^{\pm} + \overset{(-)}{\nu}_{\mu} \,, \tag{2.1.37}$$

$$\mu^{\pm} \to e^{\pm} + \overset{(-)}{\nu}_{e} + \overset{(-)}{\nu}_{\mu} \,. \tag{2.1.38}$$

The initial neutrino flux consists of $\nu_e, \bar{\nu}_e, \nu_\mu$ and $\bar{\nu}_\mu$ with a ratio $(\nu_e + \bar{\nu}_e)/(\nu_\mu + \bar{\nu}_\mu) \approx 1/2$ at low energies.[4] Atmospheric neutrino energies range from the GeV to the TeV range, although the flux rapidly decreases for large energies. The distances travelled by atmospheric neutrinos range up to the diameter of the Earth ($\sim 10^4$ km) for upward going neutrinos. The Super-Kamiokande experiment measured the $\nu_e + \overline{\nu}_e$ and $\nu_\mu + \overline{\nu}_\mu$ fluxes at different zenith angles, corresponding to different path lengths from production to detection. No significant discrepancy between the expected and measured number of electron neutrino events or down-going muon neutrino events was found. However a deficit of up-going muon neutrinos was observed, which is interpreted as oscillations of muon neutrinos into tau neutrinos. These results have been confirmed by the IceCube/DeepCore [44] experiments which also measure atmospheric neutrinos. Long baseline experiments such as K2K [45], T2K [46], Noνa [47] and MINOS [48] detect muon neutrinos from accelerators to measure the muon neutrino survival probability. Their results are compatible with the results from atmospheric neutrino experiments.

Up to now the octant of θ_{23} is unknown (i.e., if $\theta_{23} > 45°$ or $\theta_{23} < 45°$). By studying the ν_μ survival probability the degeneracy in the octant cannot be resolved, since the oscillation probability in the two-flavour regime depends on $\sin^2(2\theta_{23})$. A combination of reactor data with accelerator ν_μ disappearance and ν_e appearance measurements could resolve the octant [49, 50].

So far the solar and atmospheric neutrino oscillations have been analysed in the two-flavour approximation. This is possible because, in the solar and atmospheric regimes, the parameters governing the other type of oscillations are not relevant at leading order. Since $\Delta m^2_{21} L/E$ is small in the atmospheric regime the solar oscillations have not developed yet, and since $\sin^2(2\theta_{13})$ is small the atmospheric oscillation leads to a subleading term in the solar oscillation probability.

2.1.1.4. Reactor neutrinos

The smallest mixing angle θ_{13} has been determined through anti-electron neutrinos coming from reactors. The Daya Bay [51], RENO [52], and Double Chooz [53] experiments studied the anti-electron neutrino survival probability with reactor neutrino energies of $E \sim$ few MeV and baselines of $L \sim 1$ km. For such values of L/E the solar oscillation has not yet developed. In this case, the oscillation probability is given by

$$P_{ee} = 1 - \sin^2(2\theta_{13}) \sin^2\left(\frac{\Delta m^2_{31} L}{4E}\right) \,, \tag{2.1.39}$$

where the mass splitting is known from atmospheric neutrino oscillations. The reactor angle θ_{13} has been determined to be non-zero. This enables the possibility for CP violation in the lepton sector as all mixing angles have been determined to be non-zero. The result from reactor experiments have been confirmed by long baseline experiments like T2K [54], Noνa [47, 55], and MINOS [48, 56].

[4] At high energies the Lorentz boost of the muons prevents them from decaying before they reach the earth.

Although many neutrino oscillation parameters have been already determined to a good accuracy, there is still some unknowns in the neutrino sector. We will describe them in the next section.

2.1.1.5. Unknowns in the neutrino sector

While the error ranges for the mixing angles are rather narrow, the phases are not yet determined by experiments. There is only a weak hint for $\delta \approx \frac{3\pi}{2}$ coming from data of long-baseline experiments in the global oscillation parameter analysis. A measurement of δ is possible in the near future with long baseline experiments like DUNE [57] or T2HK [58]. The sensitivity to the phase comes from the interference of two contributions to the oscillation probability. Furthermore, neutrino appearance channels need to be considered since disappearance channels are the T conjugate of themselves which means they are also the CP conjugates since CPT is conserved. Since ν_μ are easy to produce the $\nu_\mu \to \nu_e$ or $\nu_\mu \to \nu_\tau$ channels can be considered. However, to measure the interference term in the easiest way possible the interfering terms should be of similar magnitude. Since the atmospheric oscillation in $\nu_\mu \to \nu_\tau$ is large the desired channel is electron neutrino appearance. The relevant oscillation probability is

$$P(\nu_\mu \to \nu_e) = \left|2U^*_{\mu 3}U_{e3}\mathrm{e}^{-\mathrm{i}\Delta_{32}} \sin\Delta_{31} + 2U^*_{\mu 2}U_{e2}\sin\Delta_{21}\right|^2 \ , \tag{2.1.40}$$

with $\Delta_{ij} = \Delta m^2_{ij}L/(4E)$. With the expressions for the matrix elements and up to second order in θ_{13} and Δm^2_{31} as they are small, the oscillation probability can be written as

$$\begin{aligned} P(\nu_\mu \to \nu_e) &= \sin^2\theta_{23}\sin^2 2\theta_{13}\sin^2\Delta_{31} + \cos^2\theta_{13}\cos^2\theta_{23}\sin^2\Delta_{21} && (2.1.41)\\ &\quad + J_r \sin\Delta_{21}\sin\Delta_{31}\cos(\Delta_{32}+\delta) && (2.1.42)\\ &= P_{atm} + P_{sol} + P_{int} && (2.1.43) \end{aligned}$$

where P_{atm}, P_{sol} describe the terms associated with the atmospheric and solar mass splitting. Both terms are small since θ_{13} and $\Delta_{21} = \Delta m^2_{21}L/E$ are small. P_{int} describes the interference term which depends on δ and the reduced Jarlskog invariant J_r

$$J_r = 8\sin\theta_{12}\cos\theta_{12}\sin\theta_{13}\cos^2\theta_{13}\sin\theta_{23}\cos\theta_{23} \ . \tag{2.1.44}$$

Notice that the interference terms has opposite signs for $\Delta m^2_{32} > 0$ or $\Delta m^2_{32} < 0$. Up to now the sign of Δm^2_{32} is unknown, while the sign of Δm^2_{21} has been determined due to the matter effects solar neutrinos experience. Hence both a normal neutrino mass ordering ($m_1 < m_2 \ll m_3$) and an inverted mass ordering ($m_3 \ll m_1 < m_2$) are compatible with data. Future long-baseline experiments can provide information on the mass ordering. Matter effects enable a determination of the mass ordering since forward elastic scattering can enhance or suppress the oscillation probability depending on the sign of Δm^2_{32} (see eq. (2.1.35)).

Since the oscillation probability is invariant under a phase transformation $U \to \mathrm{e}^{-\mathrm{i}\phi}U\mathrm{e}^{\mathrm{i}\Phi}$ (see eq. (2.1.11)), neutrino oscillations do not depend on the Majorana CP-violating phases and it is not possible to distinguish the Dirac and Majorana cases by the observation of neutrino oscillation. The Majorana phases only appear in lepton number violating processes such as in the observable $|m_{ee}|$ measured in neutrinoless double beta decay[5]

$$|m_{ee}| = \left|\sum_i U_{ei}m_i\right| \ . \tag{2.1.45}$$

[5] In this process two neutrons inside the nucleus decay simultaneously via β decays. If the emerging neutrinos are Majorana particles (i.e. they are their own antiparticles) they can annihilate and only two electrons are emitted.

The current upper limit is $|m_{ee}| < 0.12 - 0.26$ eV [59], where the uncertainty comes from the calculation of the nuclear matrix element.

Also the absolute mass scale m_{lightest} is currently unknown. Up to now we only have an upper bound on the sum of neutrino masses $\sum_i m_i = 0.12$ eV [60] coming from measurements of the total energy density in matter. A small amount of the DM energy density is also stored in neutrinos which are hot DM (their velocities are large compared to their mass). The more mass the neutrinos have the less energy density can be stored in cold DM. Since cold DM enables small structure formation we obtain from observations of the small structures in the Universe an upper bound on the sum of the neutrino masses.

Another observable is the effective flavour neutrino mass $m_{\nu_\alpha} = \sum_i |U_{\alpha i}|^2 \nu_i$. The best bound is on m_{ν_e} where the upper bound comes from the process ${}^3\text{H} \to {}^3\text{He} + e + \bar{\nu_e}$ [9]

$$m_{\nu_e} < 2 \text{ eV} \quad . \tag{2.1.46}$$

The KATRIN experiment is expected to lower the bound on m_{ν_e} to $m_{\nu_e} < 0.25$ eV [61] .

2.1.2. Neutrino mass generation mechanisms

In the previous section we have seen that neutrino oscillations are only possible when neutrinos are massive. However, in the SM neutrinos are massless, hence we can only accommodate for neutrino masses in beyond the SM theories. Since neutrinos are the only fermions that do not carry electric charge, there are two possibilities to construct a mass term for them.

Like quarks and charged leptons neutrinos could have a Dirac mass term which stems from the Higgs mechanism as already introduced in sec. 1.3

$$m_D \overline{\nu}_L \nu_R \ , \tag{2.1.47}$$

with the Dirac mass $m_D = y_\nu v/\sqrt{2}$. We only need to introduce right-handed neutrino fields which are total singlets under the SM gauge group. This mass term conserves total lepton number, which is defined as

$$L(\nu) = -L(\bar{\nu}) = 1 \ . \tag{2.1.48}$$

Since the neutrino masses are very small we need a Dirac Yukawa coupling of $\mathcal{O}(10^{-12})$ to achieve a neutrino mass of $\mathcal{O}(0.1 \text{ eV})$. This value is very small compared to the smallest Yukawa coupling in the SM, the electron Yukawa coupling which is $\mathcal{O}(10^{-6})$. This discrepancy in coupling strengths introduces a strong hierarchy between the fermion masses and hence worsens the flavour puzzle (see sec. 2.2.1).

The second possibility for a neutrino mass term is a Majorana mass term

$$\frac{m_M}{2} \overline{\nu}^c_L \nu_L \ , \tag{2.1.49}$$

written in Weyl notation, where a Weyl spinor satisfies $\Psi^c = \mathrm{i}\sigma_2 \Psi^*$. Note that a Majorana mass term for the neutrinos breaks $SU(2)_L \times U(1)_Y$. In order to obtain a Majorana mass term in a gauge invariant way we introduce a dimension-5-operator [62]

$$\frac{O^W}{\Lambda} = - \frac{(\overline{L^c_L} \mathrm{i}\tau_2 \Phi)(\Phi \mathrm{i}\tau_2 L_L)}{\Lambda} \tag{2.1.50}$$

that couples one lepton doublet L_L to one Higgs doublet Φ and where τ_2 is a Pauli matrix. This term was first introduced by Weinberg and it is non-renormalisable. The scale Λ indicates the high energy scale at which the new physics is integrated out. After electroweak symmetry breaking this operator reduces to a Majorana neutrino mass term. To obtain a neutrino mass of $\mathcal{O}(0.1 \text{ eV})$ we need $\Lambda \sim 10^{14}$ GeV which is close to the Grand Unification scale.

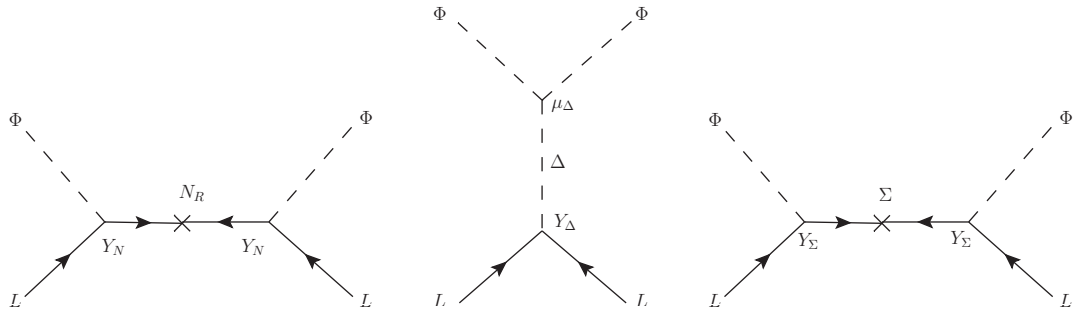

Figure 2.1.: Seesaw type I, type II, and type III (from left to right). The mechanisms differ by the exchanged heavy particle. See text for details.

There are three possibilities for generating the Weinberg operator at tree-level. They are known as seesaw type I [63–68], seesaw type II [68–72] and seesaw type III [73]. They differ by the heavy field Ξ that is exchanged (see Fig. 2.1) with mass M_Ξ and coupling Y_Ξ.

- Seesaw type I:

  Here the leptons and the Higgs doublets are coupled via the exchange of a heavy right-handed fermion N_R which is a SM singlet. It is then possible to construct a Majorana mass term for N_R and a Dirac mass term. The relevant Lagrangian describing neutrino masses reads

  $$\mathcal{L}_\nu = M_N \overline{N}_R^c N_R + Y_N \overline{L}_L \Phi^c N_R + \text{h.c.} \; . \tag{2.1.51}$$

  After electroweak symmetry breaking the light neutrino masses are generated and at leading order in $\frac{vY_N}{M_N}$ they read

  $$m_\nu = Y_N^T \frac{1}{M_N} Y_N v^2 \; . \tag{2.1.52}$$

  Notice that to obtain neutrino masses compatible with data a minimal set of two N_R need to be introduced.

- Seesaw type II: In this mechanism a heavy scalar $SU(2)_L$ triplet Δ is exchanged. The neutrino mass arises from

  $$\mathcal{L}_\nu = Y_\Delta L_L^c \mathrm{i}\tau_2 \Delta L_L + h.c. \; . \tag{2.1.53}$$

  Since Δ is a $SU(2)_L$ triplet with hypercharge -1, it also interacts with the Higgs as well as with the electroweak gauge bosons

  $$\mathcal{L}_\Delta \supset \mathrm{Tr}((D_\mu \Delta)^\dagger (D_\mu \Delta)) - (\mu_\Delta \Phi^T \mathrm{i}\tau_2 \Delta^\dagger \Phi + h.c.) \; . \tag{2.1.54}$$

  From the coupling to the Higgs Δ obtains an induced vev $v_\Delta = \mu_\Delta v^2/(\sqrt{2}M_\Delta^2)$ on which the neutrino masses depend (to leading order in $\frac{vY_\Delta}{M_\Delta}$)

  $$m_\nu = Y_\Delta \frac{\mu_\Delta}{M_\Delta^2} v^2 \; . \tag{2.1.55}$$

  Notice that there are no right-handed neutrinos in the type II seesaw.

- Seesaw type III:

  In this seesaw type, the right-handed fermion from type I is replaced by a $SU(2)_L$ fermion triplet Σ. The Lagrangian that describes the interactions of Σ is

$$\mathcal{L}_\Sigma = \overline{\Sigma} \not{D} \Sigma - Y_\Sigma (\overline{L}_L \Phi) \Sigma - \mathrm{Tr}(M_\Sigma \overline{\Sigma} \Sigma^c + h.c.) \ . \tag{2.1.56}$$

  The neutrino mass term reads (to leading order in $\frac{vY_\Sigma}{M_\Sigma}$)

$$m_\nu = Y_\Sigma^T \frac{1}{M_\Sigma} Y_\Sigma v^2 \ . \tag{2.1.57}$$

The type I and type III seesaw mechanisms rely on a hierarchy of scales (i.e. the electroweak scale over the new physics scale M_Ξ) to accommodate small neutrino masses. Hence in these mechanisms the detection of the additional fermions is experimentally challenging due to their large mass and their suppressed mixing with the SM neutrinos (with mixing angle $\theta \sim Y_\Xi v / M_\Xi$). Furthermore, these models introduce a hierarchy problem since the new particles introduce large corrections to the Higgs mass. In the type II seesaw the smallness of the neutrino masses is either achieved by a hierarchy of scales or via a small dimensionfull parameter μ_Δ while keeping M_Δ at the electroweak scale. Since μ_Δ is the only parameter in the model which breaks lepton number its value can be small, assuming an approximate lepton number symmetry. In chapter 5 we introduce a model where we promote μ_Δ to a dynamical quantity by identifying it with a vev of a scalar which breaks the global lepton number symmetry of the SM.

Assuming an approximate lepton number symmetry is also the idea behind another class of neutrino mass models. These models allow for the possible detection of the extra fermions, since their masses can then be around the electroweak scale. For example in the inverse seesaw scenario [74] two species of additional fermions N_R and $N_R^{'}$ are introduced (see fig. 2.2).[6] In the inverse seesaw the neutrino masses come from the following Lagrangian

$$-\mathcal{L}_\nu = m_D \overline{\nu_L} N_R + \overline{N_R^c} M_N N_R' + + \mu \overline{(N_R')^c}\, N_R' + \text{h.c.}, \tag{2.1.58}$$

which leads to the mass matrix (in the basis $(\nu_L^c,\ N_R, N_R^{'})$)

$$M = \begin{pmatrix} 0 & m_D & 0 \\ m_D^T & 0 & M_N \\ 0 & M_N^T & \mu \end{pmatrix} \ , \tag{2.1.59}$$

where M_N is the mass matrix of the heavy neutrinos. The matrix μ breaks lepton number, hence if this symmetry is only mildly broken the neutrino masses are necessarily small. For $\mu \neq 0$ the light neutrino masses are given by

$$m_\nu \sim m_D M_N^{-1} \mu \left(M_N^T\right)^{-1} m_D^T \ . \tag{2.1.60}$$

With TeV-scale right-handed neutrinos and $\mathcal{O}(1)$ Yukawa couplings we would need $\mu \sim \mathcal{O}(\text{keV})$ to obtain sub eV neutrino masses. Implementing this dimensionfull parameter by hand is unsatisfying. In chapter 4 we propose a model where μ arises as a dynamical quantity.

A Majorana mass term also breaks global lepton number symmetry by two units since a Majorana mass term mixes ν and $\bar{\nu}$. As already explained in the previous section, neutrino oscillation experiments are not able to distinguish Dirac neutrinos from Majorana neutrinos. Only a measurement of lepton number breaking observables (for example the observable $|m_{ee}|$ in neutrinoless double beta decay) is a smoking gun for Majorana neutrinos because this process violates lepton number [68].

[6] The same idea is also behind the linear [75, 76] or double seesaw [74, 77–79], which also allow for TeV scale neutrinos.

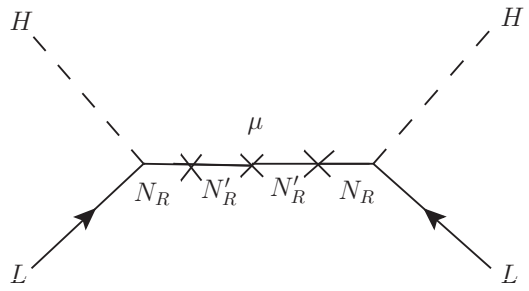

Figure 2.2.: Inverse seesaw scenario. Two species of right-handed neutrinos N_R and $N_R^{'}$ need to be introduced.

2.1.3. Leptogenesis

Massive neutrinos might also be connected to another open question in the SM, the baryon asymmetry of the Universe, i.e., the excess of matter over antimatter. Experiments such as AMS did not find any evidence for antimatter in the Universe and constrained the ratio of the number of antihelium over helium nuclei in cosmic rays to be [80]

$$\frac{N_{\overline{\mathrm{He}}}}{N_{\mathrm{He}}} < 1.1 \cdot 10^{-6} \ . \tag{2.1.61}$$

A way to quantify the baryon asymmetry of the universe (BAU) is [9, 60, 81, 82]

$$Y_{\Delta B} = \left.\frac{n_B - n_{\bar{B}}}{s}\right|_0 \approx \left.\frac{n_B}{s}\right|_0 = (8.75 \pm 0.23) \cdot 10^{-11} \ , \tag{2.1.62}$$

where n_B and $n_{\bar{B}}$ are the number densities of the (anti-)baryons and s is the entropy at current time (indicated by the subscript 0). The measurement of $Y_{\Delta B}$ comes from the primordial abundance of light elements [82, 83] and from the power spectrum of temperature fluctuations in the CMB [60]. If the Universe was matter-antimatter symmetric at early times an asymmetry needs to be generated during the evolution of the Universe. A model to successfully generate the baryon asymmetry needs to fulfil the Sakharov conditions [84]:

- Baryon number violation: Necessary to evolve from a state without a baryon number asymmetry to a state with a baryon number asymmetry.
- C and CP violation: Otherwise the processes involving baryons are at precisely the same rate as the C or CP conjugated processes involving antibaryons and no net baryon asymmetry would be generated.
- Out of equilibrium process: If processes would be in chemical equilibrium any generated baryon asymmetry would be immediately erased.

These conditions are fulfilled in the SM. However, a sufficiently large baryon asymmetry cannot be produced by SM processes alone [85, 86]. One of the problems is that the CP violation coming from the quark sector is not large enough.

A new physics scenario that can successfully generate a sufficient BAU is the leptogenesis mechanism [87]. In this mechanism heavy sterile neutrinos decay out of equilibrium leading to a lepton asymmetry followed by a conversion of this lepton asymmetry into a baryon asymmetry by non-perturbative processes (sphalerons), which are already present in the SM.

In detail, the lightest heavy neutrino N_1 with mass M_1 decays into a light neutrino and a Higgs

$$N_1 \leftrightarrow \Phi + L \ , \tag{2.1.63}$$

where in the early Universe ($T \gg M_1$) these processes are in thermal equilibrium. When the temperature drops below its mass and the lifetime of the neutrino is long enough, N_1 decays out of equilibrium. The interference between the tree-level diagram and the loop-level diagram of the N_1 decay leads to a non-zero CP asymmetry produced in the decay of N_1

$$\epsilon = \frac{\Gamma(N_1 \to \Phi L) - \Gamma(N_1^c \to \Phi^\dagger \bar{L})}{\Gamma(N_1 \to \Phi L) + \Gamma(N_1^c \to \Phi^\dagger \bar{L})} \,, \tag{2.1.64}$$

which describes the difference in the rate of decays into particles and the rate of decays into anti-particles normalized by the total decay rate. If the heavy neutrinos are nearly degenerate in mass, resonance effects from the decay of the next to lightest right-handed neutrino N_2 need to be taken into account. In general, the final lepton asymmetry is a result of the competition between production processes and washout processes that tend to erase any generated asymmetry. For a calculation of the produced lepton asymmetry the decays of the right-handed neutrinos, inverse decays ($\Phi L \to N$), $\Delta L = 1$ scatterings of heavy neutrinos involving top quarks (for example $q_L t_R \to \Phi \to N_1 L$) and $\Delta L = 2$ processes mediated by virtual heavy neutrinos need to be taken into account in the Boltzmann equation of the right-handed neutrinos [88].

The generated lepton asymmetry is then converted into a baryon asymmetry by sphaleron processes present in the SM [89–91]. These non-perturbative processes violate $B+L$ while conserving $B-L$. They arise in the electroweak theory where several topologically distinct energy minima of the field configurations exist, which are not related by continuous gauge transformations. The different minima have different values of $B+L$ and hence changing from one minimum to another implies a conversion from a lepton asymmetry to a baryon asymmetry.

To obtain the resulting baryon asymmetry N_B after sphaleron transitions, we need to calculate the change of number of particles of different species by the various SM processes. If the processes happen fast compared to the expansion rate of the Universe H, they lead to an equilibrium state, where the comoving number densities of the participating particles remain constant. This is described by conditions of chemical equilibrium: The sum of chemical potentials of all particles entering the interaction, should be zero. For example the lepton-Higgs interaction term $y_l^{ij} \overline{L}_L^i \phi e_R^j$ (see eq. (1.3.1)) changes a $SU(2)_L$ doublet lepton into a $SU(2)_L$ singlet lepton and a Higgs. In terms of chemical potentials μ_i

$$\mu_{e_R^j} + \mu_\phi - \mu_{L_L^i} = 0 \,. \tag{2.1.65}$$

The asymmetry in the individual particle number densities can be related to the chemical potentials via

$$\Delta y_i = \frac{n_i - \bar{n}_i}{s} = \begin{cases} \frac{g_i}{6s} T^2 \mu_i, & \text{for fermions} \\ \frac{g_i}{3s} T^2 \mu_i, & \text{for bosons} \end{cases} \tag{2.1.66}$$

where g_i is the internal number of degrees of freedom. Above the electroweak phase transition all SM interactions are fast and the Yukawa interactions lead to relations between the chemical potentials among the fermions and the Higgs. The electroweak sphalerons conserve $B-L$ so we additionally get $\sum_{i=1}^{3}(3\mu_{Q^i} + \mu_{L^i}) = 0$. Together with the requirement that the total hypercharge of the plasma vanishes we can solve for the chemical potentials of the particles. The baryon and lepton asymmetries are the sum over the individual baryon and lepton number densities $\Delta y_B, \Delta y_L$, respectively. Finally, we arrive at the resulting baryon asymmetry [90, 91]

$$Y_{\Delta B} = \frac{28}{79} Y_{\Delta(B-L)} \tag{2.1.67}$$

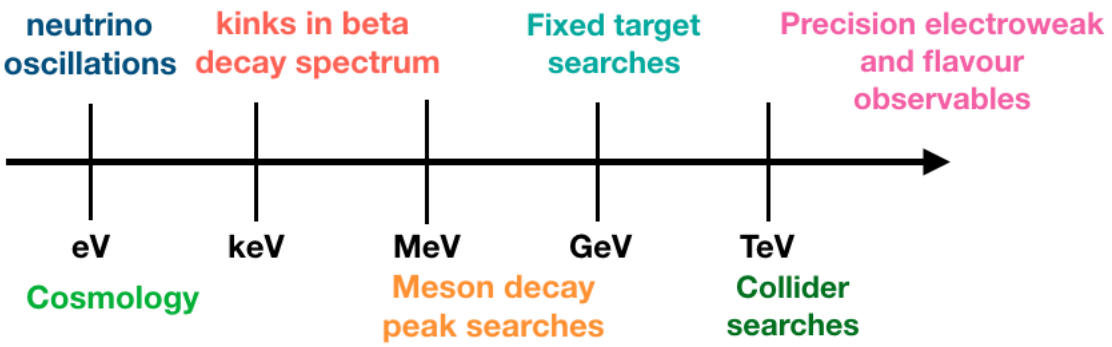

Figure 2.3.: Impact of sterile neutrinos on different observables.

in terms of the $B - L$ asymmetry $Y_{\Delta(B-L)}$.

This mechanism for leptogenesis based on the out-of-equilibrium decay of the right-handed neutrinos requires large Majorana neutrino masses $> 10^8$ GeV [92]($\gtrsim 10^6$ GeV when flavour effects are included [93]). There is an alternative leptogenesis scenario allowing for lighter right-handed neutrinos (1-100 GeV scale). The lepton asymmetry in this case is produced by freeze-in of the sterile states via their CP-violating oscillations [94–96].

2.1.4. Sterile neutrino search

In sec. 2.1.2 we saw that the easiest extension to generate neutrino masses is to add SM singlet fermions to the particle content. The mass of the right-handed neutrinos is not related to the electroweak scale and can therefore range over several orders of magnitude. Constraining the existence of additional neutrino generations is of great interest. In the following we will give a short overview of the current status of sterile neutrino searches.

Depending on the mass of the sterile neutrino they leave an imprint in different observables (see fig. 2.3):

- $m_4 \sim$ eV: Sterile neutrinos leave an imprint in neutrino oscillations as well as in cosmological observables.
- $m_4 \sim$ keV: Kinks in the β spectrum as well as cosmological observables.
- $m_4 \sim$ MeV: Peaks in the spectrum of electrons in meson decays and direct N_4 decay.
- $m_4 \sim$ GeV: Fixed target experiments.
- $m_4 \sim$ TeV: Collider constraints, precision electroweak and flavour observable.

The current experimental bounds on the mixing between the sterile neutrino and the SM neutrinos is shown in fig. 2.4 in the $|V_{\alpha 4}|^2$-m_4 mass plane (figure from [97]). The mixing with electron neutrinos $|V_{e4}|^2$ can be constraint from kinks in the β spectrum, peaks in the spectrum of electrons in meson decays (where the meson decays to a sterile neutrino instead of SM neutrino), or from the decay of N_4 to electron-positron pairs in reactor and accelerator experiments. Constraints on the mixing with muon neutrinos $|V_{\mu 4}|^2$ come from peak searches in the spectrum of muons in meson decays (pion decays for $M_4 < 34$ MeV and kaon decays for higher masses), and of the decays of N_4 produced in beam dump experiments and e^+e^- collisions. Finally, the mixing with tau neutrinos $|V_{\tau 4}|^2$ can be constrained from N_4 decays. For more details on the derivation of the bounds see [97].

The impact of sterile neutrinos in electroweak precision observables has been studied in [98], where the mixing was constrained to be $V_{\alpha 4} \lesssim 10^{-2}$.

Up to now no positive evidence of sterile neutrinos has been found, but there are several anomalies that might point to the existence of sterile neutrinos. The LSND [99] and

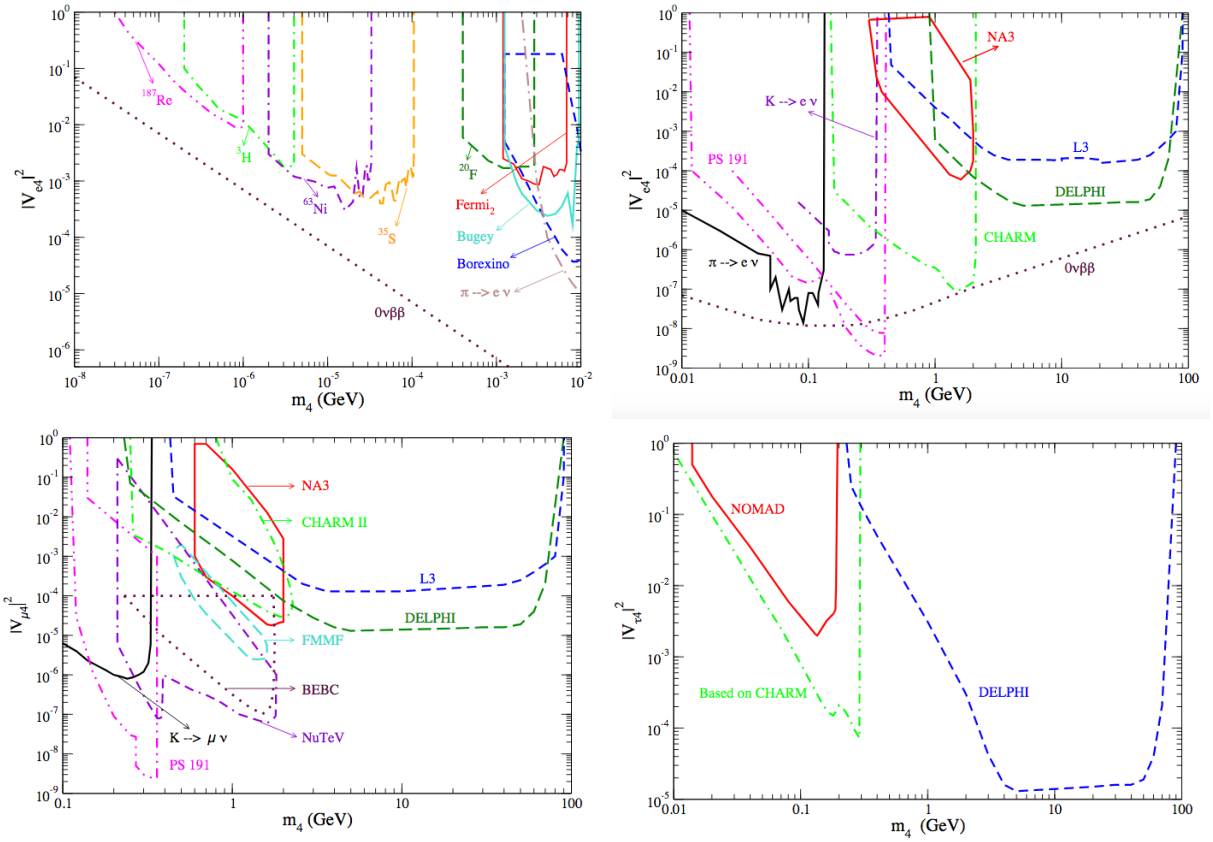

Figure 2.4.: Bounds on sterile mixing matrix element over the mass of the sterile neutrino from [97].

MiniBooNE [100] experiments found results that cannot be explained within the three-neutrino framework. The LSND experiment observed an excess of $\overline{\nu}_e$ events from a source of pions decaying at rest while the MiniBooNE experiment observed an excess of electron like events in both ν_μ and $\overline{\nu}_\mu$ beams. Both results are compatible with $\nu_\mu \to \nu_e$ oscillations at short baselines with a relativly large mass splitting [101]. Furthermore, fluxes from gallium experiments [102–107] and reactors [108, 109] shown a deficit of ν_e events relative to the theoretical expectation. All of these results can be explained with a sterile neutrino with $m_4 \sim 1$ eV. However, this explanation is not compatible with muon neutrino disappearance results $\nu_\mu \to \nu_\mu$ [110,111]. The discrepancy between electron neutrino appearance $\nu_\mu \to \nu_e$ data and disappearance data $\nu_\mu \to \nu_\mu$ is around 4.7σ [101, 112, 113]. The MiniBooNE and LSND excesses will be further studied within the Fermilab Short Baseline programme [114].

In chap. 3 of this work we will focus on sterile neutrinos with larger masses, which cannot explain the LSND and MiniBooNE result. In fact, in sec. 2.1.4 we present current constraints on the matrix elements $V_{\mu 4}$ and $V_{\tau 4}$ assuming one additional sterile neutrino.

2.2. Flavour physics and the hierarchy problem

Most of the free parameters in the SM are related to the flavour sector. Finding a deeper insight on the origin to their values and the hierarchies between them is compelling and would imply physics beyond the SM, since there is no explanation from the SM. Indeed, the numerical values of the flavour parameters need to be inserted by hand and are rather ad hoc.

In the past, flavour physics has proven to be a discovery ground for new physics. For example, the charm quark was predicted [115] before its discovery by the observation

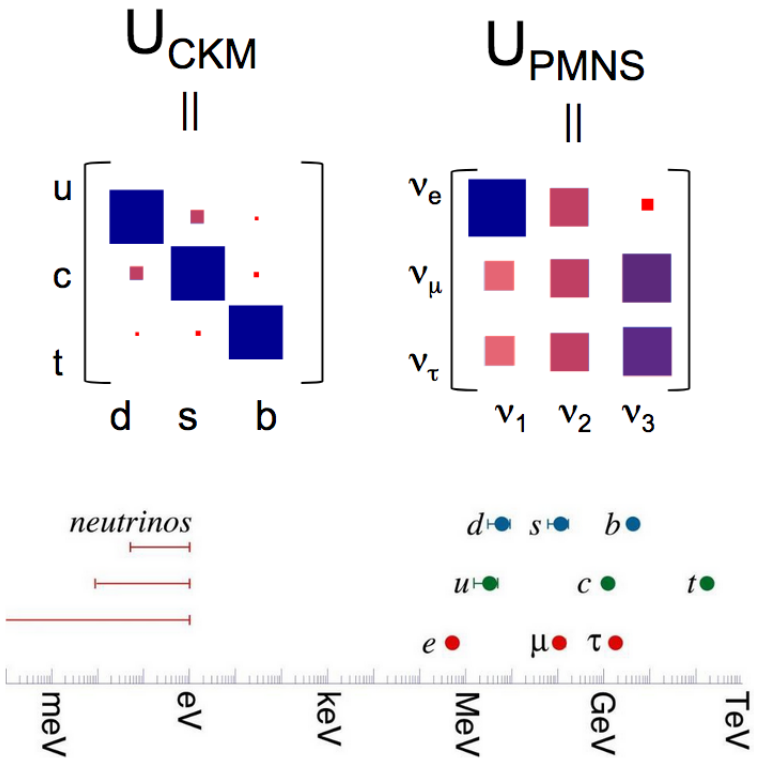

Figure 2.5.: Comparision of the CKM and PMNS matrix elements and of the fermion masses (image credit: Hitoshi Murayama).

of the tiny branching ratio (BR) of $K_L \to \mu\mu$ and the third generation of quarks was predicted [17, 18] to accommodate for CP violation in kaon mixing.

In the following we will introduce the flavour puzzle and discuss possible explanations based on symmetries, and review the flavour problem. Many new physics models which for example propose solutions to the flavour puzzle or explanations for the smallness of neutrino masses introduce new particles at a high scale. These new particles lead to large contributions to the Higgs mass which gives rise to the hierarchy problem which we will also introduce in this section.

2.2.1. Flavour puzzle

Out of the 18 free parameters in the SM, 13 are related to flavour. Inserting the numerical values of these parameters by hand seems unsatisfactory and we would like to have a fundamental understanding of the origin of these parameters. In fact, the fermion masses show a striking hierarchy among the different generations [9]

$$(m_e,\ m_\mu,\ m_\tau) = (0.511\ \text{MeV},\ 105.7\ \text{MeV},\ 1776.9\ \text{MeV})\ , \tag{2.2.1}$$
$$(m_u,\ m_c,\ m_t) = (2.2\ \text{MeV},\ 1.275\ \text{GeV},\ 173.0\ \text{GeV})\ , \tag{2.2.2}$$
$$(m_d,\ m_s,\ m_b) = (4.7\ \text{MeV},\ 95\ \text{MeV},\ 4.18\ \text{GeV})\ . \tag{2.2.3}$$

The mixings in the quark and lepton sectors are also very different (e.g., compare eq. (1.3.7) to tab. 2.1). The difference is even more striking when shown schematically in fig. 2.5.[7]

Hence questions such as " Why are there three families of quarks and leptons?", "Why do the fermion masses exhibit a strong hierarchical structure spanning several orders of

[7] The ratio of the mass of the lightest fermion, the neutrino, over the heaviest fermion, the top quark, is roughly the same as comparing the weight of an ant to a whale.

magnitude?" and "Why are the mixing angles in the quark sector so different from the ones in the lepton sector?" arise and call for answers.

Several ideas to explain the different masses and mixings have been proposed:

- Frogatt-Nielsen: This mechanism is based on the assumption of a flavour $U(1)_{FN}$ symmetry under which the fermions have different charges [116]. A SM singlet S with $U(1)_{FN}$ charge -1 acquires a vev and breaks the symmetry. The different masses of the fermions can be realised assuming different orders of the small parameter $\epsilon = \langle S \rangle / M_*$, where M_* is the scale of flavour symmetry breaking, typically associated with the mass of extra chiral fermions that have been integrated out. The fermion mass terms then read $\mathcal{L} \subset \overline{\Psi}_L^i \Phi \epsilon^{n_{ij}} \Psi_R^j$, where the SM Yukawa couplings are identified with $y_{ij} = Y_{ij} \epsilon^{n_{ij}}$ with $Y \sim \mathcal{O}(1)$. The masses of the fermions are suppressed by powers of ϵ depending on their $U(1)_{FN}$ charges $\epsilon^{-a_i + a_j}$ with $Q(\Psi_L) = a_i$ and $Q(\Psi_R) = a_j$. Assuming that the $U(1)_{FN}$ charge differences for the lighter generations are larger than for the heavier generations leads to smaller masses while all Yukawa coupling Y_{ij} are the same order of magnitude. The mass ratios are therefore given by $m_i/m_j = \epsilon^{-a_i + a_j + b_i - b_j}$. The mass hierarchy and the mixing angles can be correctly reproduced just by assuming different suitable $U(1)_{FN}$ charges.

- Discrete symmetries: Symmetries were good guidelines to build the SM. The measured values of the atmospheric and solar mixing angles motivated explanations based on modelling their values as ratios of integers. A very popular example is tribimaximal mixing [117] based on the numerology $\sin^2\theta_{12} = 1/3, \sin^2\theta_{23} = 1/2, \sin^2\theta_{13} = 0$. These values can be realised motivated by a discrete symmetry like A_4. However, the measured non-vanishing value of the reactor angle and the deviation from maximal atmospheric mixing call for deviations from the exact values predicted by the discrete symmetries.[8] A drawback of the discrete symmetry approach might be that the chosen group is arbitrary and the different mixing patterns in the quark and lepton sectors are not related to each other from the discrete symmetry alone.[9]

- Continuous symmetries: An alternative approach to explain the flavour puzzle is to generate the Yukawa couplings of the fermions through scalar fields that spontaneously break the continuous global flavour symmetry present in the SM Lagrangian with massless fermions [122]

$$G_{Fl} = U(3)_{Q_L} \times U(3)_{U_R} \times U(3)_{D_R} \times U(3)_{L_L} \times U(3)_{E_R} \, . \tag{2.2.4}$$

  Notice that the Yukawas do not break the complete flavour symmetry but leave out the accidental global symmetries of the SM: baryon and individual lepton number. Spontaneous breaking of a global symmetry leads to unwanted massless Goldstone bosons in the spectrum. A way out is to gauge the flavour symmetry [123,124] where as an ansatz $SU(3)_{L_L} \times SU(3)_{E_R}$, and $SU(3)_{Q_L} \times SU(3)_{U_R} \times SU(3)_{D_R}$ have been gauged. Cubic and mixed hypercharge anomalies arise which are cancelled by the introduction of mirror fermions such that the fermions are vector-like with respect to the flavour gauge group. The Yukawa terms in the Lagrangian lead to fermion mass matrices that present a seesaw-like structure and where the SM fermion masses are inversely proportional to the mirror fermion masses.

  Hence, with this ansatz, the flavour puzzle could be solved by a scalar potential which predicts different scales at which the corresponding flavour group is broken and by different values of the parameters in the fermion mass terms.

[8] Such corrections could come from assuming a non-diagonal charged lepton mixing matrix, in particular $\theta_{13} \approx 9^\circ$ can be achieved by assuming a 1-2 mixing in the charged lepton sector of the size of the Cabbibo angle [118–121].

[9] In $SU(5)$ Grand Unified Theories the down type Yukawa matrix is related to the charged lepton Yukawa matrix as $Y_d \sim Y_e^T$.

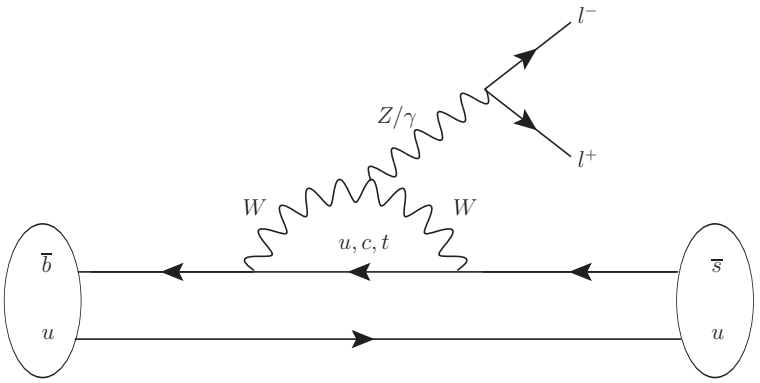

Figure 2.6.: An example for a FCNC arising in the SM at loop level: $B^+ \to K^+ l^+ l^-$.

The observed smallness of neutrino masses contributes to the flavour puzzle. In this sense, the new physics extensions proposed in chapters 4 and 5 also address the flavour puzzle as they propose an explanation for the smallness of neutrino masses in comparison to the other fermion masses.

Most models addressing the flavour puzzle necessarily introduce new particles that modify the predictions for flavour observables. However, many searches for deviations in those observables have turned up empty handed. We will address this topic in the next subsection.

2.2.2. Flavour problem

The flavour problem refers to the non-observation of new physics in flavour observables.[10] Flavour observables are very sensitive to new physics contributions since in general new physics models are not expected to have the same flavour structure as the SM.

First let us discuss flavour physics in the SM. From eq. (1.3.5) we see that the flavour changing processes are mediated by the $W^\pm$ boson, since it couples to the different components of the $SU(2)_L$ doublets. This is due to the off-diagonal generator $\tau^\pm = \tau_1 \pm \mathrm{i}\tau_2$ in the coupling of the $W^\pm$ boson. The Z boson (and the photon) on the other hand is a mixture of W^3 and B (see eq. 1.2.7) which couples with a diagonal generator and hence it always couples the same entries of the $SU(2)_L$ doublet. The CKM/PMNS matrices introduced in eqs. (1.3.6, 2.1.1) are only involved in the coupling to the W boson while leaving the rest of the SM Lagrangian unaffected. Since the couplings of the neutral gauge bosons, the Z and the photon, are flavour diagonal, there are no flavour changing neutral currents (FCNC) in the SM at tree-level. This argument does not apply to processes that are generated at loop level, for example $B^+ \to K^+ l^+ l^-$ transitions (see fig. 2.6). Nevertheless, in the SM, there is a suppression of FCNC also at loop level due to the Glashow-Iliopoulos-Maiani (GIM) [115] mechanism. As an example we consider $s \to d$ transitions and summing over the intermediate quarks u, c and t the amplitude is

$$\mathcal{M}(\bar{s}d \to Z) = V_{ud}V_{us}^* f(m_u^2/m_W^2) + V_{cd}V_{cs}^* f(m_c^2/m_W^2) + V_{td}V_{ts}^* f(m_t^2/m_W^2) \ , \qquad (2.2.5)$$

where f is the loop function that keeps track of the dependence on the quark masses via the ratio $x_{q'} = m_{q'}^2/m_W^2$. This dependence is crucial, if all up-quark masses would be equal this function would be factored out which leads to $\mathcal{M} = 0$, since from the unitarity of the CKM matrix, $V_{ud}V_{us}^* + V_{cd}V_{cs}^* + V_{td}V_{ts}^* = 0$. We know that the quark masses are not equal but due to the hierarchy between them we can neglect all quark masses apart from the top mass. In this case $\mathcal{M} \sim V_{td}V_{ts}^* f(m_t^2/m_W^2)$, which is suppressed by the product of the

[10] Recently, deviations in $b \to sll$ and $b \to c\nu l$ observables have been observed [125–131]. The discrepancy to the SM predictions accumulate to $4 - 6\sigma$ [132–137].

small CKM matrix elements V_{td} and V_{ts}. Hence, the suppression of FCNCs in the SM comes from the unitarity relations of the mixing matrix, which allows us to express the amplitude of FCNC processes as the small quark mass differences and mixing parameters. Note that in the case of a non-unitary CKM or PMNS matrix, due to the introduction of new heavy fermions, FCNC are not necessarily suppressed anymore.

Let us now turn to flavour physics beyond the SM. To account for new physics contributions we consider the SM as an effective field theory (EFT) valid up to some scale Λ. All BSM operators will then be suppressed by inverse powers of this scale

$$\mathcal{L} = \mathcal{L}_{SM} + \frac{O^W}{\Lambda} + \sum_i \frac{c_i}{\Lambda^2} O_i + \mathcal{O}\left(\frac{1}{\Lambda^3}\right) \tag{2.2.6}$$

where O^W is the Weinberg operator, the only gauge invariant dimension 5 operator that can be built with the SM fields, already introduced in sec. 2.1.2. In general, these higher dimension operators would induce large effects in processes that are not mediated by tree-level SM amplitudes like FCNC transitions with $\Delta F = 1$ and $\Delta F = 2$. However, up to now we have not observed any deviations from SM predictions. This pushes the scale of new physics above the TeV scale [138]. In the case of K^0-$\overline{K^0}$ mixing, the scale for $\Delta S = 2$ operators is $\Lambda > 10^2$ TeV, assuming $c_i = 1$. The flavour problem states that if we insist that the new physics scale should be around a few TeV, then the possible BSM models should have a non-generic flavour structure. In general one does not expect that a BSM theory follows the same flavour pattern as the SM.

2.2.3. Hierarchy problem

The expectation that the new physics scale Λ should not exceed a few TeV comes from arguments of naturalness. The t'Hooft definition of naturalness [139] states that a physical parameter or set of parameters $\alpha(\mu)$ is allowed to be very small at any energy scale μ, only if the replacement $\alpha(\mu) = 0$ would increase the symmetry of the system.

On the other hand it would also be unnatural if two contributions to a physical parameter cancel to a high accuracy. For example the loop corrections to fermion masses can only be proportional to the masses themselves since in the limit of vanishing mass a chiral symmetry is restored. Fermion masses are hence natural and protected by this symmetry. Similarly, the gauge boson masses are protected. Setting gauge boson masses in a broken gauge theory to zero restores the gauge symmetry. An issue arises when considering the mass of a scalar particle, for example the Higgs boson in the SM. Since the Higgs mass is not protected by any symmetry the loop corrections can be large and proportional to the new physics scale. Hence to obtain the Higgs mass around the electroweak scale the new physics scale also needs to be around the electroweak scale or a large fine tuning between the bare mass parameter and the loop correction needs to be involved. The fact that the Higgs mass is sensitive to the cutoff scale Λ of the SM through loop corrections is known as the hierarchy problem. Chapters 4 and 5 treat new physics models where all new particles are found at the electroweak scale which means they do not lead to a hierarchy problem. Furthermore the introduced dimensionfull parameters are technically natural according to the t'Hooft definition of naturalness. These models also do not contribute to the flavour problem since the new particles couple flavour diagonal.

2.3. Dark Matter

The SM particles described in the previous sections make up only 5% of the energy content of the Universe. The remaining energy is stored in dark energy and dark datter (DM). In this section we will give an overview of the evidence for DM and describe experimental search strategies for it. Although there is a wealth of DM candidates we will focus on heavy DM with mass at the TeV scale.

2.3.1. Experimental evidence

There is plenty of evidence for DM. However, all such evidence comes from gravitational observations, we have not seen any other interactions of DM so far. We will give a short overview of the observations.

2.3.1.1. Kinematical observation

The earliest evidence for DM came from the observation of velocity dispersions of galaxies within clusters. Zwicky noticed [140] that galaxies of the Coma cluster were moving far too quickly to be explained by the gravitational potential of the visible cluster mass only. Using the virial theorem

$$\langle V \rangle = -2\langle T \rangle \ , \tag{2.3.1}$$

which relates the average over the total gravitational potential energy V to the time average over the total kinetic energy T, one obtains as total gravitational mass M_{tot} in the cluster

$$M_{\text{tot}}\bar{v}^2 = \frac{GM_{\text{tot}}^2}{2R} \tag{2.3.2}$$

with the average velocity of the galaxies $\bar{v}$ and the cluster radius R. Comparing the obtained value of M_{tot} to results obtained from observations of luminous matter leads to the conclusion that clusters also must contain a large non-luminous matter component: dark matter. This result has been confirmed also for other galaxy clusters [141].

2.3.1.2. Rotation curves

Observations of the orbital velocity of stars in the outer regions of spiral galaxies show that stars move faster than what would be expected if the galaxies consisted only of the visible matter [142–144]. Using Newtonian mechanics the orbital velocity is

$$v(r) = \sqrt{GM(r)/(2r)} \tag{2.3.3}$$

where $M(r)$ is the mass enclosed at radius r. For large r one expects that $v(r)$ decreases like $r^{-1/2}$ but observations indicate that $v(r) \to$ constant. This means that $M(r) \propto r$. This result can be explained by the existence of a DM halo that is far more extended than the observed galactic disk.

2.3.1.3. Gravitational lesing

Mass acts as a source of spacetime curvature. This curvature of spacetime leads to bending of light rays around massive bodies. In this way light from distant sources passing through the gravitational field of a massive foreground source can be bent towards the observer. The distant source will then appear distorted or stretched depending on the mass distribution of the foreground. Hence from gravitational lensing we obtain information on the mass of the foreground, even if the foreground does not interact electromagnetically.

The most famous example where DM lensing has been used to determine the amount of non-luminous matter is the Bullet Cluster [145]. This object consists of two galaxy clusters that have recently collided (see fig. 2.7). The mass distribution of the clusters has been inferred from lensing observations (shown in blue) whereas the mass distribution of luminous matter has been inferred from X-ray emissions and is shown in pink. The offset between the two distributions indicate that the clusters contains mass which has passed through the collision unimpeded whereas the luminous matter interacts giving X-rays. The gas clouds have exerted friction on each other during the collision and decelerated. This is visible from the observation that the pink areas are closer together than the blue areas. This observation supports that DM does not necessarily track the behaviour of normal matter and that it is essentially collisionless with respect to baryons but also with respect to itself.

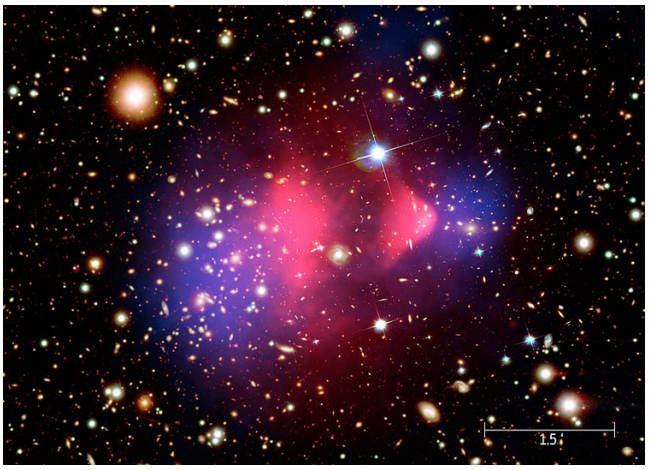

Figure 2.7.: Gravitatonal and X-ray observations of the Bullet cluster mass distributions from [145].

2.3.1.4. Structure formation

Large scale structures like galaxies or clusters of galaxies, superclusters should reflect the history of gravitational clustering of matter since the Big Bang. If DM was present in the early Universe during structure formation it should impact these large scale structures. Large scale N-body simulations show that the observed large-scale structures could only have been formed in the presence of a substantial amount of dark matter [146–150]. These simulations also show that DM needs to be cold and non-dissipative. In this context cold means that DM needs to be non-relativistic and have a short free-streaming length.

2.3.1.5. Cosmic microwave background & baryon acoustic oscillations

DM also left an imprint on the cosmic microwave background (CMB) which has been very precisely measured by the Planck satellite [60]. From the scales of anisotropies in the CMB, cosmological parameters such as the total energy density, the baryonic fraction, and the dark matter abundance can be determined. After a period of exponential expansion of space in the early universe (inflation) the Universe had small overdense regions due to density fluctuations where the DM could gravitationally collapse. The baryons also fall into these dense regions, but since baryons interact with photons, regular matter starts to heat up and provides a pressure to support against the gravitational collapse. This causes an oscillatory "bounce" for overdense regions. At the same time, the Universe expands and cools down. When the recombination temperature, where protons and electrons combine to form Hydrogen, is reached the photons are no longer coupled to matter and can free-stream. Since the CMB is a picture from this recombination, there is a sharp cut-off to the oscillations. The strength and size of these baryon acoustic oscillations are therefore imprinted in the CMB spectrum [151]. The relative amplitudes of the oscillations indicate the ratio of dark matter to regular matter, more baryonic matter means a bigger bounce, more dark matter means more compression. The results show that the energy density of DM is around five times larger than the baryonic energy density [60].

2.3.2. Dark matter characteristics

Although we have plenty of evidence for the existence of DM we know only very little about its nature. We know that DM needs to be massive since we observe its gravitational influence. DM needs to be dark, which means that it should have a very small coupling to photons and it needs to be non-dissipative in order to produce the correct structures in the early Universe. This means that the coupling between ordinary matter and DM needs to be small otherwise energy would be efficiently transferred from DM to the normal matter and radiated away as photons, allowing the DM to form disks along with normal

matter. Thus, DM behaves collisionless with respect to normal matter and the Bullet Cluster observation shows that it does not couple substantially to itself. Finally, DM must be produced with the correct observed relic abundance $\Omega_\chi h^2 = 0.12$ [60] today. This also means that DM must be stable, or at least very long-lived, in order to be still abundant today.

2.3.3. Weakly interacting massive particles

In the following we will describe the DM production mechanism assuming that dark matter is a thermally produced WIMP (weakly interacting massive particle), i.e., a species that was in thermal equilibrium before freezing out and leaving a relic density. In this case the cosmological evolution of the WIMP number density $n_\chi(t)$ can be described by the Boltzman equation

$$\dot{n_\chi} + 3Hn_\chi = -\langle\sigma v\rangle(n_\chi^2 - n_{\chi,\mathrm{eq}}^2) \ . \tag{2.3.4}$$

where H is the Hubble rate and the number density n_χ being given by

$$n_\chi(T) = \int \frac{\mathrm{d}p}{(2\pi)^3} f_\chi(p,T) \ , \tag{2.3.5}$$

and $f_\chi(p,T)$ the DM distribution function. For the equilibrium number density $n_{\chi,\mathrm{eq}}$, f_χ is replaced by the equilibrium distribution function which to a reasonable approximation is the Maxwell-Boltzman distribution

$$n_{\chi,\mathrm{eq}}(T) = g_i \frac{m_\chi^2 T}{2\pi} K_2\left(\frac{m_\chi}{T}\right) \ , \tag{2.3.6}$$

where g_i is the number of internal degrees of freedom, the DM mass m_χ, and K_2 is the modified Bessel function of second kind. The quantity $\langle\sigma v\rangle$ is the thermally averaged pair annihilation cross-section for the process $\chi\chi \to$ SM SM. Freeze-out occurs when the annihilation rate becomes smaller than the expansion rate of the Universe $\Gamma = n_\chi\langle\sigma v\rangle \ll H$. With the yield $Y(t) = n(t)/s$ to eliminate the linear term in eq. (2.3.4) and the new variable $x = m_\chi/T$ eq. (2.3.4) reads

$$\frac{\mathrm{d}Y(x)}{\mathrm{d}x} = -\frac{\lambda}{x^2}(Y^2 - Y_{\mathrm{eq}}^2) \ , \tag{2.3.7}$$

where

$$\lambda(x) \equiv \left[\frac{x\langle\sigma v\rangle s}{H(m)}\right]_{x=1} \ . \tag{2.3.8}$$

With the expression for the entropy s and the Hubble parameter

$$H^2 = \frac{8\pi}{3M_{\mathrm{Pl}}^2}\frac{\pi^2}{30} g_* T^4 \ , \tag{2.3.9}$$

$$s = \frac{2\pi^2}{45} g_{*,s} T^3 \ , \tag{2.3.10}$$

$$\Rightarrow \lambda = \frac{\sqrt{\pi/5}}{3}\frac{g_{*,s}}{\sqrt{g_*}}\langle\sigma v\rangle m_\chi M_{\mathrm{Pl}} \ , \tag{2.3.11}$$

with the active degrees of freedom $g_{*,s}$ in entropy. In general, there is no exact analytical solution to this equation. Figure 2.8 shows an example of a numerical solution. We can estimate the behaviour of Y for the limiting cases $x \gg 1$ and $x \ll 1$. At high temperatures ($x \ll 1$) $\Gamma \sim T\langle\sigma v\rangle$ is much larger than H which means the number density Y remains in thermal equilibrium and follows Y_{eq} because the particles are close enough to interact. Due

to the expansion of the universe the equilibrium number density becomes exponentially suppressed with $\mathrm{e}^{-m_\chi/T}$. At low temperatures, when $x \gg 1$ and $\Gamma \ll H$ the DM particles can no longer find each other fast enough compared to the expansion rate and fall out of equilibrium. The equilibrium abundance becomes exponentially suppressed $n_{\mathrm{eq}} \sim \mathrm{e}^{-x}$ whereas Y is approximately constant. The temperature at which this happens is called the freeze-out temperature x_f. Typically one gets $x_f \sim 20$. After freeze out, Y_{eq} will continue to decrease according to the Boltzman suppression so that $Y \gg Y_{\mathrm{eq}}$. For $x \gg 1$ eq. (2.3.7) is then

$$\frac{\mathrm{d}Y(x)}{\mathrm{d}x} \simeq -\frac{\lambda Y^2}{x^2} \ . \tag{2.3.12}$$

This equation can be integrated from freeze out x_f with freeze-out abundance Y_f until very late times x_∞ with abundance Y_∞. We get

$$Y_\infty = \left(\frac{\lambda}{x_f} + \frac{1}{Y_f}\right)^{-1} \rightarrow Y_\infty = \frac{x_f}{\lambda} \tag{2.3.13}$$

since $\lambda Y_f > x_f$ typically. To obtain the fraction of critical density ρ_{cr} contributed by DM today

$$\Omega_\chi = \frac{\rho_\chi(T_0)}{\rho_{\mathrm{cr}}} \tag{2.3.14}$$

we use

$$\rho_\chi = m_\chi n_\chi(T_0) = m_\chi n_\chi(T_f)\left(\frac{a(T_f)}{a(T_0)}\right) = m_\chi Y_\infty T_f^3 \left(\frac{a(T_f)T_f}{a(T_0)T_0}\right)^3 \ . \tag{2.3.15}$$

From conservation of entropy

$$\left(\frac{a(T_f)T_f}{a(T_0)T_0}\right)^3 = \frac{g_*(T_0)}{g_*(T_f)} \approx 1/30 \tag{2.3.16}$$

with the active degrees of freedom g_* in radiation at different temperatures. With the expression for Y_∞ from eq. (2.3.13) with eq. (2.3.11) the final expression for the relic density is (assuming also $g_{*,s} \approx g_*$)

$$\Omega h^2 = 2.5 \cdot 10^{28} \frac{m_\chi}{T_{\mathrm{dec}}\sqrt{g_*} M_{\mathrm{Pl}}^2 \langle\sigma v\rangle} \ . \tag{2.3.17}$$

If one assumes interaction cross sections of the order of the electroweak one the correct relic density can be obtained for DM roughly around the electroweak scale. This observation is called the WIMP miracle. The reason to call it a miracle is that solutions to the hierarchy problem introduce a neutral $SU(2)_L$ field which can be a DM candidate. There is a rich experimental program targeting this parameter space.

2.3.4. Experimental searches

An extensive experimental program is being conducted to detect DM. There is a large effort, both from the theoretical and experimental side, to exploit and probe the plethora of DM candidates and models. In the following we will give a short summary of the three experimental avenues to search for WIMP DM.

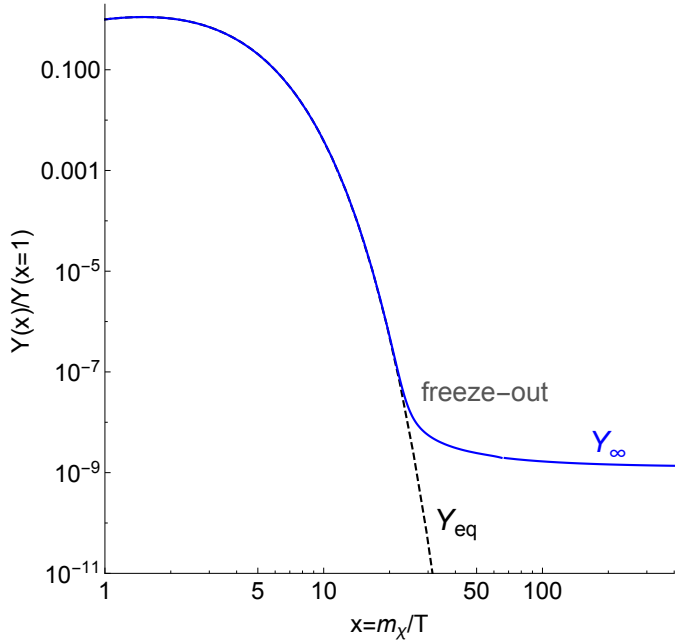

Figure 2.8.: Abundance Y of a WIMP as a function of $x = m_\chi/T$. The dashed line shows the equilibrium abundance. Freeze-out occurs when Y does not follow the equilibrium abundance any more around $x_f \sim 20$.

2.3.4.1. Colliders

Since DM is a stable neutral particle it would manifest itself at colliders as missing energy. However, a missing energy signal is not necessarily associated to a DM particle, also any other stable (on collider-scales) neutral particle could be responsible for such a signal. DM searches are generally based on the observation of the visible counterpart of the event such as charged leptons, jets, or a photon. For example in mono-jet searches events with a jet with a high transverse momentum and large missing energy are selected to suppress the SM background (for recent results by ATLAS and CMS see refs. [152, 153]). If the DM mass is smaller than half of the Higgs mass, constraints from the invisible branching ratio of the Higgs boson apply (BR($H \to$ inv) $< 0.25\%$ at 95% C.L.) [154, 155]. In the same way constraints from the invisible decay width of the Z apply for $m_\chi < m_Z/2$ with $\Gamma(Z \to \text{inv}) < 499 \pm 1.5$ MeV.

2.3.4.2. Indirect detection

The idea behind indirect detection is to search for the products of DM annihilation using Earth based telescopes like HESS [156], CTA [157] or IceCube [158] or satellites like Fermi-LAT [159] or AMS [160]. Experiments constrain the DM annihilation cross section times the DM velocity σv over the DM mass using various annihilation channels.[11] Notice that indirect detection experiments constrain the DM annihilation cross section and the DM velocity whereas, to obtain the correct relic abundance, the thermally averaged cross section times velocity at freeze out temperature is relevant. For example, the gamma ray flux from WIMP annihilation is given by [161]

$$\underbrace{\frac{\mathrm{d}\Phi}{\mathrm{d}E\mathrm{d}\Omega}}_{\text{diff. flux}} = \frac{\sigma v}{8\pi m_\chi^2} \times \underbrace{\frac{\mathrm{d}N}{\mathrm{d}E}}_{\text{energy spectrum}} \times \underbrace{\int_{l.o.s} \mathrm{d}s}_{\text{line of sight integral}} \times \underbrace{\rho^2(\vec{r}(s,\Omega))}_{\text{DM distribution}} \,. \tag{2.3.18}$$

The DM density distribution is not well known and several profiles are considered which lead to more spiked or cored DM densities towards the center of galaxies.

[11] Studied annihilation channels include gamma rays, electrons/positrons, neutrinos or (anti-)protons.

2.3.4.3. Direct detection

Direct detection experiments search for DM scattering off nuclei and hence constrain the DM-nucleus scattering cross section and, from the kinematics of the scattering, the DM mass. The observable in these experiments is the nuclear recoil coming from the scattering of a DM particle. The WIMP-nucleus differential scattering rate is

$$\frac{\mathrm{d}R}{\mathrm{d}E}(E,t) = \frac{N_T \rho_\chi}{m_\chi m_A} \int_{v_{\min}}^{v_{\mathrm{esc}}} v f_E(\vec{v},t) \frac{\mathrm{d}\sigma}{\mathrm{d}E}(v,E)\mathrm{d}\vec{v} \,, \tag{2.3.19}$$

where N_T is the number of target nuclei per kilogram of the detector, ρ_χ the local DM density ($\rho_\chi = 0.3$ GeV/cm^3 [9]), $\vec{v}$ the velocity of the DM particle relative to the Earth, $f_E(\vec{v},t)$ the distribution of velocities of the WIMP in the frame of the Earth. The minimum velocity required to produce a detectable event at energy E is $v_{\min} = \sqrt{m_N E/(2\mu^2)}$ and v_{esc} is the local galactic escape velocity. The DM-nucleus reduced mass is $\mu = m_\chi m_N/(m_\chi + m_N)$ with nucleus mass m_N, $\frac{\mathrm{d}\sigma}{\mathrm{d}E}(v,E)$ is the differential cross section for DM- nucleus scattering. In order to discriminate signal from background the detectors need the best shielding possible (to avoid background signals), a low energy threshold to access low DM masses, and large target mass to increase the scattering rate. Notice that in order to get constraints in the cross section-DM mass plane assumptions on the velocity distribution, nuclear form factor, type of DM-nucleon scattering, and local DM density have been made. In fig. 2.9 we show a compilation of the current bounds on spin-independent and spin-dependent cross sections.

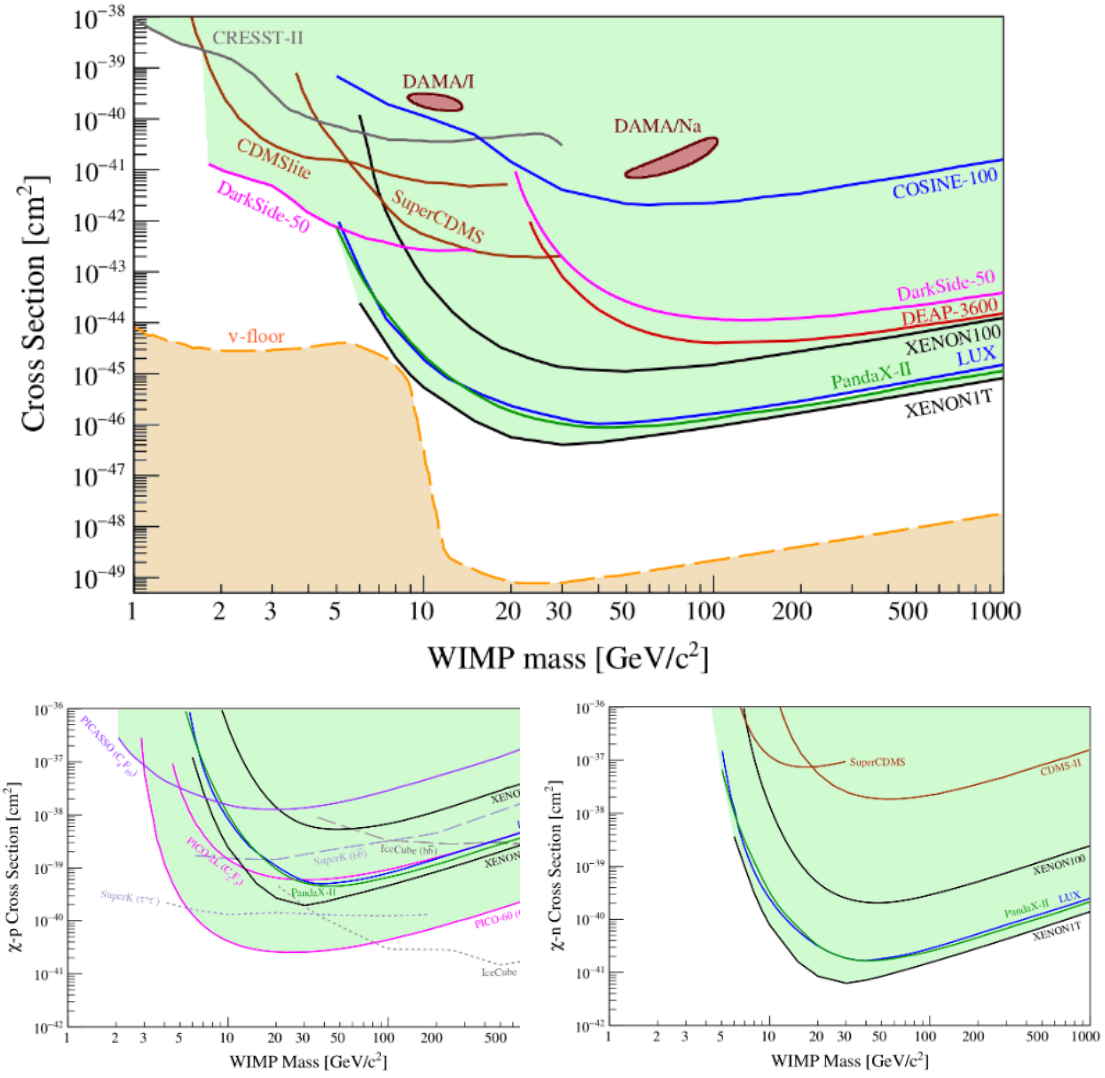

Figure 2.9.: Exclusion upper-limits for spin-independent WIMP-nucleon cross section (upper plot) and spin-dependent WIMP-nucleon cross-section (lower plots) assuming pure proton coupling (left) and pure neutron coupling (right) as of early 2019 from [162].

3. IceCube bounds on sterile neutrinos above 10 eV

3.1. Introduction

Over the last 20 years neutrino oscillations have been established as the explanation of the experimental evidence for neutrino flavour transitions [163,164] with the mixing angles and mass squared differences measured to high accuracy (see Tab. 3.1 for recent global fit results of the mass and mixing parameters). The simplest extension of the Standard Model accommodating neutrino masses is the addition of sterile (right-handed) neutrinos to its content. The mass of these extra singlets, unlike all other fermions, would not be related to the Higgs mechanism and the electroweak scale due to their singlet nature. Therefore, it is vital to probe their existence experimentally at all possible scales.

For instance, short baseline (SBL) experiments like LSND [99] and MiniBOONE [165, 166] as well as reactor experiments combined with a recent reevaluation of their expected fluxes [108, 109] and Gallium source experiments [104, 167, 168] have reported oscillation results that are consistent with a mass squared difference with a possible fourth neutrino mass eigenstate of $\Delta m^2_{41} \approx 1$ eV^2, although this interpretation is in strong tension with other searches [105,113]. With an even higher mass, around the keV scale, sterile neutrinos are a viable dark matter candidate [169, 170] that can be probed via their decay to light neutrinos and X-rays with both stringent constraints [171] and a possible hint at 3.5 keV [172, 173], which could come from the decay of such neutrinos. At larger masses, sterile neutrinos would leave their imprint altering the kinematics of beta decays and meson decays and can also be probed for at beam dump and collider experiments [97,174]. Even when beyond the reach of collider searches, sterile neutrino mixing can be tested indirectly via precision electroweak and flavour observables [68, 98, 175–190].

Through neutrino oscillation data, MINOS [191], IceCube [110], SuperKamiokande [192], MiniBOONE [193], and CDHS [194], among others, have published limits on the sterile mixing parameters for mass squared differences in the range $\Delta m^2_{41} = 0.01 - 10$ eV^2. The impact of sterile neutrino oscillations in this mass range at IceCube has also been previously discussed in refs. [195–197]. These results have been combined to global analyses in refs. [105, 198–201].

In this study we will consider larger sterile mass squared differences and investigate the sensitivity to the mixing of the sterile neutrinos to the μ and τ flavours of the presently released 1 year data, as well as forecasts for 8 years and 20 years, of atmospheric muon neutrino disappearance data at IceCube. In particular, we will study mass squared differences large enough for the sterile-neutrino-driven oscillations to be averaged out at IceCube energies ($\Delta m^2_{41} \gtrsim 100$ eV^2) for atmospheric neutrinos traveling through the Earth

Parameter	best-fit ($\pm 1\sigma$)	3σ range
θ_{12} [°]	$33.63^{+0.78}_{-0.75}$	$31.44 \to 36.07$
θ_{13} [°]	$8.52^{+0.15}_{-0.15} \oplus 8.55^{+0.14}_{-0.14}$	$8.07 \to 8.98$
θ_{23} [°]	$48.7^{+1.4}_{-6.9} \oplus 49.1^{+1.2}_{-1.6}$	$39.3 \to 52.4$
δ [°]	$228^{+51}_{-33} \oplus 281^{+30}_{-33}$	$128 \to 390$
Δm^2_{21} [10^{-5} eV^2]	$7.40^{+0.21}_{-0.20}$	$6.80 \to 8.02$
Δm^2_{31} [10^{-3} eV^2] (NO)	$2.515^{+0.035}_{-0.035}$	$2.408 \to 2.621$
Δm^2_{32} [10^{-3} eV^2] (IO)	$-2.483^{+0.034}_{-0.035}$	$-2.580 \to -2.389$

Table 3.1.: The best-fit values and the 3σ ranges for the mixing and mass parameters taken from ref. [36]. There are two minima for θ_{13}, θ_{23} and δ. The first one corresponds to the normal mass ordering whereas the second one corresponds to the inverted mass ordering. The 3σ ranges are given for either ordering.

($L \lesssim 12000$ km). Such mass squared differences are too big to explain the SBL anomalies but are compatible with the sterile neutrino interpretation [202] of the upward directed cosmic ray shower observed by ANITA [203]. These mixings are however ruled out by cosmological constraints [204] and some non-standard effect suppressing the production of these sterile neutrinos in the early Universe would be necessary to reconcile the results [205]. Our results apply for sterile neutrino masses $\Delta m^2_{41} \gtrsim 100$ eV^2. Note that for sterile masses above 10 MeV stronger bounds on the active-heavy mixing with muon and tau neutrinos are present from laboratory experiments where the sterile neutrino could be detected directly [97].[1]

SuperKamiokande [192] and DeepCore [206] have already published constraints on the sterile mixing parameters in the averaged out regime. It should be noted that the energy threshold of SuperKamiokande is lower than the IceCube one and the averaged out regime for SuperKamiokande therefore starts at smaller mass squared differences ($\Delta m^2_{41} > 10^{-1}$ eV^2). The same parameter space has also been probed by experiments like CHORUS [207] and NOMAD [208] although, instead of analyzing the disappearance of atmospheric ν_μ and the effect of the matter potential from neutral current interactions in presence of steriles, they searched for the appearance of ν_τ in a ν_μ beam through vacuum oscillations. We will compare our results to these current experimental bounds.

This chapter is organized as follows: In section 3.2 we give an overview of the muon neutrino survival probability when the oscillations driven by the new mass eigenvalues are averaged out, in section 4.5 we analyse one year of though-going muon data in IceCube and give forecasts for the 8 years and 20 years sensitivities. Finally, in section 3.4 we summarise our results and give our concluding remarks.

3.2. Sterile neutrino mixing

Upon the addition of several sterile neutrinos, the flavour eigenstates of the weak interactions $|\nu_\alpha\rangle$ ($\alpha = e,\ \mu,\ \tau,\ s_1,\ s_2, ...$) are related to the neutrino mass eigenstates $|\nu_i\rangle$, with masses m_i ($i = 1, 2, 3, 4, 5, ...$) via the elements $U_{\alpha i}$ of the lepton mixing matrix according to

$$|\nu_\alpha\rangle = \sum_i U^*_{\alpha i} |\nu_i\rangle \ . \tag{3.2.1}$$

[1] Electron neutrino-sterile mixing can be constrained for even smaller mass squared differences via kink searches in β spectra of certain isotopes and in neutrinoless double beta decay experiments [97].

In general, the mixing matrix for n neutrino flavours can be decomposed as the product of $n(n-1)/2$ rotations with mixing angles θ_{ij}, with $(n-1)(n-2)/2$ physical phases δ_{ij}. The usual parametrization is through a series of unitary rotations V_{ij} in the i-j-plane given by

$$U = V_{3n}V_{2n}V_{1n}V_{3(n-1)}V_{2(n-1)}V_{1(n-1)}\cdots V_{34}V_{24}V_{14}\underbrace{V_{23}V_{13}V_{12}}_{=U_0}, \tag{3.2.2}$$

with

$$(V_{ij})_{ab} = \begin{cases} \cos(\theta_{ij}), & a = b \in \{i,j\} \\ \sin(\theta_{ij})e^{i\delta_{ij}}, & a = i,\ b = j \\ -\sin(\theta_{ij})e^{-i\delta_{ij}}, & a = j,\ b = i \\ 1, & a = b \notin \{i,j\} \\ 0, & \text{otherwise} \end{cases}, \tag{3.2.3}$$

and where U_0 has the usual PMNS matrix, U_ν, as the upper left 3×3 block. Note that we have not included rotations in the purely sterile sector, e.g., V_{45}, as such rotations are unphysical. Written in this fashion, the full mixing matrix takes the block form

$$U = \mathcal{U}U_0 = \begin{pmatrix} 1-\alpha & \Theta \\ X & Y \end{pmatrix}\begin{pmatrix} U_\nu & 0 \\ 0 & 1 \end{pmatrix} = \begin{pmatrix} (1-\alpha)U_\nu & \Theta \\ XU_\nu & Y \end{pmatrix}. \tag{3.2.4}$$

Here, if the rotations are performed in the order given by Eq. (3.2.2), α is a lower triangular matrix of the form [209–213]

$$\alpha = \begin{pmatrix} \alpha_{ee} & 0 & 0 \\ \alpha_{\mu e} & \alpha_{\mu\mu} & 0 \\ \alpha_{\tau e} & \alpha_{\tau\mu} & \alpha_{\tau\tau} \end{pmatrix}, \tag{3.2.5}$$

whose components to leading order in the active-heavy mixing elements are given by

$$\alpha_{\beta\gamma} \simeq \begin{cases} \frac{1}{2}\sum_{i=4}^{n}|U_{\beta i}|^2, & \beta = \gamma \\ \sum_{i=4}^{n}U_{\beta i}U^*_{\gamma_i}, & \beta > \gamma \\ 0, & \gamma > \beta \end{cases}. \tag{3.2.6}$$

The $\nu_\mu \to \nu_\mu$ oscillation probability, $P_{\mu\mu}$, will here be derived and discussed in the case where the active-heavy mixing angles are small, the corresponding mass squared differences are large enough for the oscillations to average out, and where the electron neutrinos do not participate in the oscillations[2] (i.e., $\Delta m^2_{21}L/2E \ll 1$ and $\theta_{1i} = 0$). We do so by considering a basis that is rotated by $\mathcal{U}$ relative to the flavour basis. In this basis, the neutrino oscillation Hamiltonian in matter takes the form

$$\tilde{H} = \begin{pmatrix} H_0 & 0 \\ 0 & H_1 \end{pmatrix} + V_{\text{NC}}\mathcal{U}^\dagger\begin{pmatrix} 1 & 0 \\ 0 & 0 \end{pmatrix}\mathcal{U}, \tag{3.2.7}$$

where H_0 is the standard Hamiltonian for μ-τ oscillations in vacuum, H_1 is a diagonal matrix containing large entries, and $V_{\text{NC}} = \mp G_F N_n/\sqrt{2}$ (with the upper sign for neutrinos and the lower sign for anti-neutrinos). The upper left 2×2 block describing the ν_μ-ν_τ oscillations (not including the electron neutrino states) can be treated separately, leading to the 2×2 effective Hamiltonian

$$\tilde{H}_0 = H_0 + V_{\text{NC}}(1-\alpha^\dagger)(1-\alpha) \simeq H_0 - V_{\text{NC}}(\alpha + \alpha^\dagger)$$

[2] The oscillation of ν_μ to ν_e at the energies and baselines that characterize the IceCube data are strongly suppressed. Indeed, θ_{13} is small and the solar mass squared difference Δm^2_{21} is too small for the oscillations with θ_{12} to develop. Finally, θ_{14} has been tightly constrained by electron neutrino disappearance experiments [105] and would also play a subleading role.

$$= \frac{\Delta m^2_{31}}{4E}\begin{pmatrix} -\cos(2\theta_{23}) & \sin(2\theta_{23}) \\ \sin(2\theta_{23}) & \cos(2\theta_{23}) \end{pmatrix} - V_{\rm NC}\begin{pmatrix} 2\alpha_{\mu\mu} & \alpha^*_{\tau\mu} \\ \alpha_{\tau\mu} & 2\alpha_{\tau\tau} \end{pmatrix}, \tag{3.2.8}$$

where the $\simeq$ represents equality up to a matrix proportional to unity and to leading order in α. This can be rewritten as

$$\tilde{H}_0 \simeq \frac{\Delta_m}{2}\begin{pmatrix} -\cos(2\theta_m) & \sin(2\theta_m)\lambda^* \\ \sin(2\theta_m)\lambda & \cos(2\theta_m) \end{pmatrix}, \tag{3.2.9}$$

where

$$\begin{aligned} \Delta^2_m &= \left[\frac{\Delta m^2_{31}}{2E}\cos(2\theta_{23}) + 2V_{\rm NC}(\alpha_{\mu\mu} - \alpha_{\tau\tau})\right]^2 + \left|\frac{\Delta m^2_{31}}{2E}\sin(2\theta_{23}) - 2V_{\rm NC}\alpha_{\tau\mu}\right|^2, \\ \sin^2(2\theta_m) &= \frac{1}{\Delta^2_m}\left|\frac{\Delta m^2_{31}}{2E}\sin(2\theta_{23}) - 2V_{\rm NC}\alpha_{\tau\mu}\right|^2, \end{aligned} \tag{3.2.10}$$

and λ is a phase factor of modulus one. Rotating back to the flavour basis, the muon neutrino survival probability is given by

$$P_{\mu\mu} = (1-\alpha_{\mu\mu})^4\left(1 - \sin^2(2\theta_m)\sin^2\left(\frac{\Delta_m L}{2}\right)\right) + \sum_{i=4}^{n}|U_{\mu i}|^4, \tag{3.2.11}$$

where the last term is a constant leaking term [214]. Note that, except for the leaking term, all the sterile neutrino effects are encoded in the matrix α, in particular in the elements $\alpha_{\mu\mu}$, $\alpha_{\tau\tau}$, and $\alpha_{\tau\mu}$, regardless of how many sterile neutrinos are considered as long as they are all in the averaged out regime [213]. However, in our analysis of IceCube data we will allow a free normalization of the events, given the large uncertainties in the atmospheric neutrino fluxes, thus there will be no sensitivity to the normalization factor $(1-\alpha_{\mu\mu})^4$ nor to the leaking term, which does not depend on energy nor baseline.

At leading order in α, and neglecting Δm^2_{31} whose effect is negligible at the energies of the IceCube data sample, the following probability is obtained

$$P_{\mu\mu} \simeq 1 - V^2_{\rm NC}|\alpha_{\tau\mu}|^2 L^2, \tag{3.2.12}$$

where the overall normalization has also been dropped since we allow a free normalization in the analysis. In order to ease the comparison with existing constraints from SuperKamiokande [192] and DeepCore [206] and to make use of the nuSQuIDS software [215, 216] for numerical calculations without approximations, we will now particularize these expressions for the addition of a single sterile neutrino. With our given parametrization, we find that

$$U_{\mu 4} = s_{24}e^{-i\delta_{24}} \quad \text{and} \quad U_{\tau 4} = c_{24}s_{34}, \tag{3.2.13}$$

so that

$$\alpha_{\mu\mu} = 1 - c_{24} \simeq |U_{\mu 4}|^2/2, \quad \alpha_{\tau\tau} = 1 - c_{34} \simeq |U_{\tau 4}|^2/2, \quad \alpha_{\tau\mu} = s_{24}s_{34}e^{i\delta_{24}} \simeq U_{\tau 4}U^*_{\mu 4}, \tag{3.2.14}$$

and thus

$$P_{\mu\mu} \simeq 1 - V^2_{\rm NC}|U_{\tau 4}|^2|U_{\mu 4}|^2 L^2. \tag{3.2.15}$$

Therefore, the bounds will essentially follow a hyperbola in the $|U_{\mu 4}|^2$-$|U_{\tau 4}|^2$-plane.

Note that, in contrast to IceCube, for the SuperKamiokande and DeepCore energies the atmospheric oscillation driven by Δm^2_{31} is relevant. Thus, the approximate Eq. (3.2.15) is not valid and the sensitivity mainly stems from the interference between the standard and sterile oscillations in Eqs. (3.2.10). Therefore, the phase of $\alpha_{\tau\mu}$, i.e., δ_{24} in the one extra sterile neutrino scenario, has an impact on the oscillation probability. Specifically,

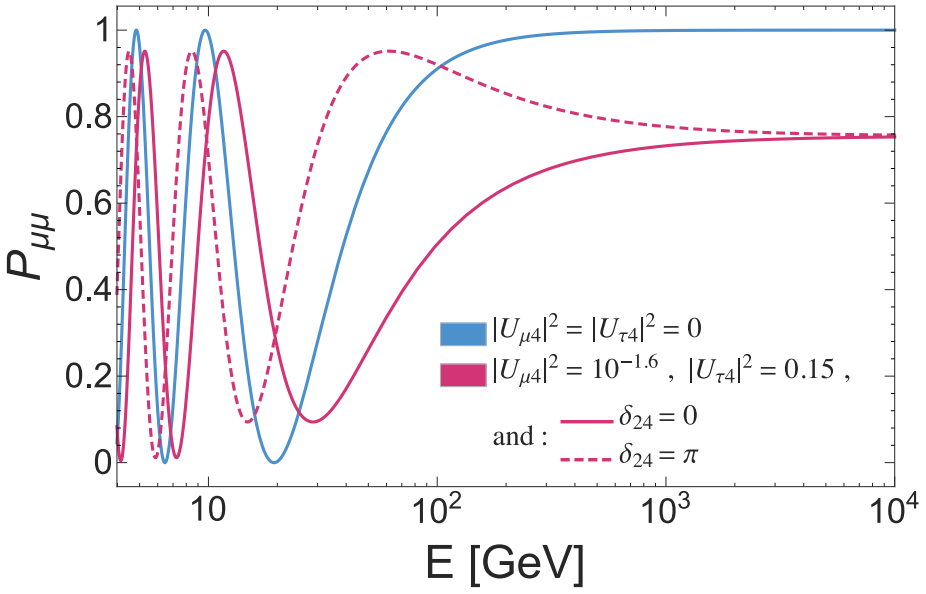

Figure 3.1.: Muon neutrino survival probability using Eq. (3.2.11) as a function of energy. The blue curve shows the oscillation probability without sterile mixing, while the magenta solid (dashed) curve shows the probability for $|U_{\mu 4}|^2 = 10^{-1.6}$, $|U_{\tau 4}|^2 = 0.15$, and $\delta_{24} = 0$ ($\delta_{24} = \pi$). The baseline has been set to the diameter of the Earth.

it can change the sign of the interference term between the atmospheric and the sterile terms in the expression for the energy and the mixing angle in matter. As an example of the impact of the phase, in Figure 3.1 the muon neutrino survival probability as a function of the energy for $|U_{\mu 4}|^2 = 10^{-1.6}$, $|U_{\tau 4}|^2 = 0.15$, $L = 1.2 \times 10^4$ km, and two different values of the phase, $\delta_{24} = 0$ (solid line) and $\delta_{24} = \pi$ (dashed line) is shown. As comparison, the muon neutrino disappearance oscillation probability for zero sterile mixing is also shown. These values of the sterile matrix elements are at the border of the 90% C.L. region of SuperKamiokande. The sign of the interference term can also be changed by changing the mass ordering (i.e., the sign of Δm^2_{31}) or by switching between neutrinos and antineutrinos (i.e., changing the sign of $V_{\rm NC}$). However, neither IceCube nor SuperKamiokande or DeepCore can distinguish between neutrinos and antineutrinos so this dependence is diluted in their data.

Conversely, experiments such as CHORUS and NOMAD explored the same parameter space but instead exploiting the ν_μ to ν_τ appearance channel with negligible matter effects leading to

$$P_{\mu\tau} \simeq 4|U_{\tau 4}|^2|U_{\mu 4}|^2 \sin^2\left(\frac{\Delta m^2_{41} L}{4E}\right). \tag{3.2.16}$$

3.3. Simulation and results

One year of high-energy through-going muons released by the IceCube collaboration [110] for the last IceCube detector stage with 86 strings will be analyzed. The data sample consists of up-going track events so as to avoid the background from cosmic ray muons giving, after all cuts, a sample purity better than 99.9%. Hence, the distances the signal neutrinos travel are of the order of 10^4 km. The selected events have reconstructed energies between 400 GeV and 20 TeV and cosine of the reconstructed zenith angle between -1 and 0.2. The sensitivity that a full 8-year IceCube sample would have as well as the prospects for an exposure equivalent to 20 years of IceCube data will also be forecasted. For our simulations, the neutrino flux computed with the analytic air shower code [217] using the cosmic

ray flux from HondaGaisser model with Gaissser-Hillas H3a correction [218] together with the hadronic model QGSJET II-04 [219] have been adopted. We have also verified that our results do not change significantly under the assumption of different fluxes, such as using the cosmic ray flux from the poly-gonato model [220,221] or the Zatsepin-Sokolskaya [222] model updated with measurements by PAMELA [223] together with the hadronic model SIBYLL2.3, RC1, point-like [224] or QGSJET II-04.

The propagation of the neutrinos was simulated using the nuSQuIDS software [215,216], where the PREM profile [225] is implemented for the Earth matter density. Since we are interested in the averaged out regime our simulations were performed with a sterile mass squared difference of $\Delta m^2_{41} = 10^3$ eV^2, but we have verified that changing this parameter does not alter the results as long as $\Delta m^2_{41} \gtrsim 100$ eV^2 as expected.

Since neutrino and antineutrino interactions cannot be distinguished on an event basis, the signal will contain both ν_μ and $\bar{\nu}_\mu$ events. After propagating the flux for every value of the sterile neutrino parameter, the Monte Carlo provided with the data releas [110] has been used to compute the expected number of events $N_{\mathrm{th},i}$ in every bin of reconstructed zenith angle.

In order to obtain the expected significance of the bounds on the sterile mixing parameters, we adopt a Poisson log-likelihood given by

$$L = -\sum_i \left[N_{\mathrm{th},i} - N_{\mathrm{d},i} + N_{\mathrm{d},i} \log\left(\frac{N_{\mathrm{d},i}}{N_{\mathrm{th},i}}\right)\right] , \tag{3.3.1}$$

where the $N_{\mathrm{th},i}$ and $N_{\mathrm{d},i}$ are the predicted and observed number of events given a set of parameters in bin i, respectively, and the sum is taken over all the reconstructed zenith angle bins i.

The log-likelihood has been maximized for a number of nuisance parameters to include the effect of possible systematic errors. In particular, the uncertainty in the pion-kaon ratio of the initial flux (π/k), the efficiency of the digital optical modules (DOMs), and the overall flux normalization have been considered. Since the observable is energy independent for large values of the sterile neutrino mass (see Eq. (3.2.15)), only one energy bin has been considered and the uncertainty in the energy spectrum slope has been neglected, while 40 bins for the reconstructed zenith angle have been adopted. For the pion-kaon ratio a Gaussian prior with $\sigma_{\pi/k} = 0.05$ has been adopted and no prior for the DOM efficiency or the overall flux normalization has been assumed. The standard oscillation parameters used in the simulations were set to their respective best-fit values from Tab. 3.1. To find the confidence regions from the log-likelihood differences we assume that the prerequisites for Wilks' theorem [226] holds so that likelihood ratios can be directly converted to a confidence level.

In the left panel of Figure 3.2, the 90% C.L. constraints (for 2 degrees of freedom) obtained for the public 1-year data (pink contours) in the $|U_{\mu 4}|^2$-$|U_{\tau 4}|^2$-plane is presented. The existing bounds from SuperKamiokande [192] and DeepCore [206] at the same C.L. are also shown for comparison by the hatched gray area. At 90% C.L. present data prefer some degree of sterile mixing and we find that zero sterile mixing is disfavoured at 2.3σ (1 degree of freedom[3]). The preference for non-zero sterile mixing is independent on the atmospheric sterile neutrino flux adopted in the analysis but its significance varies between 1.6 and 3.0 σ with the different models tested. Given this preference for non-zero sterile mixing, the current constraints from IceCube do not improve upon the combined bounds from SuperKamiokande and DeepCore at 90% C.L. In the right panel, the same information is shown at 99% C.L. In this case, the present 1-year data gives an upper bound that already slightly improves upon the present SuperKamiokande and DeepCore constraints, ruling out the white region in the plot. We have also checked how these results

[3]Note that if $U_{\mu 4} = 0$, the ν_μ survival oscillation probability is insensitive to $U_{\tau 4}$.

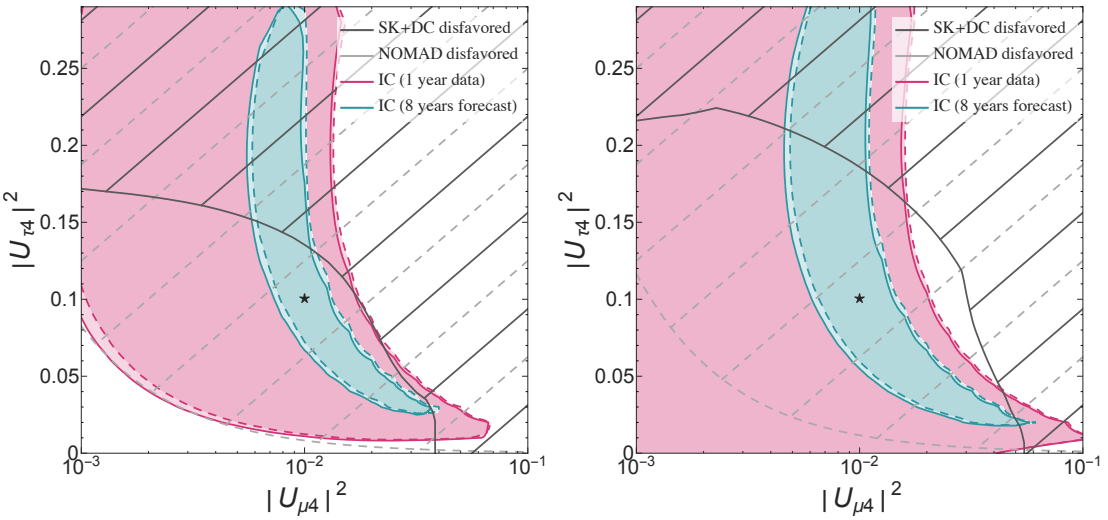

Figure 3.2.: The left (right) panel shows in pink the constraints at 90% (99%) C.L. for the sterile mixing elements from the released 1-year data. The cyan region shows at the same C.L. the forecast for 8 years of IceCube data assuming as true values $|U_{\mu 4}|^2 = 10^{-2}$, $|U_{\tau 4}|^2 = 0.1$, $\delta_{24} = 0$ (marked with a star). The full (dashed) lines show the bounds for $\delta_{24} = 0$ ($\delta_{24} = \pi$). The solid (dashed) hatched regions are disfavoured by SuperKamiokande [192] and DeepCore [206] (NOMAD [208]) data at the same C.L.

depend on the binning in energy and zenith angle. We have seen that when the data is also binned in energy, the case of no active-sterile mixing becomes slightly less disfavoured. Using different combinations of fluxes and binning, the no-mixing scenario is disfavoured at between 0.74 and 3.1 σ, depending on the combination. In particular, for the case of 10 energy bins and 21 bins in the zenith angle, as presented in ref. [110], the significance varies between 0.75 and 3.0 σ.[4]

The physics reach of an 8-year run of IceCube data if the present preference for sterile mixing is maintained is also shown in cyan. In particular, the present best-fit value of $|U_{\mu 4}|^2 = 10^{-2}$, $|U_{\tau 4}|^2 = 0.29$ lies in the already disfavoured region by DeepCore and SuperKamiokande. Due to the hyperbola-shaped degeneracy of the oscillation probability in the $|U_{\mu 4}|^2$-$|U_{\tau 4}|^2$-plane, there are values of the sterile oscillation parameters that provide an almost equally good fit without being in tension with the other ν_μ disappearance present data. Remarkably, theses values of $U_{\tau 4}$ are also compatible with the sterile neutrino interpretation [202] of the upward directed cosmic ray shower observed by ANITA [203]. Indeed, the sterile neutrino interpretation of the ANITA results requires that the sterile neutrino mass is between $\sim 10^2$ and $\sim 10^6$ eV, which would also fall in the averaged out regime for IceCube studied here. However, all the parameter space preferred by IceCube at the 90% C.L. is disfavoured by NOMAD [208] with the same significance. Indeed, the null results in their ν_τ search translates through Eq. (3.2.16) into $|U_{\mu 4}|^2 |U_{\tau 4}|^2 < 8.3 \cdot 10^{-5}$ at the 90% C.L. for $\Delta m^2_{41} \gtrsim 100$ eV^2. Nevertheless, the channel and underlying physics explored to obtain the bounds are very different in the two sets of experiments. While

[4] After this work was submitted to the arXiv, a different analysis [101] did not find any preference for non-zero active-sterile mixing. In particular ref. [101] adopts the same binning as ref. [110] and marginalizes over fluxes. Since in this case we find that no sterile mixing is disfavoured by only $\Delta\chi^2 = 0.56$, the different approaches to the treatment of systematic errors can easily account for the small discrepancy between the two results.

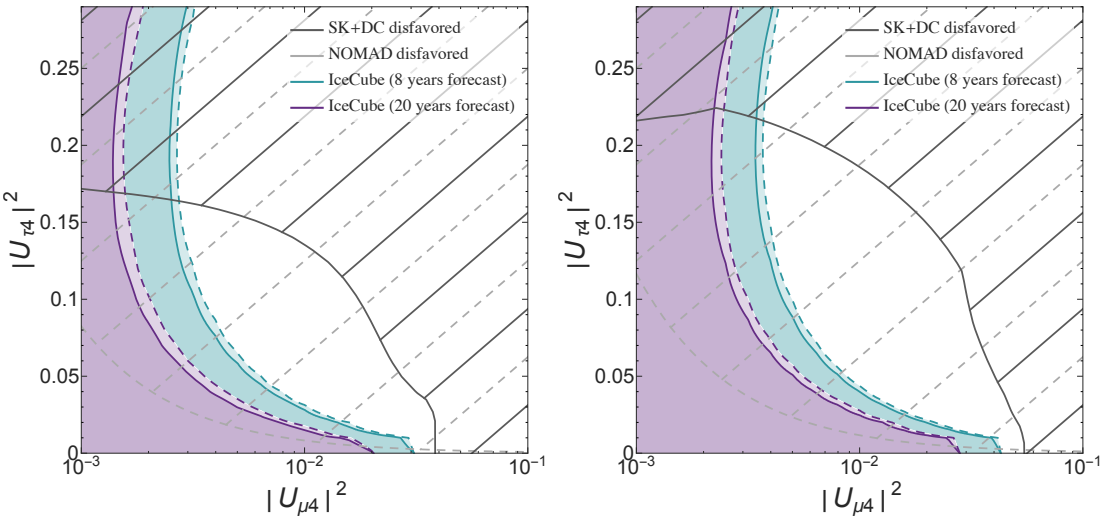

Figure 3.3.: The left (right) panel shows the expected constraints in absence of sterile neutrino mixing at 90% (99%) C.L. for the sterile mixing elements from datasets composed of 8-year (cyan) or 20-year (purple) of IceCube data. The full (dashed) curves show the bounds for $\delta_{24} = 0$ ($\delta_{24} = \pi$). The solid (dashed) gray hatched regions are disfavoured by SuperKamiokande [192] and DeepCore [206] (NOMAD [208]) data at the same C.L.

SuperKamiokande, DeepCore and IceCube analyze ν_μ disappearance and the steriles are probed via their matter effects as shown in Eq. (3.2.15), NOMAD and CHORUS searched for ν_τ appearance essentially in vacuum through Eq. (3.2.16). Thus, in presence of non-standard matter effects (also conceivably in the sterile sector) the two results could still be reconciled if a stronger tension should remain upon including more IceCube data. We therefore simulate 8 years of IceCube data assuming $|U_{\mu 4}|^2 = 10^{-2}$, $|U_{\tau 4}|^2 = 0.1$, and $\delta_{24} = 0$ as the true oscillation parameters. As can be seen in Figure 3.2, the expected confidence region region shrinks significantly with the additional statistics, while keeping its shape. In particular, if the values of the sterile neutrino mixing marked by the star were realized in nature, 8-years of IceCube data would disfavour no sterile mixing around the 5σ level.

The capability of larger IceCube samples to improve the present constraints on sterile mixing in absence of sterile neutrinos have been also studied. In Figure 3.3, the contours for 90% (left panel) and 99% C.L. (right panel) expected exclusion limits in the $|U_{\mu 4}|^2$-$|U_{\tau 4}|^2$-plane together with the existing bounds from SuperKamiokande and DeepCore are presented. The bound on $|U_{\mu 4}|^2$ from 8 years of IceCube would improve over present constraints between a factor 1.3 for vanishing values of $|U_{\tau 4}|^2$ to around an order of magnitude for $|U_{\tau 4}|^2$ close to 0.1. Similarly, for $|U_{\mu 4}|^2 \sim 10^{-2}$, the constraint on $|U_{\tau 4}|^2$ would improve around a factor 5. In particular, the present best fit for non-zero sterile mixing would be excluded at high significance (more than 5σ) and most of the currently preferred parameter space at 90% C.L. (pink area in the left panel of Figure 3.2) disfavoured. Comparatively, increasing the statistics up to 20-year of IceCube data yields a more modest improvement in sensitivity. Remarkably, not even the 20-year scenario would improve over the present NOMAD limit of $|U_{\mu 4}|^2 |U_{\tau 4}|^2 < 8.3 \cdot 10^{-5}$ at the 90% C.L. Nevertheless, we consider the two constraints complementary given the different physics probed by each of them.

The effect of the CP-violating phase δ_{24} is also shown. In particular, the solid lines correspond to $\delta_{24} = 0$ and the dashed lines to $\delta_{24} = \pi$. As can be seen, IceCube is not very

sensitive to the sterile phase as oscillations due to the atmospheric mass squared difference at energies above 100 GeV do not have time to develop. Indeed, from Figure 3.1 the ν_μ survival probability is essentially 1 in absence of sterile mixing for $E > 100$ GeV.

3.4. Summary and conclusions

In this chapter we have presented the current constraints from the public 1-year IceCube data as well as the expectations of a full 8-year dataset and forecasts for 20 years worth of statistics to the mixing of sterile neutrinos with the μ and τ flavours. In particular, we concentrated for the first time on larger masses for the extra neutrinos ($\Delta m^2 > 100$ eV^2) than usually explored so that their oscillations are averaged out at IceCube. We find that the public 1-year IceCube data presents some preference for non-zero sterile mixing in the averaged out regime that would manifest via neutral-current-induced matter effects in the ν_μ disappearance channel. In particular, values of the squared sterile mixing with the μ flavour of order 10^{-2} and with the τ between 10^{-1} and 10^{-2} are favoured at around 2σ with respect to no sterile mixing when no binning in energy and 40 bins in zenith angle are adopted. These mixings are however in strong tension with cosmological constraints [204] and some non-standard effect suppressing the production of these sterile neutrinos in the early Universe would be necessary to reconcile these results [205]. Moreover, these mixings are also in tension with present data from CHORUS [207] and NOMAD [208] which, however, explore a different channel without matter effects. Thus, in presence of non-standard matter effects the two results could be potentially reconciled.

We have also studied the sensitivity that 8 years of IceCube data, close to the data that should be presently available, would have and find that it would be sufficient to either confirm the present preference or exclude it with high significance (more than 5σ) and set stringent constraints improving around an order of magnitude over SuperKamiokande and DeepCore present bounds in some parts of the parameter space. Since sterile neutrinos at some mass scale are a general expectation of many extensions of the SM accounting for neutrino masses, it will be very interesting to explore this part of the parameter space with averaged out sterile neutrino oscillations using the full data sample collected by IceCube.

4. Dark Matter and the elusive Z′ in the Dynamical Inverse Seesaw scenario

4.1. Introduction

The simplest and most popular mechanism to accommodate the evidence for neutrino masses and mixings [36, 227–231] and to naturally explain their extreme smallness, calls upon the introduction of right-handed neutrinos through the celebrated Seesaw mechanism [63–65, 67, 68, 232]. Its appeal stems from the simplicity of its particle content, consisting only of the right-handed neutrinos otherwise conspicuously missing from the Standard Model (SM) ingredients. In the Seesaw mechanism, the smallness of neutrino masses is explained through the ratio of their Dirac masses and the Majorana mass term of the extra fermion singlets. Unfortunately, this very same ratio suppresses any phenomenological probe of the existence of this mechanism. Indeed, either the right-handed neutrino masses would be too large to be reached by our highest energy colliders, or the Dirac masses, and hence the Yukawa interactions that mediate the right-handed neutrino phenomenology, would be too small for even our more accurate precision probes through flavour and precision electroweak observables.

However, a large hierarchy of scales is not the only possibility to naturally explain the smallness of neutrino masses. Indeed, neutrino masses are protected by the $B-L$ (Baryon minus Lepton number) global symmetry, otherwise exact in the SM. Thus, if this symmetry is only mildly broken, neutrino masses will be necessarily suppressed by the small $B-L$-breaking parameters. Conversely, the production and detection of the extra right-handed neutrinos at colliders as well as their indirect effects in flavour and precision electroweak observables are not protected by the $B-L$ symmetry and therefore not necessarily suppressed, leading to a much richer and interesting phenomenology. This is the rationale behind the popular Inverse Seesaw Mechanism [74] (ISS) as well as the Linear [76, 233] and Double Seesaw [74, 77–79] variants.

In the presence of right-handed neutrinos, $B-L$ is the only flavour-universal SM quantum number that is not anomalous, besides hypercharge. Therefore, just like the addition of right-handed neutrinos, a very natural plausible SM extension is the gauging of this symmetry. In this work these two elements are combined to explore a possible dynamical origin of the ISS pattern from the spontaneous breaking of the gauged $B-L$ symmetry.

Previous models in the literature have been constructed using the ISS idea or gauging $B-L$ to explain the smallness of the neutrino masses, see e.g. [234–239]. A minimal model in which the ISS is realised dynamically and where the smallness of the Lepton Number Violating (LNV) term is generated at the two-loop level was studied in [240]. Concerning

$U(1)_{B-L}$ extensions of the SM with an ISS generation of neutrino masses, several models have been investigated [241–244]. A common origin of both sterile neutrinos and Dark Matter (DM) has been proposed in [245, 246]. An ISS model which incorporates a keV sterile neutrino as a DM candidate was constructed in e.g. [247]. Neutrino masses break $B-L$, if this symmetry is not gauged and dynamically broken, a massless Goldstone boson, the Majoron, appears in the spectrum. Such models have been investigated for example in [245, 248].

Interestingly, since the ISS mechanism requires a chiral pattern in the neutrino sector, the gauging of $B-L$ predicts the existence of extra fermion singlets with non-trivial charges so as to cancel the anomalies. We find that these extra states may play the role of DM candidates as thermally produced Weakly Interacting Massive Particles (WIMPs) (see for instance [249, 250] for a review).

Indeed, the extra states would form a *dark sector*, only connected to the SM via the Z' gauge boson associated to the $B-L$ symmetry and, more indirectly, through the mixing of the scalar responsible for the spontaneous symmetry breaking of $B-L$ with the Higgs boson. For the simplest charge assignment, this dark sector would be constituted by one heavy Dirac and one massless Weyl fermion with large $B-L$ charges. These large charges make the Z' couple preferentially to the dark sector rather than to the SM, making it particularly *elusive*. In this work the phenomenology associated with this dark sector and the elusive Z' is investigated. We find that the heavy Dirac fermion of the dark sector can be a viable DM candidate with its relic abundance mediated by the elusive Z'. Conversely, the massless Weyl fermion can be probed through measurements of the relativistic degrees of freedom in the early Universe. The collider phenomenology of the elusive Z' is also investigated and the LHC bounds are derived.

The chapter is structured as follows. In Sec. 4.2 we describe the features of the model, namely its Lagrangian and particle content. In Sec. 4.3 we analyse the phenomenology of the DM candidate and its viability. The collider phenomenology of the Z' boson is discussed in Sec. 4.4. Finally, in Secs. 4.5 and 4.6 we summarise our results and conclude.

4.2. The model

The usual ISS model consists of the addition of a pair of right-handed SM singlet fermions (right-handed neutrinos) for each massive active neutrino [74, 251–253]. These extra fermion copies, say N_R and N'_R, carry a global Lepton Number (LN) of $+1$ and -1, respectively, and this leads to the following mass Lagrangian

$$-\mathcal{L}_{\rm ISS} = \bar{L} Y_\nu \widetilde{H} N_R + \overline{N_R^c} M_N N'_R + \overline{N'^c_R} \mu\, N'_R + \text{h.c.}, \tag{4.2.1}$$

where Y_ν is the neutrino Yukawa coupling matrix, $\widetilde{H} = i\sigma_2 H^*$ (H being the SM Higgs doublet) and L is the SM lepton doublet. Moreover, M_N is a LN conserving matrix, while the mass matrix μ breaks LN explicitly by 2 units.

The right-handed neutrinos can be integrated out, leading to the Weinberg operator [62] which generates masses for the light, active neutrinos of the form:

$$m_\nu \sim v^2 Y_\nu M_N^{-1} \mu (M_N^T)^{-1} Y_\nu^T. \tag{4.2.2}$$

Having TeV-scale right-handed neutrinos (e.g. motivated by naturalness [254, 255]) and $\mathcal{O}(1)$ Yukawa couplings would require $\mu \sim \mathcal{O}(\text{ keV})$. In the original ISS formulation [74], the smallness of this LNV parameter arises from a superstring inspired E6 scenario. Alternative explanations call upon other extensions of the SM such as Supersymmetry and Grand Unified Theories (see for instance [76, 256]). Here a dynamical origin for μ will be instead explored. The μ parameter is technically natural: since it is the only parameter that breaks LN, its running is multiplicative and thus once chosen to be small, it will remain small at all energy scales.

To promote the LN breaking parameter μ in the ISS scenario to a dynamical quantity, we choose to gauge the $B-L$ number [257]. The spontaneous breaking of this symmetry will convey LN breaking, generate neutrino masses via a scalar vev, and give rise to a massive vector boson, dubbed here Z'. $B-L$ is an accidental symmetry of the SM, and it is well motivated in theories in which quarks and leptons are unified [258–261]. In unified theories, the chiral anomalies cancel within each family, provided that SM fermion singlets with charge +1 are included. In the usual ISS framework, this is not the case due to the presence of right-handed neutrinos with charges +1 and −1. The triangle anomalies that do not cancel are those involving three $U(1)_{B-L}$ vertices, as well as one $U(1)_{B-L}$ vertex and gravity. Therefore, to achieve anomaly cancellation for gauged $B-L$ we have to include additional chiral content to the model with charges that satisfy

$$\sum Q_i = 0 \Rightarrow \sum Q_{iL} - \sum Q_{iR} = 0, \tag{4.2.3}$$

$$\sum Q_i^3 = 0 \Rightarrow \sum Q_{iL}^3 - \sum Q_{iR}^3 = 0, \tag{4.2.4}$$

where the first and second equation refer to the mixed gravity-$U(1)_{B-L}$ and $U(1)_{B-L}^3$ anomalies, respectively. The index i runs through all fermions of the model.

In the following subsections we will discuss the fermion and the scalar sectors of the model in more detail.

4.2.1. The fermion sector

Besides the anomaly constraint, the ISS mechanism can only work with a certain number of N_R and N'_R fields (see, e.g., Ref. [262]). We find a phenomenologically interesting and viable scenario which consists of the following copies of SM fermion singlets and their respective $B-L$ charges: 3 N_R with charge −1; 3 N'_R with charge +1; 1 χ_R with charge +5; 1 χ_L with charge +4 and 1 ω with charge +4[1] Some of these right-handed neutrinos allow for a mass term, namely, $M_N \overline{N_R^c} N'_R$, but to lift the mass of the other sterile fermions and to generate SM neutrino masses, two extra scalars are introduced. Thus, besides the Higgs doublet H, the scalar fields ϕ_1 with $B-L$ charge +1 and ϕ_2 with charge +2 are considered. The SM leptons have $B-L$ charge −1, while the quarks have charge 1/3. The scalar and fermion content of the model, related to neutrino mass generation, is summarised in Table 4.1. The most general Lagrangian in the neutrino sector is then given by[2]

$$-\mathcal{L}_\nu = \bar{L} Y_\nu \widetilde{H} N_R + \overline{N_R^c} M_N N'_R + \phi_2 \overline{N_R^c} Y_N N_R + \phi_2^* \overline{(N'_R)^c}\, Y'_N N'_R + \phi_1^* \overline{\chi_L}\, Y_\chi \chi_R + \text{h.c.}, \tag{4.2.5}$$

where the capitalised variables are to be understood as matrices (the indices were omitted).

The singlet fermion spectrum splits into two parts, an ISS sector composed by ν_L, N_R, and N'_R, and a dark sector with χ_L and χ_R, as can be seen in the following mass matrix written in the basis $(\nu_L^c, N_R, N'_R, \chi_L^c, \chi_R)$:

$$M = \left(\begin{array}{ccc|cc} 0 & Y_\nu \widetilde{H} & 0 & 0 & 0 \\ Y_\nu^T \widetilde{H}^\dagger & Y_N \phi_2 & M_N & 0 & 0 \\ 0 & M_N^T & Y'_N \phi_2^* & 0 & 0 \\ \hline 0 & 0 & 0 & 0 & Y_\chi \phi_1^* \\ 0 & 0 & 0 & Y_\chi^T \phi_1 & 0 \end{array}\right). \tag{4.2.6}$$

[1] Introducing 2 N_R and 3 N'_R as for example in [247] leads to a keV sterile neutrino as a potentially interesting warm DM candidate [263] in the spectrum due to the mismatch between the number of N_R and N'_R. However, the relic abundance of this sterile neutrino, if thermally produced via freeze out, is an order of magnitude too large. Thus, in order to avoid its thermalisation, very small Yukawa couplings and mixings must be adopted instead.

[2] Notice that a coupling $\phi_1^* \overline{\omega} Y_\omega \chi_R$, while allowed, can always be reabsorbed into $\phi_1^* \overline{\chi_L} Y_\chi \chi_R$ through a rotation between ω and χ_L.

Particle	ϕ_1	ϕ_2	ν_L	N_R	N'_R	χ_R	χ_L	ω
$U(1)_{B-L}$ charge	+1	+2	−1	−1	+1	+5	+4	+4
Multiplicity	1	1	3	3	3	1	1	1

Table 4.1.: Neutral fermions and singlet scalars with their $U(1)_{B-L}$ charge and their multiplicity. $\phi_{1,2}$ are SM singlet scalars while N_R, N'_R and χ_R are right-handed and χ_L and ω are left-handed SM singlet fermions respectively.

The dynamical equivalent of the μ parameter can be identified with $Y'_N\phi_2^{*3}$. After ϕ_1 develops a vacuum expectation value (vev) a Dirac fermion $\chi = (\chi_L, \chi_R)$ and a massless fermion ω are formed in the dark sector. Although the cosmological impact of this extra relativistic degree of freedom may seem worrisome at first, we will show later that the contribution to N_{eff} is suppressed as this sector is well secluded from the SM.

To recover a TeV-scale ISS scenario with the correct neutrino masses and $\mathcal{O}(1)$ Yukawa couplings, $v_2 \equiv \phi_2 \sim$ keV $\ll v$ (where $v = H = 246$ GeV is the electroweak vev) and $M_R \sim$ TeV are needed. Moreover, the mass of the $B-L$ gauge boson will be linked to the vevs of ϕ_1 and ϕ_2, and hence to lift its mass above the electroweak scale will require $v_1 \equiv \phi_1 \gtrsim$ TeV. In particular, we will show that a triple scalar coupling $\eta\phi_1^2\phi_2^*$ can induce a small v_2 even when v_1 is large, similar to what occurs in the type-II seesaw [68–71, 264]. After the spontaneous symmetry breaking, the particle spectrum would then consist of a $B-L$ gauge boson, 3 pseudo-Dirac neutrino pairs and a Dirac dark fermion at the TeV scale, as well as a massless dark fermion. The SM neutrinos would in turn develop small masses via the ISS in the usual way. Interestingly, both dark fermions only interact with the SM via the new gauge boson Z' and via the suppressed mixing of ϕ_1 with the Higgs. They are also stable and thus the heavy dark fermion is a natural WIMP DM candidate. Since all new fermions carry $B-L$ charge, they all couple to the Z', but specially the ones in the dark sector which have larger $B-L$ charge.

4.2.2. The scalar sector

The scalar potential of the model can be written as

$$V = \frac{m_H^2}{2}H^\dagger H + \frac{\lambda_H}{2}(H^\dagger H)^2 + \frac{m_1^2}{2}\phi_1^*\phi_1 + \frac{m_2^2}{2}\phi_2^*\phi_2 + \frac{\lambda_1}{2}(\phi_1^*\phi_1)^2 + \frac{\lambda_2}{2}(\phi_2^*\phi_2)^2 + \frac{\lambda_{12}}{2}(\phi_1^*\phi_1)(\phi_2^*\phi_2) + \frac{\lambda_{1H}}{2}(\phi_1^*\phi_1)(H^\dagger H) + \frac{\lambda_{2H}}{2}(\phi_2^*\phi_2)(H^\dagger H) - \eta(\phi_1^2\phi_2^* + \phi_1^{*2}\phi_2). \tag{4.2.7}$$

Both m_H^2 and m_1^2 are negative, but m_2^2 is positive and large. Then, for suitable values of the quartic couplings, the vev of ϕ_2, v_2, is only induced by the vev of ϕ_1, v_1, through η and thus it can be made small. With the convention $\phi_j = (v_j + \varphi_j + i\,a_j)/\sqrt{2}$ and the neutral component of the complex Higgs field given by $H^0 = (v + h + iG_Z)/\sqrt{2}$ (where G_Z is the Goldstone associated with the Z boson mass), the minimisation of the potential yields

$$m_H^2 = -\frac{1}{2}\left(\lambda_{1H}v_1^2 + \lambda_{2H}v_2^2 + 2\lambda_H v^2\right) \simeq -\frac{1}{2}\left(\lambda_{1H}v_1^2 + 2\lambda_H v^2\right), \tag{4.2.8}$$

$$m_1^2 = -\frac{1}{2}\left(2\lambda_1 v_1^2 + \lambda_{1H}v^2 - 4\sqrt{2}\eta v_2 + \lambda_{12}v_2^2\right) \simeq -\frac{1}{2}\left(2\lambda_1 v_1^2 + \lambda_{1H}v^2\right), \tag{4.2.9}$$

$$m_2^2 = \left(\frac{\sqrt{2}\eta}{v_2} - \frac{\lambda_{12}}{2}\right)v_1^2 - \lambda_2 v_2^2 - \frac{\lambda_{2H}}{2}v^2 \simeq \frac{\sqrt{2}\eta v_1^2}{v_2}, \tag{4.2.10}$$

or, equivalently,

$$v_2 \simeq \frac{\sqrt{2}\eta v_1^2}{m_2^2}\,. \tag{4.2.11}$$

[3] The analogous term $Y_N\phi_2$ - also dynamically generated - contributes to neutrino masses only at the one-loop level and is therefore typically sub-leading.

Clearly, when $\eta \to 0$ or $m_2^2 \to \infty$, the vev of ϕ_2 goes to zero. For example, to obtain $v_2 \sim \mathcal{O}(\text{ keV})$, one could have $m_2 \sim 10$ TeV, $v_1 \sim 10$ TeV, and $\eta \sim 10^{-5}$ GeV. The neutral scalar mass matrix is then given by

$$M_0^2 \simeq \begin{pmatrix} \lambda_H v^2 & \lambda_{1H} v_1 v/2 & 0 \\ \lambda_{1H} v_1 v/2 & \lambda_1 v_1^2 & -\sqrt{2}\eta v_1 \\ 0 & -\sqrt{2}\eta v_1 & \eta v_1^2/\sqrt{2} v_2 \end{pmatrix}. \tag{4.2.12}$$

Higgs data constrain the mixing angle between $\text{Re}(H^0)$ and $\text{Re}(\phi_1^0)$ to be below $\sim 30\%$ [265]. Moreover, since $\eta \ll m_2, v_1$, the mixing between the new scalars is also small. Thus, the masses of the physical scalars h, φ_1 and φ_2 are approximately

$$m_h^2 = \lambda_H v^2, \quad m_{\varphi_1}^2 = \lambda_1 v_1^2, \quad \text{and} \quad m_{\varphi_2}^2 = m_2^2/2, \tag{4.2.13}$$

while the mixing angles α_1 and α_2 between $h - \varphi_1$ and $\varphi_1 - \varphi_2$, respectively, are

$$\tan\alpha_1 \simeq \frac{\lambda_{1H}}{\lambda_1}\frac{v}{2v_1}, \quad \text{and} \quad \tan\alpha_2 \simeq 2\frac{v_2}{v_1}. \tag{4.2.14}$$

If $v_1 \sim$ TeV and the quartics λ_1 and λ_{1H} are $\mathcal{O}(1)$, the mixing α_1 is expected to be small but non-negligible. A mixing between the Higgs doublet and a scalar singlet can only diminish the Higgs couplings to SM particles. Concretely, the couplings of the Higgs to gauge bosons and fermions, relative to the SM couplings, are

$$\kappa_F = \kappa_V = \cos\alpha_1, \tag{4.2.15}$$

which is constrained to be $\cos\alpha_1 > 0.92$ (or equivalently $\sin\alpha_1 < 0.39$) [266]. Since the massless fermion does not couple to any scalar, and all other extra particles in the model are heavy, the modifications to the SM Higgs couplings are the only phenomenological impact of the model on Higgs physics. The other mixing angle, α_2, is very small since it is proportional to the LN breaking vev and thus is related to neutrino masses. Its presence will induce a mixing between the Higgs and φ_2, but for the parameters of interest here it is unobservable.
Besides Higgs physics, the direct production of φ_1 at LHC via its mixing with the Higgs would be possible if it is light enough. Otherwise, loop effects that would change the W mass bound can also test this scenario imposing $\sin\alpha_1 \lesssim 0.2$ for $m_{\varphi_1} = 800$ GeV [265].

Apart from that, the only physical pseudoscalar degree of freedom is

$$A = \frac{1}{\sqrt{v_1^2 + 4v_2^2}}\left[2v_2 a_1 - v_1 a_2\right] \tag{4.2.16}$$

and its mass is degenerate with the heavy scalar mass, $m_A \simeq m_{\varphi_2}$.

We have built this model in `SARAH` 4.9 [267–270]. This Mathematica package produces the model files for `SPheno` 3.3.8 [271, 272] and `CalcHep` [273] which are then used to study the DM phenomenology with `Micromegas` 4.3 [274]. We have used these packages to compute the results presented in the following sections. Moreover, we will present analytical estimations to further interpret the numerical results.

4.3. Dark matter phenomenology

As discussed in the previous section, in this dynamical realisation of the ISS mechanism we have two stable fermions. One of them is a Dirac fermion, $\chi = (\chi_L, \chi_R)$, which acquires a mass from ϕ_1, and therefore is manifest at the TeV scale. The other, ω, is massless and will contribute to the number of relativistic species in the early Universe. First we analyse if χ can yield the observed DM abundance of the Universe.

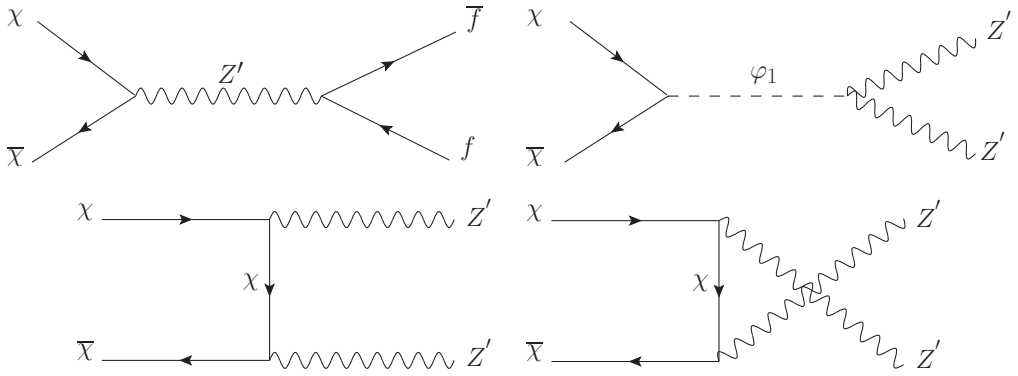

Figure 4.1.: DM annihilation channels $\chi\bar{\chi} \to f\bar{f}$ via the Z' boson and $\chi\bar{\chi} \to Z'Z'$. The $\chi\bar{\chi} \to Z'Z'$ channel opens up when $M_{Z'}^2 < m_\chi^2$. Since the process $\chi\bar{\chi} \to \varphi_1 \to Z'Z'$ is velocity suppressed this diagram is typically subleading.

4.3.1. Relic density

In the early Universe, χ is in thermal equilibrium with the plasma due to its gauge interaction with Z'. The relevant part of the Lagrangian is

$$\mathcal{L}_{DM} = -g_{\rm BL}\bar{\chi}\gamma^\mu(5P_R + 4P_L)\chi Z'_\mu + \frac{1}{2}M_{Z'}^2 Z'_\mu Z'^\mu - m_\chi\bar{\chi}\chi, \tag{4.3.1}$$

where

$$M_{Z'} = g_{\rm BL}\sqrt{v_1^2 + 4v_2^2} \simeq g_{\rm BL}v_1, \quad \text{and} \quad m_\chi = Y_\chi v_1/\sqrt{2}, \tag{4.3.2}$$

and $P_{R,L}$ are the chirality projectors.

The main annihilation channels of χ are $\chi\bar{\chi} \to f\bar{f}$ via the Z' boson exchange and $\chi\bar{\chi} \to Z'Z'$ - if kinematically allowed (see fig. 4.1).

The annihilation cross section to a fermion species f, at leading order in v, reads:

$$\sigma {\rm v}_{f\bar{f}} \simeq n_c(q_{\chi_L} + q_{\chi_R})^2 \, \frac{q_{f_L}^2 + q_{f_R}^2}{8\pi} \frac{g_{\rm BL}^4 m_\chi^2}{(4m_\chi^2 - M_{Z'}^2)^2 + \Gamma_{Z'}^2 M_{Z'}^2} + \mathcal{O}\left(v^2\right), \tag{4.3.3}$$

see e.g. [275, 276], where n_c is the color factor of the final state fermion (=1 for leptons), $q_{\chi_L} = 4$ and $q_{\chi_R} = 5$ and $q_{f_{L,R}}$ are the $B - L$ charges of the left- and right-handed components of the DM candidate χ and of the fermion f, respectively. Moreover, the partial decay width of the Z' into a pair of fermions (including the DM, for which $f = \chi$) is given by

$$\Gamma_{Z'}^{f\bar{f}} = n_c \, g_{\rm BL}^2 \frac{\left(6q_{f_L}q_{f_R}m_f^2 + \left(q_{f_L}^2 + q_{f_R}^2\right)\left(M_{Z'}^2 - m_f^2\right)\right)\sqrt{M_{Z'}^2 - 4m_f^2}}{24\pi M_{Z'}^2}. \tag{4.3.4}$$

When $M_{Z'}^2 < m_\chi^2$, the annihilation channel $\chi\bar{\chi} \to Z'Z'$ is also available. The cross section for this process (lower diagrams in fig. 4.1) is given by (to leading order in the relative velocity) [275]

$$\begin{aligned}\sigma {\rm v}_{Z'Z'} \simeq \frac{1}{256\pi m_\chi^2 M_{Z'}^2}&\left(1 - \frac{M_{Z'}^2}{m_\chi^2}\right)^{3/2}\left(1 - \frac{M_{Z'}^2}{2m_\chi^2}\right)^{-2} \\ &\left(8g_{\rm BL}^4(q_{\chi R} + q_{\chi L})^2(q_{\chi R} - q_{\chi L})^2 m_\chi^2 + \left((q_{\chi R} - q_{\chi L})^4 + (q_{\chi R} + q_{\chi L})^4\right.\right. \\ &\left.\left. -6(q_{\chi R} - q_{\chi L})^2(q_{\chi R} + q_{\chi L})^2\right) g_{\rm BL}^4 M_{Z'}^2\right),\end{aligned} \tag{4.3.5}$$

The $\chi\bar{\chi} \to \varphi_1 \to Z'Z'$ (upper right diagram in fig. 4.1) channel is velocity suppressed and hence typically subleading. Further decay channels like $\chi\bar{\chi} \to \varphi_1\varphi_1$ and $\chi\bar{\chi} \to Z'\varphi_1$ open when $2m_\chi > m_{\varphi_1} + m_{\varphi_1}(m_{\varphi_1} + m_{Z'})$. With $m_\chi = Y_\chi/\sqrt{2}v_1$, $m_{\varphi_1} = \sqrt{\lambda_1}v_1$, $m_{Z'} = g_{\rm BL}v_1$ and the additional constraint from perturbativity $Y_\chi \leq 1$ we get only small kinematically allowed regions which play a subleading role for the relic abundance. The cross section for the annihilation channel $\chi\bar{\chi} \to Z'h^0$ is also subleading due to the mixing angle α_1 between $\varphi_1 - h^0$ which is small although non-negligible (cf. Eq. (4.2.14)).

The relic density of χ has been computed numerically with `Micromegas` obtaining also, for several points of the parameter space, the DM freeze-out temperature at which the annihilation rate becomes smaller than the Hubble rate $\sigma{\rm v}n_\chi \lesssim H$. Given the freeze-out temperature and the annihilation cross sections of Eqs. (4.3.3) and (4.3.5), the DM relic density can thus be estimated by [277]:

$$\Omega_\chi h^2 = \frac{2.5 \cdot 10^{28} m_\chi}{T_\chi^{\rm f.o.} M_{Pl}^2 \sqrt{g_\star}\sigma{\rm v}}, \tag{4.3.6}$$

where $g_\star$ is the number of degrees of freedom in radiation at the temperature of freeze-out of the DM ($T_\chi^{\rm f.o.}$), σv is its thermally averaged annihilation cross section and $M_{Pl} = 1.2 \cdot 10^{19}$ GeV is the Planck mass. In Sec. 4.5 we will use this estimation of $\Omega_\chi h^2$ together with its constraint $\Omega_\chi h^2 \simeq 0.1186 \pm 0.0020$ [81, 278] to explore the regions of the parameter space for which the correct DM relic abundance is obtained.

4.3.2. Direct Detection

The same Z' couplings that contribute to the relic abundance can give rise to signals in DM direct detection experiments. The DM-SM interactions in the model via the Z' are either vector-vector or axial-vector interactions. Indeed, the Z'- SM interactions are vectorial (with the exception of the couplings to neutrinos) while χ has different left- and right-handed charges. The axial-vector interaction does not lead to a signal in direct detection and the vector-vector interaction leads to a spin-independent cross section [279].

The cross section for coherent elastic scattering on a nucleon is

$$\sigma_\chi^{\rm DD} = \frac{\mu_{\chi{\rm N}}^2}{\pi}\left(\frac{9}{2}\frac{g_{\rm BL}^2}{M_{Z'}^2}\right)^2 \tag{4.3.7}$$

where $\mu_{\chi{\rm N}}$ is the reduced mass of the DM-nucleon system. The strongest bounds on the spin-independent scattering cross section come from LUX [280] and XENON1T [281]. The constraint on the DM-nucleon scattering cross section is $\sigma_\chi^{\rm DD} < 10^{-9}$ pb for $m_\chi = 1$ TeV and $\sigma_\chi^{\rm DD} < 10^{-8}$ pb for $m_\chi = 10$ TeV. The experimental bound on the spin-independent cross section (Eq. (4.3.7)) allows to derive a lower bound on the vev of ϕ_1:

$$v_1\ [\text{GeV}] > \left(\frac{2.2 \cdot 10^9}{\sigma_\chi^{\rm DD}\ [\text{pb}]}\right)^{1/4}. \tag{4.3.8}$$

This bound pushes the DM mass to be $m_\chi \gtrsim$ TeV. For instance, for $g_{\rm BL} = 0.25$ and $m_{Z'} = 10$ TeV, a DM mass $m_\chi = 3.8$ TeV is required to have $\sigma_\chi^{\rm DD} \sim 9 \times 10^{-10}$ pb. In turn, this bound translates into a lower limit on the vev of ϕ_1: $v_1 \gtrsim 40$ TeV (with $Y_\chi \gtrsim 0.1$). Next generation experiments such as XENON1T [282] and LZ [283] are expected to improve the current bounds by an order of magnitude and could test the parameter space of this model, as it will be discussed in Sec. 4.5.

4.3.3. Indirect Detection

In full generality, the annihilation of χ today could lead also to indirect detection signatures, in the form of charged cosmic rays, neutrinos and gamma rays. However, since the main annihilation channel of χ is via the Z' which couples dominantly to the dark sector, the bounds from indirect detection searches turn out to be subdominant.

The strongest experimental bounds come from gamma rays produced through direct emission from the annihilation of χ into $\tau^+\tau^-$. Both the constraints from the Fermi-LAT Space Telescope (6-year observation of gamma rays from dwarf spheroidal galaxies) [159] and H.E.S.S. (10-year observation of gamma rays from the Galactic Center) [156] are not very stringent for the range of DM masses considered here. Indeed, the current experimental bounds on the velocity-weighted annihilation cross section $< \sigma v > (\chi\bar{\chi} \to \tau^+\tau^-)$ range from 10^{-25} cm^{3}s^{-1} to 10^{-22} cm^{3}s^{-1} for DM masses between 1 and 10 TeV. These values are more than two orders of magnitude above the values obtained for the regions of the parameter space in which we obtain the correct relic abundance (notice that the branching ratio of the DM annihilation to χ into $\tau^+\tau^-$ is only about 5%). Future experiments like CTA [157] could be suited to sensitively address DM masses in the range of interest of this model ($m_\chi \gtrsim 1$ TeV).

4.3.4. Effective number of neutrino species, $N_{\rm eff}$

The presence of the massless fermion ω implies a contribution to the number of relativistic degrees of freedom in the early Universe. In the following, we discuss its contribution to the effective number of neutrino species, $N_{\rm eff}$, which has been measured to be $N_{\rm eff}^{exp} = 3.04 \pm 0.33$ [81]. Since the massless ω only interacts with the SM via the Z', its contribution to $N_{\rm eff}$ will be washed out through entropy injection to the thermal bath by the number of relativistic degrees of freedom $g_\star(T)$ at the time of its decoupling:

$$\Delta N_{\rm eff} = \left(\frac{T_\omega^{\rm f.o.}}{T_\nu}\right)^4 = \left(\frac{11}{2g_\star(T_\omega^{\rm f.o.})}\right)^{4/3} , \tag{4.3.9}$$

where $T_\omega^{\rm f.o.}$ is the freeze-out temperature of ω and T_ν is the temperature of the neutrino background. The freeze-out temperature can be estimated when the Hubble expansion rate of the Universe $H = 1.66\sqrt{g_\star}T^2/M_{Pl}$ overcomes the ω interaction rate $\Gamma =< \sigma v > n_\omega$ leading to:

$$(T_\omega^{\rm f.o.})^3 \sim \frac{2.16\sqrt{g_\star}M_{Z'}^4}{M_{Pl}g_{\rm BL}^4 \sum_f (q_{f_L}^2 + q_{f_R}^2)} . \tag{4.3.10}$$

With the typical values that satisfy the correct DM relic abundance: $m_{Z'} \sim \mathcal{O}(10$ TeV) and $g_{\rm BL} \sim \mathcal{O}(0.1)$ ω would therefore freeze out at $T_\omega^{\rm f.o.} \sim 4$ GeV, before the QCD phase transition. Thus, the SM bath will heat significantly after ω decouples and the contribution of the latter to the number of degrees of freedom in radiation will be suppressed:

$$\Delta N_{\rm eff} \approx 0.026 \tag{4.3.11}$$

which is one order of magnitude smaller than the current uncertainty on $N_{\rm eff}$. For gauge boson masses between 1-50 TeV and gauge couplings between 0.01 and 0.5, $\Delta N_{\rm eff} \in [0.02, 0.04]$. Nevertheless, this deviation from $N_{\rm eff}$ matches the sensitivity expected from a EUCLID-like survey [284, 285] and would be an interesting probe of the model in the future.

4.4. Collider phenomenology

The new gauge boson can lead to resonant signals at the LHC. Dissimilarly from the widely studied case of a sequential Z' boson, where the new boson decays dominantly to dijets, the elusive Z' couples more strongly to leptons than to quarks (due to the $B-L$ number). Furthermore, it has large couplings to the SM singlets, specially χ and ω which carry large $B-L$ charges. Thus, typical branching ratios are ∼70% invisible (i.e. into SM

neutrinos and ω), $\sim$12% to quarks and $\sim$18% to charged leptons.[4] LHC $Z' \to e^+e^-, \mu^+\mu^-$ resonant searches [286, 287] can be easily recast into constraints on the elusive Z'. The production cross section times branching ratio to dileptons is given by

$$\sigma(pp \to Z' \to \ell\bar{\ell}) = \sum_q \frac{C_{qq}}{sM_{Z'}} \Gamma(Z' \to q\bar{q}) \mathrm{BR}(Z' \to \ell\bar{\ell}), \tag{4.4.1}$$

where s is the center of mass energy, $\Gamma(Z' \to q\bar{q})$ is the partial width to $q\bar{q}$ pair given by Eq. (4.3.4), and C_{qq} is the $q\bar{q}$ luminosity function obtained here using the parton distribution function MSTW2008NLO [288]. To have some insight on what to expect, we compare our Z' with the usual sequential standard model (SSM) Z', in which all couplings to fermions are equal to the Z couplings. The dominant production mode is again $q\bar{q} \to Z'$ though the coupling in our case is mostly vectorial. The main dissimilarity arrives from the branching ratio to dileptons, as there are many additional fermions charged under the new gauge group. In summary, only $\mathcal{O}(1)$ differences in the gauge coupling bounds are expected, between the SSM Z' and our elusive Z'.

4.5. Results

We now combine in fig. 4.2 the constraints coming from DM relic abundance, DM direct detection experiments and collider searches. We can clearly see the synergy between these different observables. Since the DM candidate in our model is a thermal WIMP, the relic abundance constraint puts a lower bound on the gauge coupling, excluding the blue shaded region in the panels of fig. 4.2. On the other hand, LHC resonant searches essentially put a lower bound on the mass of the Z' (red shaded region), while the LUX direct detection experiment constrains the product $g_{\mathrm{BL}} \cdot M_{Z'}$ from above (orange shaded region). For reference, we also show the prospects for future direct detection experiments, namely, XENON1T (orange short-dashed line, projected sensitivity assuming $2t \cdot y$) and LZ (orange long-dashed line, projected sensitivity for 1000d of data taking). Finally, if the gauge coupling is too large, perturbativity will be lost. To estimate this region we adopt the constraint $g_{\mathrm{BL}} \cdot q_{\max} \leq \sqrt{2\pi}$ and being the largest $B - L$ charge $q_{\max} = 5$, we obtain $g_{\mathrm{BL}} > 0.5$ for the non-perturbative region. The white region in these panels represents the allowed region. We present four different DM masses so as to exemplify the dependence on m_χ. First, we see that for DM masses at 1 TeV (upper left panel), there is only a tiny allowed region in which the relic abundance is set via resonant $\chi\bar{\chi} \to Z' \to f\bar{f}$ annihilation. For larger masses, the allowed region grows but some amount of enhancement is in any case needed so that the Z' mass needs to be around twice the DM mass in order to obtain the correct relic abundance. For m_χ above 20 TeV (lower right panel), the allowed parameter space cannot be fully probed even with generation-2 DM direct detection experiments.

On top of the DM and collider phenomenology discussed here, this model allows for a rich phenomenology in other sectors. In full analogy to the standard ISS model, the dynamical ISS mechanism here considered is also capable of generating a large CP asymmetry in the lepton sector at the TeV scale, thus allowing for a possible explanation of the baryon asymmetry of the Universe via *leptogenesis* [289–292].
Moreover, the heavy sterile states typically introduced in ISS scenarios, namely the three pseudo-Dirac pairs from the states N_R and $N_R^{'}$ can lead to new contributions to a wide array of observables [68,175–185,188–190,293–302] such as weak universality, lepton flavour violating or precision electroweak observables, which allow to constrain the mixing of the SM neutrinos with the extra heavy pseudo-Dirac pairs to the level of 10^{-2} or even better for some elements [98, 187].

[4] If the decay channels to the other SM singlets are kinematically accessible, specially into χ and into the N_R, N_R' pseudo-Dirac pairs, the invisible branching ratio can go up to $\sim 87\%$, making the Z' even more elusive and rendering these collider constraints irrelevant with respect to direct DM searches.

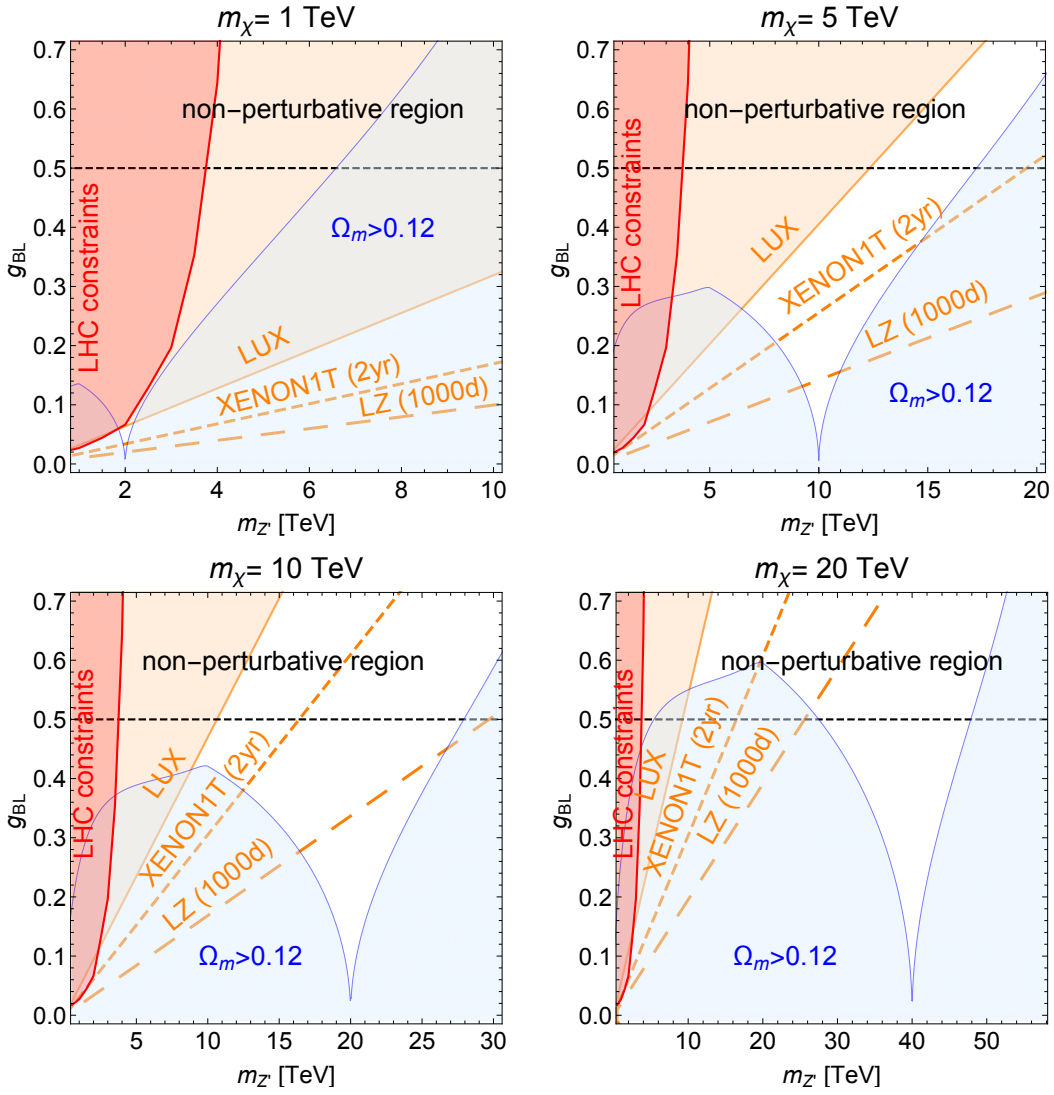

Figure 4.2.: Summary plots of our results. The red region to the left is excluded by LHC constraints on the Z' (see text for details), the region above $g_{\rm BL} > 0.5$ is non-perturbative due to $g_{\rm BL} \cdot q_{\rm max} \leq \sqrt{2\pi}$. In the blue shaded region DM is overabundant. The orange coloured region is already excluded by direct detection constraints from LUX [280], the short-dashed line indicates the future constraints from XENON1T [282] (projected sensitivity assuming $2t \cdot y$), the long-dashed line the future constraints from LZ [283] (projected sensitivity for 1000d of data taking).

4.6. Conclusions

The simplest extension to the SM particle content so as to accommodate the experimental evidence for neutrino masses and mixings is the addition of right-handed neutrinos, making the neutrino sector more symmetric to its charged lepton and quark counterparts. In this context, the popular Seesaw mechanism also gives a rationale for the extreme smallness of these neutrino masses as compared to the rest of the SM fermions through a hierarchy between two different energy scales: the electroweak scale – at which Dirac neutrino masses are induced – and a much larger energy scale tantalizingly close to the Grand Unification scale at which Lepton Number is explicitly broken by the Majorana mass of the right-handed neutrinos. On the other hand, this very natural option to explain the smallness of neutrino masses automatically makes the mass of the Higgs extremely unnatural, given the hierarchy problem that is hence introduced between the electroweak scale and the heavy Seesaw scale.

The ISS mechanism provides an elegant solution to this tension by lowering the Seesaw scale close to the electroweak scale, thus avoiding the Higgs hierarchy problem altogether. In the ISS the smallness of neutrino masses is thus not explained by a strong hierarchy between these scales but rather by a symmetry argument. Since neutrino masses are protected by the Lepton Number symmetry, or rather $B-L$ in its non-anomalous version, if this symmetry is only mildly broken, neutrino masses will be naturally suppressed by the small parameters breaking this symmetry. In this work, the possibility of breaking this gauged symmetry dynamically has been explored.

Since the ISS mechanism requires a chiral structure of the extra right-handed neutrinos under the $B-L$ symmetry, some extra states are predicted for this symmetry to be gauged due to anomaly cancellation. The minimal such extension requires the addition of three new fields with large non-trivial $B-L$ charges. Upon the spontaneous breaking of the $B-L$ symmetry, two of these extra fields become a massive heavy fermion around the TeV scale while the third remains massless. Given their large charges, the Z' gauge boson mediating the $B-L$ symmetry couples preferentially to this new *dark sector* and much more weakly to the SM leptons and particularly to quarks, making it rather *elusive*.

The phenomenology of this new dark sector and the elusive Z' has been investigated. We find that the heavy Dirac fermion is a viable DM candidate in some regions of the parameter space. While the elusive nature of the heavy Z' makes its search rather challenging at the LHC, it would also mediate spin-independent direct detection cross sections for the DM candidate, which place very stringent constraints in the scenario. Given its preference to couple to the dark sector and its suppressed couplings to quarks, the strong tension between direct detection searches and the correct relic abundance for Z' mediated DM is mildly alleviated and some parts of the parameter space, not far from the resonance, survive present constraints. Future DM searches by XENON1T and LZ will be able to constrain this possibility even further. Finally, the massless dark fermion will contribute to the amount of relativistic degrees of freedom in the early Universe. While its contribution to the effective number of neutrinos is too small to be constrained with present data, future EUCLID-like surveys could reach a sensitivity close to their expected contribution, making this alternative probe a promising complementary way to test this scenario.

5. Natural and Dynamical Neutrino Mass Mechanism at the LHC

5.1. Introduction

The presence of non-zero neutrino masses, as inferred by neutrino oscillation experiments, is the only laboratory-based evidence of physics beyond the standard model [163, 164]. Strictly speaking, neutrinos have no mass in the standard model (SM). There is no unique prescription of how neutrino could become massive. Perhaps the simplest way of generating neutrino masses is via the seesaw framework. In its naïve realizations, seesaw types I, II and III [64, 65, 67, 68, 70, 71, 74], a large suppression of the electroweak breaking scale provides an explanation for the smallness of neutrino masses. Without a full underlying framework, like Grand Unified Theories or Supersymmetry, these mechanisms typically introduce a hierarchy problem due to the large mass gap [255] or rely on very small (but technically natural [139]) parameters.

In general, the seesaw mechanism generates a small parameter from the ratio of two disparate physics scales, e.g., electroweak versus Grand Unification scales. Therefore, when we set the new heavy states to the weak scale (such as done in studies of type II seesaw at colliders [303, 304]), the "seesaw" mechanism is exchanged by a small parameter. This can be appreciated in a model independent way by writing down schematically the Weinberg effective operator that generates neutrino masses [62], namely

$$\mathcal{L}_5 = \frac{c}{\Lambda} LLHH \tag{5.1.1}$$

(H and L are the Higgs and lepton doublets) and observing that if $\Lambda \sim \langle H \rangle$ then the Wilson coefficient c needs to be tiny in order to obtain sub-electronvolt neutrino masses. We will show in this Letter that a simple generalization of the type II seesaw can dynamically generate this small parameter by replacing the seesaw by a chain of seesaws.

More concretely, in type II seesaw a scalar triplet

$$\Delta = \begin{pmatrix} \delta^+/\sqrt{2} & \delta^{++} \\ (v_\Delta + \delta + i a_\delta)/\sqrt{2} & -\delta^+/\sqrt{2} \end{pmatrix} \tag{5.1.2}$$

obtains its vacuum expectation value (vev) after electroweak symmetry breaking

$$v_\Delta \simeq \frac{\mu}{\sqrt{2}} \frac{v^2}{M_\Delta^2}, \tag{5.1.3}$$

where μ is a dimensionful lepton number breaking parameter of the scalar potential, $v = 246$ GeV is the Higgs doublet vev, and M_Δ is approximately the physical mass of Δ. Neutrino masses are given by $m_\nu = \sqrt{2} Y v_\Delta$, with Y being a matrix of Yukawa couplings.

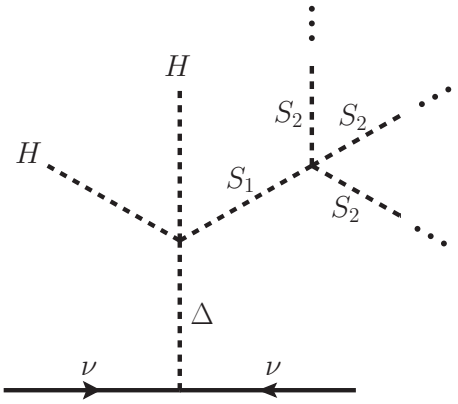

Figure 5.1.: Illustration of the generalized type II seesaw mechanism for neutrino mass generation.

We can immediately see that the smallness of neutrino masses can only be obtained by having small Yukawas, large M_Δ, and/or small ad hoc lepton number breaking parameter μ. For instance, if M_Δ is accessible at the LHC, say at the TeV scale, and the Yukawas are taken to be of order 1, we obtain

$$\mu \simeq 1.6 \text{ eV } \left(\frac{m_\nu}{0.1 \text{ eV}}\right). \tag{5.1.4}$$

Since $\mu = 0$ restores a symmetry of the Lagrangian, it is not generated by other couplings due to quantum corrections, thus being technically natural in the t'Hooft sense [139]. Nevertheless, it is unappealing to have this enormous hierarchy of scales $\mu/v \lesssim \mathcal{O}(10^{-11})$ put in arbitrarily. As suggested by the considerations made before regarding the Weinberg operator, this is not exclusive to type II seesaw.

In this Letter we present a generalization of the type II seesaw scenario which dynamically generates a very low lepton number breaking scale from a small hierarchy. The model is naturally found at the weak scale, introducing no new fine-tuning neither arbitrarily small couplings. Our mechanism engenders a rich and vast phenomenology, including deviations of SM Higgs couplings, the presence of a massless Majoron, lepton flavor violation and a smoking gun signature at the LHC which allows to distinguish this model from the usual type II seesaw.

5.2. The mechanism

The idea simply amounts to replicate the induced vev suppression mechanism with additional scalar singlets, as shown in Fig. 5.1. In our concrete setup, all mass parameters are near the electroweak scale and all dimensionless couplings are of similar order, thus yielding a natural model of neutrino masses accessible at the LHC. We will focus on a scenario with two extra scalar singlets, as this is the most minimal realization that successfully implements the mechanism and also exhibits all important phenomenological features of our framework.

First we require dynamical lepton number breaking. To that end, we promote $U(1)_\ell$ lepton number to a global symmetry in which leptons have charge $\ell_{\text{leptons}} = +1/2$ (the normalization has been chosen for convenience) and quarks have no charge. The neutrino Yukawa coupling

$$\mathcal{L}^\nu_{\text{Yuk}} = -Y(L^c)^T i\sigma_2 \Delta\, L + \text{h. c.} \tag{5.2.1}$$

(σ_2 is the second Pauli matrix, Y is a matrix of Yukawa couplings in flavor space, and ^{c} denotes charge conjugation) requires $\ell_\Delta = -1$, forbidding the triple coupling $\mu H^T i\sigma_2 \Delta^\dagger H$. We introduce the first complex SM singlet scalar S_1 with lepton number $\ell_1 = +1$ so its

vev may play the role of the lepton number violating parameter μ. Then, we generalize the type II seesaw model by invoking another extra scalar singlet with charge $\ell_2 = 1/3$, allowing for a term $S_1^* S_2^3$ in the scalar potential. All scalars but the Higgs and S_2 have positive bare mass terms.The crucial point is that when S_2 develops a vev spontaneously, it induces a suppressed vev for S_1, which then induces an even smaller vev for Δ. The model can easily be generalized for any number N of scalar singlets, see Appendix A.1. We identify the usual type II seesaw with a $N = 1$-step version of the generalized model in which S_1 is integrated out. Our model bears similarities with multiple seesaw and clockwork models (see, for instance, Refs. [305–313]).

As we will see later, a simple 2-step realization can lead to small neutrino masses given that some quartic couplings and neutrino Yukawas are of order $10^{-2} \sim 10^{-3}$ (larger couplings can be obtained in realizations with extra steps). Without further ado, we write down the scalar potential

$$\begin{aligned} V = & -\frac{m_H^2}{2}H + m_\Delta^2\Delta + m_1^2 S_1 - \frac{m_2^2}{2}S_2 + \frac{\lambda_H}{4}(H)^2 + \frac{\lambda_2}{4}(S_2)^2 \\ & + \lambda_{1H}(S_1)(H) + \lambda_{2H}(S_2)(H) + \left[\lambda_A H^T i\sigma_2 \Delta^\dagger H S_1^* - \frac{2}{3}\lambda'_{12} S_1^* S_2^3 + \text{h. c.}\right] \\ & \left.\begin{aligned} & + \frac{\lambda_\Delta}{4}\Delta^2 + \frac{\lambda'_\Delta}{4}\Delta\Delta + \frac{\lambda_1}{4}(S_1)^2 + \lambda_{12}(S_1)(S_2) \\ & + \lambda_{H\Delta}(H)\Delta + \lambda'_{H\Delta} H^\dagger \Delta\Delta^\dagger H + \lambda_{1\Delta}\Delta(S_1) + \lambda_{2\Delta}\Delta(S_2), \end{aligned}\right\} \text{“incidental” terms} \end{aligned} \tag{5.2.2}$$

where the parameters more relevant for the mechanism and the phenomenology are in the first two lines. Although the quartic couplings on the third and fourth lines are important for the stability of the potential, they play almost no role otherwise (thus called “incidental”). The stability of the potential is not a primary concern of this manuscript, but it is important to note that the quartic couplings λ_A and λ'_{12} tend to destabilize the potential, and hence are expected to be small. For more considerations regarding stability see Appendix A.2. We define the neutral components of the fields as $H^0 = (v+h+ia)/\sqrt{2}$, $\Delta^0 = (v_\Delta + \delta + ia_\delta)/\sqrt{2}$ and $S_j = (v_j + s_j + ia_j)/\sqrt{2}$, for $j = 1, 2$.

The positive mass terms for Δ and S_1 ensure that if $\lambda_A = \lambda'_{12} = 0$ then the vevs for these fields are zero. Notice that these two quartic couplings are protected from loop corrections by accidental global $U(1)$ symmetries. Moreover, λ_A and λ'_{12} can be made real by rephasing the scalar singlet fields. As long as v_Δ and v_1 are much smaller than v and v_2, we can obtain the former vevs by treating H and S_2 as background fields. First we obtain the approximate vevs of H and S_2 by setting the other scalar fields to zero, that is,

$$m_H^2 = \frac{1}{2}\lambda_H v^2 + \lambda_{2H} v_2^2, \qquad m_2^2 = \frac{1}{2}\lambda_2 v_2^2 + \lambda_{2H} v^2. \tag{5.2.3}$$

Then, by replacing H and S_2 by their vevs, we can easily calculate the vevs and the spectrum of the other scalars:

$$v_1 = \frac{\lambda'_{12} v_2^3}{3M_1^2}, \qquad v_\Delta = \frac{\lambda_A v^2 v_1}{2M_\Delta^2}, \tag{5.2.4}$$

and

$$M_h^2 = \frac{1}{2}\lambda_H v^2, \tag{5.2.5a}$$

$$M_1^2 = m_1^2 + \frac{1}{2}(\lambda_{1H} v^2 + \lambda_{12} v_2^2), \tag{5.2.5b}$$

$$M_2^2 = \frac{1}{2}\lambda_2 v_2^2, \tag{5.2.5c}$$

$$M_\Delta^2 = m_\Delta^2 + \frac{1}{2}\left[\lambda_{2\Delta} v_2^2 + (\lambda_{H\Delta} + \lambda'_{H\Delta})v^2\right]. \tag{5.2.5d}$$

Mixing	Phenomenology
$h - s_2$	Higgs observables, direct s_2 production
$\delta - s_1$	New LHC signatures, s_1 decay modes
$h - s_1$	s_1 decay modes
$s_1 - s_2$	Irrelevant

Table 5.1.: Sizable scalar mixings and their phenomenological impact.

The physical masses of the scalars are approximately given by the M's in Eqs. (5.2.5a-5.2.5d). Here we see the mechanism at work: λ'_{12} induces a suppression from v_2 to v_1, and λ_A induces a further suppression from v_1 to v_Δ. It is useful to write these quartics in terms of the scalar masses and vevs,

$$\lambda_A = 0.008 \left(\frac{M_\Delta}{500\ \text{GeV}}\right)^2 \left(\frac{v_\Delta/\ \text{keV}}{v_1/\ \text{MeV}}\right), \tag{5.2.6a}$$

$$\lambda'_{12} = 0.03\, \frac{(M_1/100\ \text{GeV})^2 (v_1/\ \text{MeV})}{(v_2/10\ \text{GeV})^3}. \tag{5.2.6b}$$

Note that these relations do not depend on the number of steps, as long as the perturbation theory holds.

5.3. Spectrum and mixing phenomenology

The scalar spectrum of this 2-step scenario consists of the 4 aforementioned neutral scalars (h, δ, s_1, s_2), singly and doubly charged scalars δ^+ and δ^{++}, with masses approximately given by M_Δ, two massive pseudoscalar degrees of freedom (a_δ, a_1) with masses approximately given by M_Δ and M_1, and two massless Goldstone bosons. One of the Goldstones is the longitudinal polarization of the Z boson while the other one is a massless Majoron, J [314–316]. We will analyze the Majoron phenomenology in the following section.

The mixings among the CP even scalars will have important phenomenological impacts (see Table 5.1 for a summary). The mixings between $h - s_2$, $\delta - s_1$ and $h - s_1$ are given by

$$\theta_{h2} \simeq \frac{\lambda_{2H}\, v_2\, v}{M_h^2 - M_2^2} \simeq 0.16 \lambda_{2H} \left(\frac{v_2}{10\ \text{GeV}}\right) \beta_{h2}, \tag{5.3.1a}$$

$$\theta_{\delta 1} \simeq \frac{\lambda_A}{2} \frac{v^2}{M_1^2 - M_\Delta^2} \simeq 10^{-3} \left(\frac{v_\Delta/\ \text{keV}}{v_1/\ \text{MeV}}\right) \beta_{1\delta}, \tag{5.3.1b}$$

$$\theta_{h1} \simeq \frac{\lambda_{1H} v_1\, v}{M_h^2 - M_1^2} \simeq 1.5 \cdot 10^{-5} \lambda_{1H} \left(\frac{v_1}{\text{MeV}}\right) \beta_{h1}, \tag{5.3.1c}$$

where $\beta_{ab} \equiv (1 - M_b^2/M_a^2)^{-1}$. First, the Higgs mixing with s_2 could in principle be sizable. Observations of Higgs production and decay modes together with precision electroweak measurements constrain the mixing angle α with a scalar singlet to be about $\sin\theta_{h2} \lesssim 0.2 - 0.3$ for a 200−800 GeV singlet mass [265]. If the scalar is much lighter than the Higgs, for instance in the region $1 < M_2 < 10$ GeV, the constraints on the mixing range from $\sin\theta_{h2} \lesssim 10^{-3} - 10^{-1}$ [317]. This Higgs-singlet mixing can lead to very interesting phenomenology, but it is not an exclusive signature of our model. For small values of v_2, the invisible Higgs decay to a pair of Majorons strongly constrains this mixing, as we will see later.

The mixing between δ and s_1 is quite special, as it leads to drastic deviations from the usual type II seesaw phenomenology. For δ^{++}, a new decay channel may open up,

scalar	Type II	Generalized type II	parameters
δ^{++}	$\ell^+\ell^+, W^+W^+$	$W^+W^+ s_1$	$v_\Delta, \theta_{\delta 1}$
δ^+	$\ell^+\nu, W^+Z, W^+h,\ t\bar{b}$	$W^+ s_1$	$v_\Delta, \theta_{\delta 1}$
δ	$\nu\nu, W^+W^-,\ ZZ, hh$	$h\, s_1$	$v_\Delta, \theta_{\delta 1}$
a_δ	$\nu\nu,\ t\bar{t}, Zh$	$Z\, s_1$	$v_\Delta, \theta_{\delta 1}$
s_1	not present	$\nu\nu,\ q\bar{q}, W^+W^-, ZZ$	$v_\Delta, \theta_{\delta 1}, \theta_{h1}$

Table 5.2.: Typical decay modes in type II seesaw and new modes in the generalized type II framework. In the last column it is indicated the most relevant parameters governing the partial widths.

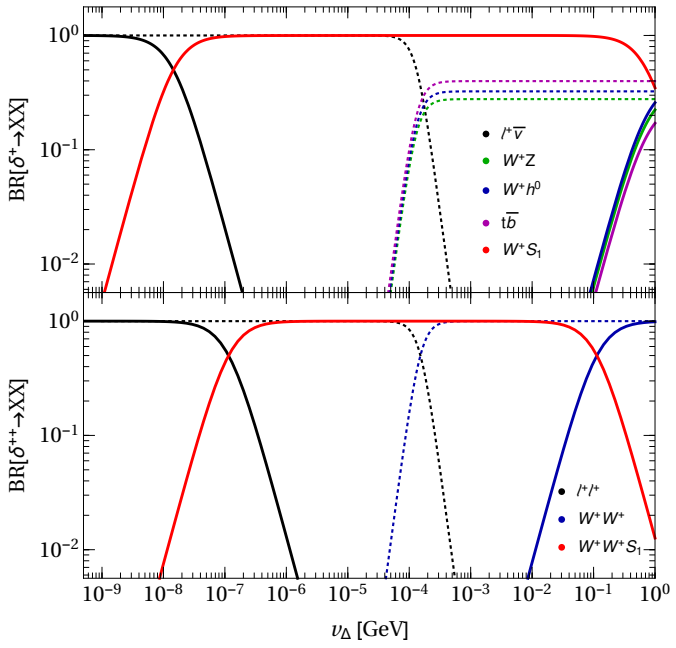

Figure 5.2.: Branching ratios of δ^+ (upper panel) and δ^{++} (lower panel) as a function of the triplet vev v_Δ for the usual type II seesaw model (dotted) and our generalized version (solid) . We considered $m_0 = 0.1$ eV, as the lightest neutrino mass, $M_{\delta^+} = M_{\delta^{++}} = 500$ GeV, $M_1 = 100$ GeV, and $\theta_{\delta 1} = 0.005$.

$\delta^{++} \to W^+W^+ s_1$ with s_1 typically decaying to neutrinos (via mixing with δ), quarks or gauge bosons (both via mixing with the Higgs) depending on its mass. Similarly, one can have $\delta^+ \to W^+ s_1$ and $\delta \to h s_1$. Another distinctive feature is the possibility of having sizable visible decays of the pseudoscalar, $a_\delta \to Z s_1$. Differently from type II seesaw, these decays are controlled uniquely by the gauge coupling and the mixing angle $\theta_{\delta 1}$. We summarize these features in Table 5.2. As can be seen in Fig. 5.2 the new decays can dominate a large region of parameter space in the generalized type II seesaw (solid lines) compared to the usual case (dotted lines). As we will see later, these new decays provide a smoking gun signature at the LHC, not only opening the possibility for discovering the new particles, but also distinguishing the model from type II seesaw.

Finally, the mixing between the Higgs and s_1 given in Eq. (5.3.1c), although small, plays a significant role in the scalar phenomenology. The s_1 decay to charged fermions, driven by θ_{h1}, will compete with the invisible decay to neutrinos, sourced by $\theta_{\delta 1}$. By analyzing the ratio of these partial widths (see Appendix A.3. for more details),

$$\frac{\Gamma_{s_1\to\nu\nu}}{\Gamma_{s_1\to ff}} \simeq \frac{3.1}{N_c}\left(\frac{\theta_{\delta 1}/10^{-3}}{\theta_{h1}/10^{-5}}\right)^2\left(\frac{m_\nu/0.1\ \text{eV}}{m_f/\ \text{GeV}}\right)^2\left(\frac{\text{keV}}{v_\Delta}\right)^2,$$

we can see that either visible or invisible s_1 decays can dominate in large natural regions of the parameter space. In this manuscript we will focus on the latter. Besides, there is some region of parameter space in which s_1 decays to b quarks and gives rise to displaced vertices at the LHC. We will nevertheless refrain from analyzing that possibility here.

5.4. Majoron phenomenology

Before dwelling on the LHC signatures, we will first discuss the Majoron phenomenology. Although a massless particle in the spectrum may at first seem problematic, its couplings to standard model fermions are extremely suppressed due to the hierarchy of vevs. The Majoron field is the linear combination

$$J \simeq \frac{1}{\ell_2 v_2}\left(\ell_1 v_1 a_1 + \ell_2 v_2 a_2 + \frac{1}{2} v_\Delta a_\delta - \frac{v_\Delta^2}{v} a\right), \tag{5.4.1}$$

where $\ell_1 = 1$ and $\ell_2 = 1/3$ are the lepton numbers of the corresponding scalars. It is straightforward to see that the Majoron has very small couplings to charged fermions given by

$$\begin{aligned} G_{Jff} &= \frac{y_f}{\sqrt{2}} \frac{v_\Delta^2}{\ell_2 v_2 v} = \frac{1.6 \cdot 10^{-18}}{\ell_2} \frac{(m_f/\text{ GeV})(v_\Delta/\text{ keV})^2}{(v_2/10\ \ \text{GeV})}, \\ G_{J\nu\nu} &= \sqrt{2} y_\nu \frac{v_\Delta}{\ell_2 v_2} = \frac{5 \cdot 10^{-12}}{\ell_2} \frac{(m_\nu/0.1\ \ \text{eV})}{(v_2/10\ \ \text{GeV})}, \end{aligned} \tag{5.4.2}$$

easily avoiding constraints from neutrinoless double beta decay with Majoron emission $G_{J\nu\nu} < (0.8 - 1.6) \times 10^{-5}$ [318], as well as astrophysical bounds $G_{Jee} < 4.3 \times 10^{-13}$ [319]. Although a thermalized Majoron would contribute to increase the effective number of relativistic degrees of freedom by 4/7, the tiny coupling in this scenario leads to very little Majoron production in the early universe.

A stringent bound on the Higgs-s_2 mixing comes from Higgs decaying invisibly to a pair of Majorons [320]. It is straightforward to obtain the approximate constraint (see e.g. Ref. [321]),

$$\theta_{h2} < 1.5 \cdot 10^{-3} \left[\frac{v_2}{10\ \ \text{GeV}}\right] \left[\frac{\Gamma_h}{4.2\ \ \text{MeV}} \frac{\text{BR}_{h\to inv}}{0.22}\right]^{1/2} \tag{5.4.3}$$

where Γ_h is the Higgs total width and $\text{BR}_{h\to\text{inv}}$ is its invisible branching ratio. The Higgs total width has only been measured indirectly, via comparison between on-shell and off-shell Higgs production, yielding the model-dependent bound $\Gamma_h^{\text{exp}} < 13$ MeV at 95% C.L. [322]. The Higgs invisible branching ratio has been bounded to be below 0.22 [154, 323]. This strong bound on θ_{h2} could be alleviated by raising v_2 to the TeV.

5.5. Collider phenomenology

In this section, we study the collider phenomenology for the generalised type II seesaw model. The leading production channels for this framework remain the same as in the usual type II, , the charged Higgs states will be dominantly produced in pairs via s-channel electroweak boson exchange, leading primarily to associated production of double and single charged Higgs bosons $\delta^{\pm\pm}\delta^{\mp}$, followed by double charged Higgs pair production $\delta^{++}\delta^{--}$[1]. Although these two production channels do not present differences in rate between the standard type II seesaw and our new model construction, their corresponding decays display new relevant phenomenological signatures. The $\delta - s_1$ mixing engenders new interaction terms from the triplet kinetic term

$$\mathcal{L} \supset \text{Tr}[(D_\mu \Delta)^\dagger D_\mu \Delta], \tag{5.5.1}$$

[1] We have checked that producing one triplet scalar in association with s_1 is typically sub-leading, as it is suppressed by the small mixing $\theta_{\delta 1}$. Thus, these production modes will be disregarded here.

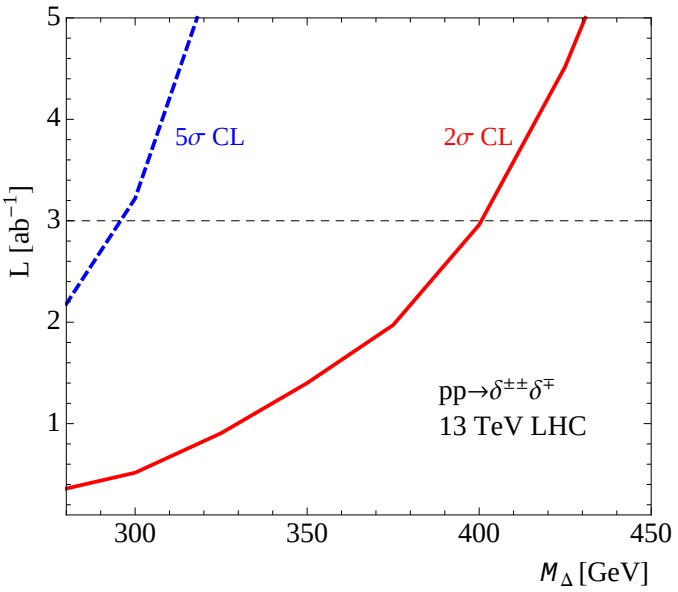

Figure 5.3.: Luminosity required to observe $pp \to \delta^{\pm\pm}\delta^{\mp}$ as a function of M_Δ at 2σ (red full) and 5σ (blue dashed) confidence level. We assume $M_1 = 100$ GeV and $v_\Delta = 10^{-6}$ GeV.

making the decays $\delta^{\pm\pm} \to W^\pm W^\pm s_1$ and $\delta^\pm \to W^\pm s_1$ available. Note that these partial widths do not present any v_Δ suppression, instead it depends only on gauge couplings, being equally large in a wide range of parameter space $v_\Delta \sim 10^{-7} - 10^{-1}$ GeV, distinctly from the usual type II, see Fig. 5.2.

Therefore, the $pp \to \delta^{\pm\pm}\delta^{\mp}$ production channel not only reveals the triplet structure nature of $\delta^{\pm\pm}$ and $\delta^\pm$ [303,304], but can also differentiate our construction from the usual type II model. To explore this phenomenology, we analyse the $pp \to \delta^{\pm\pm}\delta^{\mp}$ production at the $\sqrt{s} = 13$ TeV LHC, focusing on the trilepton plus missing energy signature, with two same flavor and same sign leptons, $e^\pm e^\pm \mu^\mp + \not{E}_T$ and $\mu^\pm \mu^\pm e^\mp + \not{E}_T$. The leptons arise from the W-boson decays and relevant extra sources of missing energy follow from the dominant s_1 decay, $s_1 \to \nu\bar{\nu}$.

Our model is implemented in FeynRules [324] and the signal sample is generated with MadGraph5 [325]. A Next-to-leading order QCD K-factor of 1.25 has been applied [326]. To obtain a robust simulation of the background components, that display large fake rates, our simulation follows the recent 13 TeV CMS study [327]. Although CMS targets a heavy neutral Majorana lepton N, it presents a set of search regions for the high mass regime $m_N > m_W$, leading to a more sizable $\not{E}_T$, that also applies to our model.

In this analysis, jets are defined with the anti-k_T clustering algorithm with $R = 0.4$, $p_{Tj} > 25$ GeV and $|\eta_j| < 2.4$ via Fastjet [328]. Events with one or more b-jets are vetoed with 70% b-tagging efficiency and 1% mistag rate. Electrons and muons are defined with $|\eta_\ell| < 2.4$ and the three leptons must satisfy $p_{T\ell} > 55, 15, 10$ GeV. Finally, the events are divided in bins associated to three observables: *i*) the trilepton mass system $m_{3\ell}$; *ii*) minimum invariant mass of all opposite sign leptons $m^{min}_{2\ell OS'}$; and *iii*) transverse mass $m_T = \sqrt{2 p_{T\ell} \not{E}_T (1 - \cos\phi)}$, where $p_{T\ell}$ corresponds to the lepton which is not used in the $m^{min}_{2\ell OS'}$ calculation and ϕ is the azimuthal angle between $\vec{p}_{T\ell}$ and $\vec{p}^{\,miss}_T$.

Using the CMS background estimate, we perfom a binned log-likelihood analysis based on the CL$_s$ method [329], exploring all search regions with $e^\pm e^\pm \mu^\mp + \not{E}_T$ and $\mu^\pm \mu^\pm e^\mp + \not{E}_T$ displayed by Ref. [327]. In Fig. 5.3, we present the luminosity required to observe $pp \to \delta^{\pm\pm}\delta^{\mp}$ as a function of M_Δ at 2σ (red full) and 5σ (blue dashed) confidence level.

At the high-luminositiy LHC, $\mathcal{L} = 3$ ab^{-1}, we can discover charged Higgses at 5σ level up to $M_\Delta = 300$ GeV and exclude it at 2σ level up to $M_\Delta = 400$ GeV.

A final comment is in order regarding two phenomenological aspects beyond the ones discussed so far. First, our model may also induce lepton flavor violation processes, very similar to the usual type II seesaw scenario [330]. Second, although the model does not have enough CP violation, adding a second $SU(2)$ triplet scalar [331] may lead to successful leptogenesis. The study of such possibilities is beyond the scope of this manuscript.

5.6. Conclusions

In this chapter we have proposed a generalization of type II seesaw in which lepton number is broken dynamically and no hierarchy problem neither arbitrarily small parameters are present. The rich phenomenology of the model includes deviations of standard Higgs couplings, the presence of a massless neutral pseudoscalar and more importantly a novel smoking gun signature at the LHC. This distinctive new signature may reveal the triplet nature of the charged scalars and at the same time disentangle the framework from the usual type II seesaw model.

6. Summary and conclusions

We have evidence that the Standard Model is not complete and that a more fundamental underlying theory remains to be unveiled. Models which explain several beyond the Standard Model indications instead of focusing on just one are particular appealing in this context.

In this work we studied possible connections between the open questions of the Standard Model: the quest for neutrino masses and mixings, the hierarchy problem, and the evidence for Dark Matter. The starting point was the origin of neutrino masses. In this sense neutrinos can serve as a window to new physics. The simplest addition to the Standard Model to explain neutrino masses is the introduction of right-handed neutrinos. Probing their mass scale and interactions is of great interest to obtain insight on the underlying physics. In chapter 3 we made a step towards this by analysing for the first time IceCube data for muon neutrino disappearance with large masses for sterile neutrinos such that their oscillations are averaged out. The 1-year of public data of atmospheric neutrino disappearance showed a mild preference (around 2σ) for non-zero sterile mixing. The preferred values of the mixing matrix elements squared for the mixing with muon flavour is around $\sim 10^{-2}$ and for the mixing with tau flavour between $10^{-1} - 10^{-2}$. We also studied the sensitivity of 8-years of IceCube data, close to the data that should be presently available, assuming no sterile neutrino mixing. Forecasted 8 and 20 years of IceCube data can improve by one order of magnitude in some regions of parameter space over current constraints by Super-Kamiokande and DeepCore. In particular, 8 years of data are enough to confirm or exclude the present preference for non-zero mixing.

Such rather large sterile mixing is in general not expected in models which explain the smallness of neutrino masses via a suppression of a new scale much higher than the electroweak. This is for case for instance of the type I seesaw and other models where the mixing of the sterile neutrinos with the active neutrinos is suppressed by the same hierarchy of scales. Alternatively, the smallness of neutrino masses can also be explained via an an approximate lepton number symmetry. Neutrino masses are protected by the accidental global baryon-lepton number symmetry of the Standard Model, if this symmetry is only mildly broken, the neutrino masses will be proportional to this small parameter. An advantage of these models is that the phenomenology of the additional right-handed neutrinos is not suppressed by this small parameter. In chapter 4 we introduced a model where we gauged the accidental baryon-lepton number symmetry of the Standard Model to obtain a dynamical realisation of this small parameter which we identified with the vacuum expectation value of the scalar which breaks baryon-lepton number. Gauging the symmetry calls for the introduction of additional fermions, one of them is a viable Dark

Matter candidate. The other additional fermion remains massless and gives a contribution to the effective number of relativistic degrees of freedom in the early Universe. The scalars needed to break the symmetry can introduce deviations in Higgs observables due to mixing with the Standard Model Higgs. Furthermore, the massive gauge boson can be searched for at colliders. Hence this model can be probed in various ways from colliders (with Higgs observables and search for a massive gauge boson at the TeV scale), Dark Matter experiments, cosmology, and via the search for heavy neutrinos with their mixing with the active neutrinos.

Similar to this gauged baryon-lepton number model the generalised type II seesaw model introduced in chapter 5 seeks to explain the striking smallness of the neutrino masses in a dynamical way without introducing a hierarchy problem. All introduced new particles have a mass around the electroweak scale without requiring fine-tuning and arbitrarily small parameters. This model presents a smoking gun signature at the LHC that allows to distinguish our model from the usual type II seesaw scenario. Furthermore, the presence of a massless Goldstone boson and deviations of standard model Higgs couplings, arise, which allows this model to be probed in various ways.

In summary, we studied the relation of neutrino mass models with other open questions of the Standard Model. We found interesting connections between a model which explains neutrino masses and at the same time gives a good Dark Matter candidate, and a model which provides an explanation for neutrino masses without introducing a hierarchy problem. Both new physics extensions also address the flavour puzzle by providing a rationale for the smallness of neutrino masses. Future experiments as well as data from current experiments can probe these models.

These studies can provide a first step to build theories which can link various open questions of the Standard Model at the same time. More data from complementary avenues (collider experiments, low-energy experiments, flavour observables, astrophysics, and cosmology) will open the way towards an understanding of a fundamental underlying theory in, hopefully, the near future.

Resultados y conclusiónes

Tenemos evidencia de que el modelo estándar no está completo y que queda por descubrir una teoría subyacente más fundamental. Los modelos que explican varias indicaciones mas allá del modelo estándar en lugar de enfocarse solo en una son particularmente atractivos en este contexto.

En este trabajo, estudiamos las posibles conexiones entre distintas preguntas abiertas del modelo estándar: la búsqueda de masas y mezclas de neutrinos, la evidencia de la materia oscura y el puzzle del sabor. El punto de partida fue el origen de las masas de neutrinos. En este sentido, los neutrinos pueden servir como una ventana a la nueva física. La incorporación más simple al modelo estándar para explicar las masas de neutrinos es la introducción de neutrinos dextróginos. Es de gran interés comprobar su escala de masa e interacciones para obtener una idea de las posibles extensiones del modelo estándar. En el capítulo 3 dimos un paso en esta dirección al analizar por primera vez los datos de IceCube para la desaparición del neutrino muón con masas grandes para los neutrinos estériles, de modo que sus oscilaciones se promedian. Los datos públicos de desaparición de neutrinos atmosféricos mostraron una preferencia leve (alrededor de 2σ) para la mezcla estéril. Los valores de los elementos de matriz de mezcla al cuadrado que mejor explican los datos son alrededor de $\sim 10^{-2}$ para mezcla con el muón y entre $10^{-1} - 10^{-2}$ para la mezcla con el tau. También estudiamos la sensibilidad que 8 años de datos de IceCube tendrían a la mezcla de neutrinos esteriles. Los datos pronosticados de 8 y 20 años de IceCube pueden mejorar en un orden de magnitud en algunas regiones del espacio de parámetros sobre las cotas actuales de Super-Kamiokande y DeepCore. En particular, 8 años de datos son suficientes para confirmar o excluir la preferencia actual por la mezcla distinta de cero.

En general, los modelos que explican la pequeñez de las masas de neutrinos mediante una supresión de la escala electrodébil, por ejemplo en el seesaw de tipo I, predicen una mezcla muy pequeña con los neutrinos estériles ya que en estos modelos la mezcla de los neutrinos estériles con los neutrinos activos se suprime por la misma jerarquía de escalas. Alternativamente, la pequeñez de las masas también puede explicarse a través de un una simetría leptónica aproximada. Las masas de neutrinos están protegidas por la simetría B-L global accidental del modelo estándar, si esta simetría se rompe levemente, las masas de neutrinos serán proporcionales a este pequeño parámetro. Una ventaja de estos modelos es que la fenomenología de los neutrinos dextróginos adicionales no se suprime con este pequeño parámetro. En el capítulo 4, presentamos un modelo en el que hacemos gauge la simetría B-L accidental del modelo estándar para obtener una realización dinámica de este pequeño parámetro que identificamos con el valor esperado en el vacío del escalar que rompe B-L. Hacer gauge la simetría exige la introducción de fermiones adicionales, uno de ellos es un candidato viable a la materia oscura. El otro fermión adicional permanece sin masa y contribuye a la cantidad efectiva de grados de libertad relativistas en el Universo primitivo. Los escalares necesarios para romper la simetría pueden introducir desviaciones en los observables de Higgs debido a la mezcla con el Higgs del modelo estándar. Además, el bosón de gauge masivo se puede buscar en los colisionadores. Por lo tanto, este modelo puede ser buscado de varias maneras: en colisionadores (con observables de Higgs y búsqueda de un bosón masivo a la escala TeV), experimentos con materia oscura, cos-

mología y mediante la búsqueda de neutrinos pesados con su mezcla con los neutrinos activos.

De manera similar a este modelo B-L gauge, el modelo de generalizado seesaw tipo II introducido en el capítulo 5 busca explicar la sorprendente pequeñez de las masas de neutrinos de una manera dinámica sin introducir un problema de jerarquía. Todas las nuevas partículas introducidas tienen una masa alrededor de la escala electrodébil sin requerir ajustes finos y parámetros arbitrariamente pequeños. Este modelo presenta una señal caracteristica en el LHC que permite distinguir nuestro modelo del escenario de seesaw tipo II habitual. Además, surgen otros aspectos fenomenológicos interesantes del modelo, como la presencia de un bosón Goldstone sin masa y las desviaciones del modelo estándar de los acoplamientos de Higgs, que permiten probar este modelo de varias maneras.

En resumen, estudiamos la relación de modelos de masa de neutrinos con otras preguntas abiertas del modelo estánda. Encontramos conexiones interesantes entre un modelo que explica las masas de neutrinos y, al mismo tiempo, ofrece un buen candidato a materia oscura, y un modelo que explica las masas de neutrinos sin introducir un problema de jerarquía. Esto dos modelos también se relacionan con el puzzle del sabor proporcionando una explicación a la pequeñez de las masas de los neutrinos. Los experimentos futuros, así como los datos de los experimentos actuales, pueden testar estos modelos.

Estos estadios pueden proporcionar un primer paso para construir teorías que puedan vincular varias preguntas abiertas del modelo estándar al mismo tiempo. Más datos de avenidas complementarias (experimentos de colisionadores, experimentos de baja energía, observables de sabor, y astrofísica y cosmología) pueden abrir el camino hacia la comprensión de la teoría fundamental subyacente.

Appendix

A. Supplemental Material for chapter 5

A.1. n-step generalized type II seesaw

Here we present the generalization of our framework for an arbitrary number of scalar singlets n. We define the following scalar bilinears,

$$B_i \equiv S_i^* S_i, \quad B_\Delta \equiv \mathrm{Tr}(\Delta^\dagger \Delta), \quad B_H \equiv H^\dagger H, \tag{A.1}$$

which allow to write the scalar potential in a compact form

$$\begin{aligned} V = &-\frac{m_H^2}{2} B_H + \sum_{\varphi}^{\Delta,1..n-1} m_\varphi^2 B_\varphi - \frac{m_n^2}{2} B_n + \sum_{\varphi}^{\text{all}} \frac{\lambda_\varphi}{4} B_\varphi^2 \\ &+ \sum_{\varphi,\varphi'>\varphi}^{\text{all}} \lambda_{\varphi\varphi'} B_\varphi B_{\varphi'} + \frac{\lambda'_\Delta}{4} \mathrm{Tr}(\Delta^\dagger \Delta \Delta^\dagger \Delta) + \lambda'_{H\Delta} H^\dagger \Delta \Delta^\dagger H \\ &+ \left[\lambda_A H^T i\sigma_2 \Delta^\dagger H S_1^* - \frac{2}{3} \sum_{i=1}^{n-1} \lambda'_{i,i+1} S_i^* S_{i+1}^3 + \text{h. c.} \right]. \end{aligned} \tag{A.2}$$

The notation in the sum of the first term of the second line indicates that permutations of $\lambda_{\varphi\varphi'}$ should not be taken (to avoid double counting). Without loss of generality, all $\lambda'_{i,i+1}$ and λ_A can be made real by rephasing the scalar singlet fields. The masses and vevs in the n-step realization are approximately given by

$$m_H^2 = \frac{1}{2}\lambda_H v^2 + \lambda_{nH} v_n^2, \tag{A.3a}$$

$$m_n^2 = \frac{1}{2}\lambda_n v_n^2 + \lambda_{nH} v^2, \tag{A.3b}$$

$$v_i = \frac{\lambda'_{i,i+1} v_{i+1}^3}{3M_i^2}, \quad \text{for } i = 1, \ldots, n-1, \tag{A.3c}$$

$$v_\Delta = \frac{\lambda_A v^2 v_1}{2M_\Delta^2}, \tag{A.3d}$$

$$M_h^2 = \frac{1}{2}\lambda_H v^2, \tag{A.3e}$$

$$M_i^2 = m_i^2 + \frac{1}{2}(\lambda_{iH} v^2 + \lambda_{in} v_n^2), \quad i = 1, \ldots, n-1, \tag{A.3f}$$

$$M_n^2 = \frac{1}{2}\lambda_n v_n^2, \tag{A.3g}$$

$$M_\Delta^2 = m_\Delta^2 + \frac{1}{2}\left[\lambda_{n\Delta} v_n^2 + (\lambda_{H\Delta} + \lambda'_{H\Delta})v^2\right]. \tag{A.3h}$$

These expressions should hold in the regime, $v_i \ll v_{i+1}$, that is,

$$\varepsilon \equiv \lambda'_{i,i+1}\frac{v_{i+1}^2}{3M_i^2} \ll 1. \tag{A.4}$$

In fact, it is straightforward to show that as long as Eq. (A.4) is satisfied, for any number n of scalar singlet fields, the vev of s_j, $j < n$, is simply given by

$$v_j = \prod_{k=0}^{n-j-1}\left(\frac{\lambda'_{j+k,j+k+1}}{3}\frac{v_n^2}{M_{j+k}^2}\right)^{3^k} v_n. \tag{A.5}$$

If, for simplicity, one takes all $\lambda'_{ij} = \lambda'$ and $M_i = M$, then we obtain a simplified expression,

$$v_j = \left(\frac{\lambda'}{3}\frac{v_n^2}{M^2}\right)^K v_n, \quad K = (3^{n-j}-1)/2. \tag{A.6}$$

We can clearly identify the parametric suppression ε^K responsible for making $v_1 \ll v_n$. For instance, if $\varepsilon = 0.01$ and $n = 3$ we obtain $v_1 \sim 10^{-8} v_n$. Note that the expressions for the mixing angles defined in Eqs. (5.3.1a-5.3.1c) are valid for any n, and thus the phenomenological considerations regarding Higgs couplings, Majoron physics and LHC signatures will still apply.

A.2. Stability of the scalar potential

Although a complete study on the stability of the scalar potential are not the main focus of this Letter, we provide here sufficient conditions for the stability. The key point is that the quartic couplings λ_A and λ'_{12} (or any $\lambda'_{i,i+1}$ in the n-step scenario) can always yield negative contributions to the potential when the values of the fields go to infinity, independently of their sign. As these couplings are the core of the generalized type II seesaw mechanism, it is important to understand how to control these contribution so that the potential is bounded from below. Although a full analysis of the stability would be very complicated, specially in the n-step scenario, we can still derive useful sufficient conditions to have stability. The idea is to split the scalar potential into pieces that will isolate each λ'_{12} or λ_A,

$$V = V_A + V_{12} + \ldots + V_0 \tag{A.7}$$

and require each piece to be independently positive. For now we will focus on $n=2$-steps and generalize the method in the end.

The first piece deals with λ_A. We define

$$\begin{aligned} V_A \equiv\ & \lambda_{1H}(S_1)(H) + \lambda_{1\Delta}\Delta(S_1) \\ & + \lambda_{H\Delta}(H)\Delta + \left(\lambda_A H^T i\sigma_2 \Delta^\dagger H S_1^* + \text{h. c.}\right) \end{aligned} \tag{A.8}$$

and require it to be positive. By performing an $SU(2)$ rotation on the field one can always write [332]

$$i\sigma_2\Delta = \begin{pmatrix} a & 0 \\ 0 & b\,e^{i\alpha} \end{pmatrix}, \quad H = \begin{pmatrix} c\,e^{i\beta} \\ d\,e^{i\gamma} \end{pmatrix}, \tag{A.9}$$

and $S_i = R_i e^{i\phi_i}$. Then, it is straightforward to obtain

$$\lambda_{H\Delta} > 0, \qquad \lambda_{1\Delta} > 0, \tag{A.10a}$$

$$\lambda_{1H} > 0, \qquad |\lambda_A|^2 < \lambda_{1H}\lambda_{H\Delta}. \tag{A.10b}$$

Now, we handle λ'_{12} by defining

$$V_{12} \equiv \frac{\lambda_2}{4}(S_2)^2 + \lambda_{12}(S_1)(S_2) - \left(\frac{2}{3}\lambda'_{12}S_1^* S_2^3 + \text{h. c.}\right), \tag{A.11}$$

and requiring $V_{12} > 0$. This yields

$$\lambda_{12} > 0, \quad \lambda_2 > 0, \quad |\lambda'_{12}|^2 < \frac{9}{16}\lambda_{12}\lambda_2. \tag{A.12}$$

We still have to deal with seven quartic couplings. First note that λ_1, λ_{2H}, and $\lambda_{2\Delta}$ need to be positive, as there is no other quartic left that can compensate for a negative contribution to the potential sourced by these couplings. The remaining parameters, λ_Δ, λ'_Δ, $\lambda_{H\Delta}$ and $\lambda'_{H\Delta}$, essentially define a usual type II seesaw potential and the stability conditions for that case are known [332]. The requirements for these seven quartics can be summarized as

$$\text{(i)} \quad \lambda_H > 0,\ \lambda_1 > 0,\ \lambda_{2H} > 0,\ \lambda_{2\Delta} > 0, \tag{A.13a}$$
$$\text{(ii)} \quad \lambda_\Delta + \lambda'_\Delta > 0,\ 2\lambda_\Delta + \lambda'_\Delta > 0, \tag{A.13b}$$
$$\text{(iii)} \quad 2\lambda'_{H\Delta} + \sqrt{\lambda_H(\lambda_\Delta + \lambda'_\Delta)} > 0, \tag{A.13c}$$
$$\text{(iv)} \quad 2\lambda'_{H\Delta}\sqrt{\lambda_\Delta + \lambda'_\Delta} + (2\lambda_\Delta + \lambda'_\Delta)\sqrt{\lambda_H} > 0. \tag{A.13d}$$

We emphasize that if inequalities (A.10), (A.12), and (A.13) are all satisfied, then the potential is stable.

The generalization to more n-steps is now straightforward. By defining

$$V_{i,i+1} \equiv \frac{\lambda_{i+1}}{4}(S_{i+1}^* S_{i+1})^2 + \lambda_{i,i+1}(S_i^* S_i)(S_{i+1}^* S_{i+1}) - \left(\frac{2}{3}\lambda'_{i,i+1}S_i^* S_{i+1}^3 + \text{h. c.}\right), \tag{A.14}$$

and requiring $V_{i,i+1} > 0$ we obtain

$$\lambda_{i,i+1} > 0, \quad \lambda_{i+1} > 0, \quad |\lambda'_{i,i+1}|^2 < \frac{9}{16}\lambda_{i,i+1}\lambda_{i+1} \tag{A.15}$$

for $i = 1..n-1$. Again, there are no quartic couplings left to compensate for λ_{iH} or $\lambda_{i\Delta}$, which demands

$$\lambda_i > 0,\ \lambda_{iH} > 0,\ \lambda_{i\Delta} > 0, \quad i = 1..n. \tag{A.16}$$

These conditions are by no means necessary, but only sufficient for having stability in the n-step realization.

A.3. Partial widths

We present in this Appendix the partial widths for the novel decay channels of some of the extra scalars in the generalized type II seesaw framework. In the case of δ, we will have three new channels: $\delta \to hs_1$, $\delta \to hhs_1$, and $\delta \to hs_1s_1$. As the latter is suppressed by v_1^2, we will safely neglect it in the remainder. The partial widths for the first two channels are

$$\Gamma(\delta \to hs_1) \simeq \frac{v^2}{1024\pi M_\Delta}(8\lambda_A \cos(2\theta_{\delta 1}) - \lambda_{1H}\sin(2\theta_{\delta 1}))^2,$$
$$\Gamma(\delta \to hhs_1) \simeq \frac{M_\Delta}{8192\pi^3}(2\lambda_A \cos(2\theta_{\delta 1}) - \lambda_{1H}\sin(2\theta_{\delta 1}))^2,$$

where we have neglected the phase space factor by assuming $M_1 + 2M_h \ll M_\Delta$. The phase space for 2-body decay can easily be incorporated by multiplying the partial width by

$$\bar{\beta}_{\delta\to hs_1} \equiv \sqrt{1 - \frac{2(M_1^2 + M_h^2)}{M_\Delta^2} + \frac{(M_1^2 - M_h^2)^2}{M_\Delta^4}}. \tag{A.17}$$

The decay width ratios with respect to the leptonic channel, $\delta \to \nu\nu + \bar{\nu}\bar{\nu}$, are approximately given by

$$\frac{\Gamma[\delta \to hs_1]}{\Gamma[\delta \to \nu\nu + \bar{\nu}\bar{\nu}]} \simeq \lambda_A^2 \frac{v_\Delta^2}{\sum_i m_{\nu_i}^2} \frac{v^2}{M_\delta^2},$$
$$\frac{\Gamma[\delta \to hhs_1]}{\Gamma[\delta \to \nu\nu + \bar{\nu}\bar{\nu}]} \simeq \frac{\lambda_A^2}{512\pi^2} \frac{v_\Delta^2}{\sum_i m_{\nu_i}^2}.$$

In the case of the single-charged scalar δ^+, the additional channel $\delta^+ \to W^+ s_1$ is the most relevant. Its decay width is given by

$$\Gamma[\delta^+ \to W^+ s_1] = \cos^2\eta \frac{\sin^2(\theta_{\delta 1})}{8\pi} \frac{M_{\delta^+}^3}{v^2} \bar{\beta}_{\delta^+}^3,$$

with

$$\cos^2\eta \equiv 1 - \frac{2v_\Delta^2}{v^2},$$
$$\bar{\beta}_{\delta^+} \equiv \sqrt{1 - \frac{2(M_1^2 + M_W^2)}{M_{\delta^+}^2} + \frac{(M_1^2 - M_W^2)^2}{M_{\delta^+}^4}}.$$

The ratio with the leptonic channel is approximately

$$\frac{\Gamma[\delta^+ \to W^+ s_1]}{\Gamma[\delta^+ \to \ell^+\nu]} \simeq 2\sin^2(\theta_{\delta 1}) \frac{v_\Delta^2}{m_{\nu_i}^2} \frac{M_{\delta^+}^2}{v^2}.$$

For s_1, we have the decay into charged fermions and neutrinos

$$\Gamma[s_1 \to f\bar{f}] = N_c \frac{M_1}{8\pi} \frac{m_f^2}{v^2} \sin^2\theta_{h1} \bar{\beta}_1, \tag{A.18a}$$
$$\Gamma[s_1 \to \nu\nu] = \frac{M_1}{16\pi} \frac{m_\nu^2}{v_\Delta^2} \sin^2\theta_{\delta 1}, \tag{A.18b}$$

where N_c is the number of colors and $\bar{\beta}_1 \equiv (1 - 4m_f^2/M_1^2)^{3/2}$. We do not present the analytic expressions for the new 3-body decay channel $\delta^{++} \to W^+W^+s_1$, as it is not particularly illuminating.

Bibliography

[1] V. De Romeri, E. Fernandez-Martinez, J. Gehrlein, P. A. N. Machado and V. Niro, *Dark Matter and the elusive Z in a dynamical Inverse Seesaw scenario*, JHEP **10** (2017) 169 [arXiv:1707.0860].

[2] M. Blennow, E. Fernandez-Martinez, J. Gehrlein, J. Hernandez-Garcia and J. Salvado, *IceCube bounds on sterile neutrinos above 10 eV*, Eur. Phys. J. **C78** (2018), no. 10 807 [arXiv:1803.0236].

[3] J. Gehrlein, D. Gonalves, P. A. N. Machado and Y. F. Perez-Gonzalez, *Natural and Dynamical Neutrino Mass Mechanism at the LHC*, Phys. Rev. **D98** (2018), no. 3 035045 [arXiv:1804.0918].

[4] H. Fritzsch, M. Gell-Mann and H. Leutwyler, *Advantages of the Color Octet Gluon Picture*, Phys. Lett. **47B** (1973) 365–368.

[5] H. Fritzsch and M. Gell-Mann, *Current algebra: Quarks and what else?*, eConf **C720906V2** (1972) 135–165 [hep-ph/0208010].

[6] S. L. Glashow, *Partial Symmetries of Weak Interactions*, Nucl. Phys. **22** (1961) 579–588.

[7] S. Weinberg, *A Model of Leptons*, Phys. Rev. Lett. **19** (1967) 1264–1266.

[8] A. Salam, *Weak and Electromagnetic Interactions*, Conf. Proc. **C680519** (1968) 367–377.

[9] **Particle Data Group** Collaboration, M. Tanabashi et. al., *Review of Particle Physics*, Phys. Rev. **D98** (2018), no. 3 030001.

[10] **CDF** Collaboration, T. Aaltonen et. al., *First Run II Measurement of the W Boson Mass*, Phys. Rev. **D77** (2008) 112001 [arXiv:0708.3642].

[11] P. W. Higgs, *Broken symmetries, massless particles and gauge fields*, Phys. Lett. **12** (1964) 132–133.

[12] P. W. Higgs, *Broken Symmetries and the Masses of Gauge Bosons*, Phys. Rev. Lett. **13** (1964) 508–509. [,160(1964)].

[13] F. Englert and R. Brout, *Broken Symmetry and the Mass of Gauge Vector Mesons*, Phys. Rev. Lett. **13** (1964) 321–323. [,157(1964)].

[14] G. S. Guralnik, C. R. Hagen and T. W. B. Kibble, *Global Conservation Laws and Massless Particles*, Phys. Rev. Lett. **13** (1964) 585–587. [,162(1964)].

[15] K. Nishijima, *Charge Independence Theory of V Particles*, Prog. Theor. Phys. **13** (1955), no. 3 285–304.

[16] M. Gell-Mann, *The interpretation of the new particles as displaced charge multiplets*, Nuovo Cim. **4** (1956), no. S2 848–866.

[17] N. Cabibbo, *Unitary Symmetry and Leptonic Decays*, Phys. Rev. Lett. **10** (1963) 531–533. [,648(1963)].

[18] M. Kobayashi and T. Maskawa, *CP Violation in the Renormalizable Theory of Weak Interaction*, Prog. Theor. Phys. **49** (1973) 652–657.

[19] R. Davis, Jr., D. S. Harmer and K. C. Hoffman, *Search for neutrinos from the sun*, Phys. Rev. Lett. **20** (1968) 1205–1209.

[20] B. T. Cleveland, T. Daily, R. Davis, Jr., J. Distel, K. Lande, C. K. Lee, P. Wildenhain and J. Ullman, *Update on the measurement of the solar neutrino flux with the Homestake chlorine detector*, Nucl. Phys. Proc. Suppl. **38** (1995) 47–53.

[21] **GALLEX** Collaboration, P. Anselmann et. al., *GALLEX results from the first 30 solar neutrino runs*, Phys. Lett. **B327** (1994) 377–385.

[22] **SAGE** Collaboration, J. N. Abdurashitov et. al., *Measurement of the solar neutrino capture rate with gallium metal*, Phys. Rev. **C60** (1999) 055801 [astro-ph/9907113].

[23] **Kamiokande-II** Collaboration, K. S. Hirata et. al., *Observation of B-8 Solar Neutrinos in the Kamiokande-II Detector*, Phys. Rev. Lett. **63** (1989) 16.

[24] **Kamiokande-II** Collaboration, K. S. Hirata et. al., *Results from one thousand days of real time directional solar neutrino data*, Phys. Rev. Lett. **65** (1990) 1297–1300. [,146(1990)].

[25] **Kamiokande-II** Collaboration, K. S. Hirata et. al., *Real time, directional measurement of B-8 solar neutrinos in the Kamiokande-II detector*, Phys. Rev. **D44** (1991) 2241. [Erratum: Phys. Rev.D45,2170(1992)].

[26] J. N. Bahcall and R. K. Ulrich, *Solar Models, Neutrino Experiments and Helioseismology*, Rev. Mod. Phys. **60** (1988) 297–372.

[27] J. N. Bahcall and M. H. Pinsonneault, *Standard solar models, with and without helium diffusion and the solar neutrino problem*, Rev. Mod. Phys. **64** (1992) 885–926.

[28] **Super-Kamiokande** Collaboration, H. Nishino et. al., *Search for Proton Decay via p —> e+ pi0 and p —> mu+ pi0 in a Large Water Cherenkov Detector*, Phys. Rev. Lett. **102** (2009) 141801 [arXiv:0903.0676].

[29] **Super-Kamiokande** Collaboration, Y. Fukuda et. al., *Evidence for oscillation of atmospheric neutrinos*, Phys. Rev. Lett. **81** (1998) 1562–1567 [hep-ex/9807003].

[30] **SNO** Collaboration, Q. R. Ahmad et. al., *Direct evidence for neutrino flavor transformation from neutral current interactions in the Sudbury Neutrino Observatory*, Phys. Rev. Lett. **89** (2002) 011301 [nucl-ex/0204008].

[31] B. Pontecorvo, *Neutrino Experiments and the Problem of Conservation of Leptonic Charge*, Sov. Phys. JETP **26** (1968) 984–988. [Zh. Eksp. Teor. Fiz.53,1717(1967)].

[32] B. Pontecorvo, *Mesonium and anti-mesonium*, Sov. Phys. JETP **6** (1957) 429. [Zh. Eksp. Teor. Fiz.33,549(1957)].

[33] Z. Maki, M. Nakagawa and S. Sakata, *Remarks on the unified model of elementary particles*, Prog. Theor. Phys. **28** (1962) 870–880. [,34(1962)].

[34] V. N. Gribov and B. Pontecorvo, *Neutrino astronomy and lepton charge*, Phys. Lett. **28B** (1969) 493.

[35] C. Jarlskog, *Commutator of the Quark Mass Matrices in the Standard Electroweak Model and a Measure of Maximal CP Violation*, Phys. Rev. Lett. **55** (1985) 1039.

[36] I. Esteban, M. C. Gonzalez-Garcia, M. Maltoni, I. Martinez-Soler and T. Schwetz, *Updated fit to three neutrino mixing: exploring the accelerator-reactor complementarity*, JHEP **01** (2017) 087 [arXiv:1611.0151].

[37] L. Wolfenstein, *Neutrino Oscillations in Matter*, Phys. Rev. **D17** (1978) 2369–2374. [,294(1977)].

[38] S. P. Mikheyev and A. Yu. Smirnov, *Resonance Amplification of Oscillations in Matter and Spectroscopy of Solar Neutrinos*, Sov. J. Nucl. Phys. **42** (1985) 913–917. [,305(1986)].

[39] S. P. Mikheev and A. Yu. Smirnov, *Neutrino Oscillations in a Variable Density Medium and Neutrino Bursts Due to the Gravitational Collapse of Stars*, Sov. Phys. JETP **64** (1986) 4–7 [arXiv:0706.0454]. [,311(1986)].

[40] S. P. Mikheev and A. Yu. Smirnov, *Resonant amplification of neutrino oscillations in matter and solar neutrino spectroscopy*, Nuovo Cim. **C9** (1986) 17–26.

[41] **Super-Kamiokande** Collaboration, K. Abe et. al., *Solar neutrino results in Super-Kamiokande-III*, Phys. Rev. **D83** (2011) 052010 [arXiv:1010.0118].

[42] **SNO** Collaboration, B. Aharmim et. al., *Combined Analysis of all Three Phases of Solar Neutrino Data from the Sudbury Neutrino Observatory*, Phys. Rev. **C88** (2013) 025501 [arXiv:1109.0763].

[43] **KamLAND** Collaboration, K. Eguchi et. al., *First results from KamLAND: Evidence for reactor anti-neutrino disappearance*, Phys. Rev. Lett. **90** (2003) 021802 [hep-ex/0212021].

[44] **IceCube** Collaboration, M. G. Aartsen et. al., *Determining neutrino oscillation parameters from atmospheric muon neutrino disappearance with three years of IceCube DeepCore data*, Phys. Rev. **D91** (2015), no. 7 072004 [arXiv:1410.7227].

[45] **K2K** Collaboration, M. H. Ahn et. al., *Indications of neutrino oscillation in a 250 km long baseline experiment*, Phys. Rev. Lett. **90** (2003) 041801 [hep-ex/0212007].

[46] **T2K** Collaboration, K. Abe et. al., *Precise Measurement of the Neutrino Mixing Parameter θ_{23} from Muon Neutrino Disappearance in an Off-Axis Beam*, Phys. Rev. Lett. **112** (2014), no. 18 181801 [arXiv:1403.1532].

[47] **NOvA** Collaboration, P. Adamson et. al., *Constraints on Oscillation Parameters from ν_e Appearance and ν_μ Disappearance in NOvA*, Phys. Rev. Lett. **118** (2017), no. 23 231801 [arXiv:1703.0332].

[48] **MINOS** Collaboration, P. Adamson et. al., *Measurement of Neutrino and Antineutrino Oscillations Using Beam and Atmospheric Data in MINOS*, Phys. Rev. Lett. **110** (2013), no. 25 251801 [arXiv:1304.6335].

[49] H. Minakata, H. Sugiyama, O. Yasuda, K. Inoue and F. Suekane, *Reactor measurement of theta(13) and its complementarity to long baseline experiments*, Phys. Rev. **D68** (2003) 033017 [hep-ph/0211111]. [Erratum: Phys. Rev.D70,059901(2004)].

[50] K. Hiraide, H. Minakata, T. Nakaya, H. Nunokawa, H. Sugiyama, W. J. C. Teves and R. Z. Funchal, *Resolving θ_{23} degeneracy by accelerator and reactor neutrino oscillation experiments*, Phys. Rev. **D73** (2006) 093008 [hep-ph/0601258].

[51] **Daya Bay** Collaboration, D. Adey et. al., *Measurement of the Electron Antineutrino Oscillation with 1958 Days of Operation at Daya Bay*, Phys. Rev. Lett. **121** (2018), no. 24 241805 [arXiv:1809.0226].

[52] **RENO** Collaboration, G. Bak et. al., *Measurement of Reactor Antineutrino Oscillation Amplitude and Frequency at RENO*, Phys. Rev. Lett. **121** (2018), no. 20 201801 [arXiv:1806.0024].

[53] **Double Chooz** Collaboration, Y. Abe et. al., *Improved measurements of the neutrino mixing angle θ_{13} with the Double Chooz detector*, JHEP **10** (2014) 086 [arXiv:1406.7763]. [Erratum: JHEP02,074(2015)].

[54] **T2K** Collaboration, K. Abe et. al., *Measurement of neutrino and antineutrino oscillations by the T2K experiment including a new additional sample of ν_e interactions at the far detector*, Phys. Rev. **D96** (2017), no. 9 092006 [arXiv:1707.0104]. [Erratum: Phys. Rev.D98,no.1,019902(2018)].

[55] **NOvA** Collaboration, M. A. Acero et. al., *New constraints on oscillation parameters from ν_e appearance and ν_μ disappearance in the NOvA experiment*, Phys. Rev. **D98** (2018) 032012 [arXiv:1806.0009].

[56] **MINOS** Collaboration, P. Adamson et. al., *Electron neutrino and antineutrino appearance in the full MINOS data sample*, Phys. Rev. Lett. **110** (2013), no. 17 171801 [arXiv:1301.4581].

[57] **DUNE** Collaboration, R. Acciarri et. al., *Long-Baseline Neutrino Facility (LBNF) and Deep Underground Neutrino Experiment (DUNE)*, [arXiv:1512.0614].

[58] **Hyper-Kamiokande Working Group** Collaboration, K. Abe et. al., *A Long Baseline Neutrino Oscillation Experiment Using J-PARC Neutrino Beam and Hyper-Kamiokande*, 2014. [arXiv:1412.4673].

[59] **GERDA** Collaboration, M. Agostini et. al., *Improved Limit on Neutrinoless Double-β Decay of ^{76}Ge from GERDA Phase II*, Phys. Rev. Lett. **120** (2018), no. 13 132503 [arXiv:1803.1110].

[60] **Planck** Collaboration, N. Aghanim et. al., *Planck 2018 results. VI. Cosmological parameters*, [arXiv:1807.0620].

[61] **KATRIN** Collaboration, J. Angrik et. al., *KATRIN design report 2004*, .

[62] S. Weinberg, *Baryon and Lepton Nonconserving Processes*, Phys. Rev. Lett. **43** (1979) 1566–1570.

[63] P. Minkowski, *$\mu \to e\gamma$ at a Rate of One Out of 10^9 Muon Decays?*, Phys. Lett. **B67** (1977) 421–428.

[64] M. Gell-Mann, P. Ramond and R. Slansky, *Complex Spinors and Unified Theories*, Conf. Proc. **C790927** (1979) 315–321 [arXiv:1306.4669].

[65] T. Yanagida, *HORIZONTAL SYMMETRY AND MASSES OF NEUTRINOS*, Conf. Proc. **C7902131** (1979) 95–99.

[66] S. L. Glashow, *The Future of Elementary Particle Physics*, NATO Sci. Ser. **B61** (1980) 687.

[67] R. N. Mohapatra and G. Senjanovic, *Neutrino Mass and Spontaneous Parity Violation*, Phys. Rev. Lett. **44** (1980) 912.

[68] J. Schechter and J. W. F. Valle, *Neutrino Masses in SU(2) x U(1) Theories*, Phys. Rev. **D22** (1980) 2227.

[69] M. Magg and C. Wetterich, *Neutrino Mass Problem and Gauge Hierarchy*, Phys. Lett. **94B** (1980) 61–64.

[70] G. Lazarides, Q. Shafi and C. Wetterich, *Proton Lifetime and Fermion Masses in an SO(10) Model*, Nucl. Phys. **B181** (1981) 287–300.

[71] R. N. Mohapatra and G. Senjanovic, *Neutrino Masses and Mixings in Gauge Models with Spontaneous Parity Violation*, Phys. Rev. **D23** (1981) 165.

[72] C. Wetterich, *Neutrino Masses and the Scale of B-L Violation*, Nucl. Phys. **B187** (1981) 343–375.

[73] R. Foot, H. Lew, X. G. He and G. C. Joshi, *Seesaw Neutrino Masses Induced by a Triplet of Leptons*, Z. Phys. **C44** (1989) 441.

[74] R. N. Mohapatra and J. W. F. Valle, *Neutrino Mass and Baryon Number Nonconservation in Superstring Models*, Phys. Rev. **D34** (1986) 1642.

[75] M. Lindner and E. Schnapka, *Dynamical electroweak symmetry breaking with a standard model limit*, Adv. Ser. Direct. High Energy Phys. **15** (1998) 707–754 [hep-ph/9712489]. [,707(1997)].

[76] M. Malinsky, J. C. Romao and J. W. F. Valle, *Novel supersymmetric SO(10) seesaw mechanism*, Phys. Rev. Lett. **95** (2005) 161801 [hep-ph/0506296].

[77] R. N. Mohapatra, *Mechanism for Understanding Small Neutrino Mass in Superstring Theories*, Phys. Rev. Lett. **56** (1986) 561–563.

[78] M. Roncadelli and D. Wyler, *Naturally Light Dirac Neutrinos in Gauge Theories*, Phys. Lett. **B133** (1983) 325–329.

[79] P. Roy and O. U. Shanker, *Observable Neutrino Dirac Mass and Supergrand Unification*, Phys. Rev. Lett. **52** (1984) 713–716. [Erratum: Phys. Rev. Lett.52,2190(1984)].

[80] **AMS** Collaboration, J. Alcaraz et. al., *Search for anti-helium in cosmic rays*, Phys. Lett. **B461** (1999) 387–396 [hep-ex/0002048].

[81] **Planck** Collaboration, P. A. R. Ade et. al., *Planck 2015 results. XIII. Cosmological parameters*, Astron. Astrophys. **594** (2016) A13 [arXiv:1502.0158].

[82] R. H. Cyburt, B. D. Fields, K. A. Olive and T.-H. Yeh, *Big Bang Nucleosynthesis: 2015*, Rev. Mod. Phys. **88** (2016) 015004 [arXiv:1505.0107].

[83] G. Steigman, *Primordial Nucleosynthesis: The Predicted and Observed Abundances and Their Consequences*, PoS **NICXI** (2010) 001 [arXiv:1008.4765].

[84] A. D. Sakharov, *Violation of CP Invariance, C asymmetry, and baryon asymmetry of the universe*, Pisma Zh. Eksp. Teor. Fiz. **5** (1967) 32–35. [Usp. Fiz. Nauk161,no.5,61(1991)].

[85] M. B. Gavela, P. Hernandez, J. Orloff, O. Pene and C. Quimbay, *Standard model CP violation and baryon asymmetry. Part 2: Finite temperature*, Nucl. Phys. **B430** (1994) 382–426 [hep-ph/9406289].

[86] M. B. Gavela, P. Hernandez, J. Orloff and O. Pene, *Standard model CP violation and baryon asymmetry*, Mod. Phys. Lett. **A9** (1994) 795–810 [hep-ph/9312215].

[87] M. Fukugita and T. Yanagida, *Baryogenesis Without Grand Unification*, Phys. Lett. **B174** (1986) 45–47.

[88] W. Buchmuller, P. Di Bari and M. Plumacher, *Leptogenesis for pedestrians*, Annals Phys. **315** (2005) 305–351 [hep-ph/0401240].

[89] V. A. Kuzmin, V. A. Rubakov and M. E. Shaposhnikov, *On the Anomalous Electroweak Baryon Number Nonconservation in the Early Universe*, Phys. Lett. **155B** (1985) 36.

[90] S. Yu. Khlebnikov and M. E. Shaposhnikov, *The Statistical Theory of Anomalous Fermion Number Nonconservation*, Nucl. Phys. **B308** (1988) 885–912.

[91] J. A. Harvey and M. S. Turner, *Cosmological baryon and lepton number in the presence of electroweak fermion number violation*, Phys. Rev. **D42** (1990) 3344–3349.

[92] S. Davidson and A. Ibarra, *A Lower bound on the right-handed neutrino mass from leptogenesis*, Phys. Lett. **B535** (2002) 25–32 [hep-ph/0202239].

[93] A. Abada, S. Davidson, A. Ibarra, F. X. Josse-Michaux, M. Losada and A. Riotto, *Flavour Matters in Leptogenesis*, JHEP **09** (2006) 010 [hep-ph/0605281].

[94] E. K. Akhmedov, V. A. Rubakov and A. Yu. Smirnov, *Baryogenesis via neutrino oscillations*, Phys. Rev. Lett. **81** (1998) 1359–1362 [hep-ph/9803255].

[95] T. Asaka and M. Shaposhnikov, *The nuMSM, dark matter and baryon asymmetry of the universe*, Phys. Lett. **B620** (2005) 17–26 [hep-ph/0505013].

[96] M. Drewes, B. Garbrecht, P. Hernandez, M. Kekic, J. Lopez-Pavon, J. Racker, N. Rius, J. Salvado and D. Teresi, *ARS Leptogenesis*, Int. J. Mod. Phys. **A33** (2018), no. 05n06 1842002 [arXiv:1711.0286].

[97] A. Atre, T. Han, S. Pascoli and B. Zhang, *The Search for Heavy Majorana Neutrinos*, JHEP **05** (2009) 030 [arXiv:0901.3589].

[98] E. Fernandez-Martínez, J. Hernandez-Garcia and J. Lopez-Pavon, *Global Constraints on Heavy Neutrino Mixing*, JHEP **08** (2016) 033 [arXiv:1605.0877].

[99] **LSND** Collaboration, A. Aguilar-Arevalo et. al., *Evidence for neutrino oscillations from the observation of anti-neutrino(electron) appearance in a anti-neutrino(muon) beam*, Phys. Rev. **D64** (2001) 112007 [hep-ex/0104049].

[100] **MiniBooNE** Collaboration, A. A. Aguilar-Arevalo et. al., *Significant Excess of ElectronLike Events in the MiniBooNE Short-Baseline Neutrino Experiment*, Phys. Rev. Lett. **121** (2018), no. 22 221801 [arXiv:1805.1202].

[101] M. Dentler, Á. Hernández-Cabezudo, J. Kopp, P. A. N. Machado, M. Maltoni, I. Martinez-Soler and T. Schwetz, *Updated Global Analysis of Neutrino Oscillations in the Presence of eV-Scale Sterile Neutrinos*, JHEP **08** (2018) 010 [arXiv:1803.1066].

[102] J. N. Bahcall, *Gallium solar neutrino experiments: Absorption cross-sections, neutrino spectra, and predicted event rates*, Phys. Rev. **C56** (1997) 3391–3409 [hep-ph/9710491].

[103] M. A. Acero, C. Giunti and M. Laveder, *Limits on nu(e) and anti-nu(e) disappearance from Gallium and reactor experiments*, Phys. Rev. **D78** (2008) 073009 [arXiv:0711.4222].

[104] C. Giunti and M. Laveder, *Statistical Significance of the Gallium Anomaly*, Phys. Rev. **C83** (2011) 065504 [arXiv:1006.3244].

[105] J. Kopp, P. A. N. Machado, M. Maltoni and T. Schwetz, *Sterile Neutrino Oscillations: The Global Picture*, JHEP **05** (2013) 050 [arXiv:1303.3011].

[106] **GALLEX** Collaboration, W. Hampel et. al., *GALLEX solar neutrino observations: Results for GALLEX IV*, Phys. Lett. **B447** (1999) 127–133.

[107] J. N. Abdurashitov et. al., *The SAGE and LNGS experiment: Measurement of solar neutrinos at LNGS using gallium from SAGE*, Astropart. Phys. **25** (2006) 349–354 [nucl-ex/0509031].

[108] G. Mention, M. Fechner, T. Lasserre, T. A. Mueller, D. Lhuillier, M. Cribier and A. Letourneau, *The Reactor Antineutrino Anomaly*, Phys. Rev. **D83** (2011) 073006 [arXiv:1101.2755].

[109] P. Huber, *On the determination of anti-neutrino spectra from nuclear reactors*, Phys. Rev. **C84** (2011) 024617 [arXiv:1106.0687]. [Erratum: Phys. Rev.C85,029901(2012)].

[110] **IceCube** Collaboration, M. G. Aartsen et. al., *Searches for Sterile Neutrinos with the IceCube Detector*, Phys. Rev. Lett. **117** (2016), no. 7 071801 [arXiv:1605.0199].

[111] **MINOS** Collaboration, P. Adamson et. al., *Search for sterile neutrinos in MINOS and MINOS+ using a two-detector fit*, [arXiv:1710.0648].

[112] G. H. Collin, C. A. Argüelles, J. M. Conrad and M. H. Shaevitz, *Sterile Neutrino Fits to Short Baseline Data*, Nucl. Phys. **B908** (2016) 354–365 [arXiv:1602.0067].

[113] S. Gariazzo, C. Giunti, M. Laveder and Y. F. Li, *Updated Global 3+1 Analysis of Short-BaseLine Neutrino Oscillations*, JHEP **06** (2017) 135 [arXiv:1703.0086].

[114] **MicroBooNE, LAr1-ND, ICARUS-WA104** Collaboration, M. Antonello et. al., *A Proposal for a Three Detector Short-Baseline Neutrino Oscillation Program in the Fermilab Booster Neutrino Beam*, [arXiv:1503.0152].

[115] S. L. Glashow, J. Iliopoulos and L. Maiani, *Weak Interactions with Lepton-Hadron Symmetry*, Phys. Rev. **D2** (1970) 1285–1292.

[116] C. D. Froggatt and H. B. Nielsen, *Hierarchy of Quark Masses, Cabibbo Angles and CP Violation*, Nucl. Phys. **B147** (1979) 277–298.

[117] P. F. Harrison, D. H. Perkins and W. G. Scott, *Tri-bimaximal mixing and the neutrino oscillation data*, Phys. Lett. **B530** (2002) 167 [hep-ph/0202074].

[118] S. Antusch and V. Maurer, *Large neutrino mixing angle θ_{13}^{MNS} and quark-lepton mass ratios in unified flavour models*, Phys. Rev. **D84** (2011) 117301 [arXiv:1107.3728].

[119] D. Marzocca, S. T. Petcov, A. Romanino and M. Spinrath, *Sizeable θ_{13} from the Charged Lepton Sector in SU(5), (Tri-)Bimaximal Neutrino Mixing and Dirac CP Violation*, JHEP **11** (2011) 009 [arXiv:1108.0614].

[120] S. Antusch and M. Spinrath, *New GUT predictions for quark and lepton mass ratios confronted with phenomenology*, Phys. Rev. **D79** (2009) 095004 [arXiv:0902.4644].

[121] S. Antusch, C. Gross, V. Maurer and C. Sluka, $\theta_{13}^{PMNS} = \theta_C/\sqrt{2}$ *from GUTs*, Nucl. Phys. **B866** (2013) 255–269 [arXiv:1205.1051].

[122] R. S. Chivukula and H. Georgi, *Composite Technicolor Standard Model*, Phys. Lett. **B188** (1987) 99–104.

[123] R. Alonso, E. Fernandez Martínez, M. B. Gavela, B. Grinstein, L. Merlo and P. Quilez, *Gauged Lepton Flavour*, JHEP **12** (2016) 119 [arXiv:1609.0590].

[124] B. Grinstein, M. Redi and G. Villadoro, *Low Scale Flavor Gauge Symmetries*, JHEP **11** (2010) 067 [arXiv:1009.2049].

[125] **LHCb** Collaboration, R. Aaij et. al., *Differential branching fractions and isospin asymmetries of $B \to K^{(*)}\mu^+\mu^-$ decays*, JHEP **06** (2014) 133 [arXiv:1403.8044].

[126] **LHCb** Collaboration, R. Aaij et. al., *Test of lepton universality using $B^+ \to K^+\ell^+\ell^-$ decays*, Phys. Rev. Lett. **113** (2014) 151601 [arXiv:1406.6482].

[127] **LHCb** Collaboration, R. Aaij et. al., *Measurements of the S-wave fraction in $B^0 \to K^+\pi^-\mu^+\mu^-$ decays and the $B^0 \to K^*(892)^0\mu^+\mu^-$ differential branching fraction*, JHEP **11** (2016) 047 [arXiv:1606.0473]. [Erratum: JHEP04,142(2017)].

[128] **LHCb** Collaboration, R. Aaij et. al., *Test of lepton universality with $B^0 \to K^{*0}\ell^+\ell^-$ decays*, JHEP **08** (2017) 055 [arXiv:1705.0580].

[129] **BaBar** Collaboration, J. P. Lees et. al., *Measurement of an Excess of $\bar{B} \to D^{(*)}\tau^-\bar{\nu}_\tau$ Decays and Implications for Charged Higgs Bosons*, Phys. Rev. **D88** (2013), no. 7 072012 [arXiv:1303.0571].

[130] **LHCb** Collaboration, R. Aaij et. al., *Measurement of the ratio of branching fractions $\mathcal{B}(\bar{B}^0 \to D^{*+}\tau^-\bar{\nu}_\tau)/\mathcal{B}(\bar{B}^0 \to D^{*+}\mu^-\bar{\nu}_\mu)$*, Phys. Rev. Lett. **115** (2015), no. 11 111803 [arXiv:1506.0861]. [Erratum: Phys. Rev. Lett.115,no.15,159901(2015)].

[131] **Belle** Collaboration, S. Hirose et. al., *Measurement of the τ lepton polarization and $R(D^*)$ in the decay $\bar{B} \to D^*\tau^-\bar{\nu}_\tau$*, Phys. Rev. Lett. **118** (2017), no. 21 211801 [arXiv:1612.0052].

[132] F. Beaujean, C. Bobeth and D. van Dyk, *Comprehensive Bayesian analysis of rare (semi)leptonic and radiative B decays*, Eur. Phys. J. **C74** (2014) 2897 [arXiv:1310.2478]. [Erratum: Eur. Phys. J.C74,3179(2014)].

[133] R. Alonso, B. Grinstein and J. Martin Camalich, *Lepton universality violation and lepton flavor conservation in B-meson decays*, JHEP **10** (2015) 184 [arXiv:1505.0516].

[134] S. Descotes-Genon, L. Hofer, J. Matias and J. Virto, *Global analysis of $b \to s\ell\ell$ anomalies*, JHEP **06** (2016) 092 [arXiv:1510.0423].

[135] T. Hurth, F. Mahmoudi and S. Neshatpour, *On the Anomalies in the Latest Lhcb Data*, Nucl. Phys. **B909** (2016) 737–777 [arXiv:1603.0086].

[136] W. Altmannshofer, C. Niehoff, P. Stangl and D. M. Straub, *Status of the $B \to K^*\mu^+\mu^-$ anomaly after Moriond 2017*, [arXiv:1703.0918].

[137] W. Altmannshofer, P. Stangl and D. M. Straub, *Interpreting Hints for Lepton Flavor Universality Violation*, [arXiv:1704.0543].

[138] G. Isidori, Y. Nir and G. Perez, *Flavor Physics Constraints for Physics Beyond the Standard Model*, Ann. Rev. Nucl. Part. Sci. **60** (2010) 355 [arXiv:1002.0900].

[139] G. 't Hooft, *Naturalness, chiral symmetry, and spontaneous chiral symmetry breaking*, NATO Sci. Ser. B **59** (1980) 135–157.

[140] F. Zwicky, *Die Rotverschiebung von extragalaktischen Nebeln*, Helv. Phys. Acta **6** (1933) 110–127. [Gen. Rel. Grav.41,207(2009)].

[141] S. Smith, *The Mass of the Virgo Cluster*, Astrophys. J. **83** (1936) 23–30.

[142] G. Bertone and D. Hooper, *History of dark matter*, Rev. Mod. Phys. **90** (2018), no. 4 045002 [arXiv:1605.0490].

[143] K. Freese, *Review of Observational Evidence for Dark Matter in the Universe and in upcoming searches for Dark Stars*, EAS Publ. Ser. **36** (2009) 113–126 [arXiv:0812.4005].

[144] L. Bergstrom, *Dark Matter Evidence, Particle Physics Candidates and Detection Methods*, Annalen Phys. **524** (2012) 479–496 [arXiv:1205.4882].

[145] D. Clowe, M. Bradac, A. H. Gonzalez, M. Markevitch, S. W. Randall, C. Jones and D. Zaritsky, *A direct empirical proof of the existence of dark matter*, Astrophys. J. **648** (2006) L109–L113 [astro-ph/0608407].

[146] J. F. Navarro, E. Hayashi, C. Power, A. Jenkins, C. S. Frenk, S. D. M. White, V. Springel, J. Stadel and T. R. Quinn, *The Inner structure of Lambda-CDM halos 3: Universality and asymptotic slopes*, Mon. Not. Roy. Astron. Soc. **349** (2004) 1039 [astro-ph/0311231].

[147] V. Springel et. al., *Simulating the joint evolution of quasars, galaxies and their large-scale distribution*, Nature **435** (2005) 629–636 [astro-ph/0504097].

[148] J. Diemand, M. Kuhlen and P. Madau, *Dark matter substructure and gamma-ray annihilation in the Milky Way halo*, Astrophys. J. **657** (2007) 262–270 [astro-ph/0611370].

[149] V. Springel, J. Wang, M. Vogelsberger, A. Ludlow, A. Jenkins, A. Helmi, J. F. Navarro, C. S. Frenk and S. D. M. White, *The Aquarius Project: the subhalos of galactic halos*, Mon. Not. Roy. Astron. Soc. **391** (2008) 1685–1711 [arXiv:0809.0898].

[150] J. Diemand, M. Kuhlen, P. Madau, M. Zemp, B. Moore, D. Potter and J. Stadel, *Clumps and streams in the local dark matter distribution*, Nature **454** (2008) 735–738 [arXiv:0805.1244].

[151] **SDSS** Collaboration, D. J. Eisenstein et. al., *Detection of the Baryon Acoustic Peak in the Large-Scale Correlation Function of SDSS Luminous Red Galaxies*, Astrophys. J. **633** (2005) 560–574 [astro-ph/0501171].

[152] **CMS** Collaboration, A. M. Sirunyan et. al., *Search for new physics in final states with an energetic jet or a hadronically decaying W or Z boson and transverse momentum imbalance at* $\sqrt{s} = 13$ TeV, Phys. Rev. **D97** (2018), no. 9 092005 [arXiv:1712.0234].

[153] **ATLAS** Collaboration, M. Aaboud et. al., *Search for new phenomena in final states with an energetic jet and large missing transverse momentum in pp collisions at* $\sqrt{s} = 13 TeV$ *using the ATLAS detector*, Phys. Rev. **D94** (2016), no. 3 032005 [arXiv:1604.0777].

[154] **ATLAS** Collaboration, G. Aad et. al., *Constraints on new phenomena via Higgs boson couplings and invisible decays with the ATLAS detector*, JHEP **11** (2015) 206 [arXiv:1509.0067].

[155] **CMS** Collaboration, V. Khachatryan et. al., *Searches for invisible decays of the Higgs boson in pp collisions at* $\sqrt{s}$ *= 7, 8, and 13 TeV*, JHEP **02** (2017) 135 [arXiv:1610.0921].

[156] **H.E.S.S.** Collaboration, A. Abramowski et. al., *Search for a Dark Matter annihilation signal from the Galactic Center halo with H.E.S.S*, Phys. Rev. Lett. **106** (2011) 161301 [arXiv:1103.3266].

[157] M. Wood, J. Buckley, S. Digel, S. Funk, D. Nieto and M. A. Sanchez-Conde, *Prospects for Indirect Detection of Dark Matter with CTA*, in Proceedings, Community Summer Study 2013: Snowmass on the Mississippi (CSS2013): Minneapolis, MN, USA, July 29-August 6, 2013, 2013. [arXiv:1305.0302].

[158] **IceCube** Collaboration, M. G. Aartsen et. al., *Search for Neutrinos from Dark Matter Self-Annihilations in the center of the Milky Way with 3 years of IceCube/DeepCore*, Eur. Phys. J. **C77** (2017), no. 9 627 [arXiv:1705.0810].

[159] **Fermi-LAT** Collaboration, M. Ackermann et. al., *Searching for Dark Matter Annihilation from Milky Way Dwarf Spheroidal Galaxies with Six Years of Fermi Large Area Telescope Data*, Phys. Rev. Lett. **115** (2015), no. 23 231301 [arXiv:1503.0264].

[160] **AMS 02** Collaboration, F. Palmonari, V. Bindi, A. Contin, N. Masi and L. Quadrani, *Search for dark matter in cosmic rays with the AMS-02 space spectrometer*, J. Phys. Conf. Ser. **335** (2011) 012066.

[161] G. Arcadi, M. Dutra, P. Ghosh, M. Lindner, Y. Mambrini, M. Pierre, S. Profumo and F. S. Queiroz, *The waning of the WIMP? A review of models, searches, and constraints*, Eur. Phys. J. **C78** (2018), no. 3 203 [arXiv:1703.0736].

[162] M. Schumann, *Direct Detection of WIMP Dark Matter: Concepts and Status*, [arXiv:1903.0302].

[163] A. B. McDonald, *Nobel Lecture: The Sudbury Neutrino Observatory: Observation of flavor change for solar neutrinos*, Rev. Mod. Phys. **88** (2016), no. 3 030502.

[164] T. Kajita, *Nobel Lecture: Discovery of atmospheric neutrino oscillations*, Rev. Mod. Phys. **88** (2016), no. 3 030501.

[165] **MiniBooNE** Collaboration, A. A. Aguilar-Arevalo et. al., *A Combined $\nu_\mu \to \nu_e$ and $\bar{\nu}_\mu \to \bar{\nu}_e$ Oscillation Analysis of the MiniBooNE Excesses*, 2012. [arXiv:1207.4809].

[166] **MiniBooNE** Collaboration, A. A. Aguilar-Arevalo et. al., *Unexplained Excess of Electron-Like Events From a 1-GeV Neutrino Beam*, Phys. Rev. Lett. **102** (2009) 101802 [arXiv:0812.2243].

[167] **SAGE** Collaboration, J. N. Abdurashitov et. al., *Measurement of the solar neutrino capture rate with gallium metal. III: Results for the 2002–2007 data-taking period*, Phys. Rev. **C80** (2009) 015807 [arXiv:0901.2200].

[168] F. Kaether, W. Hampel, G. Heusser, J. Kiko and T. Kirsten, *Reanalysis of the GALLEX solar neutrino flux and source experiments*, Phys. Lett. **B685** (2010) 47–54 [arXiv:1001.2731].

[169] S. Dodelson and L. M. Widrow, *Sterile-neutrinos as dark matter*, Phys. Rev. Lett. **72** (1994) 17–20 [hep-ph/9303287].

[170] X.-D. Shi and G. M. Fuller, *A New dark matter candidate: Nonthermal sterile neutrinos*, Phys. Rev. Lett. **82** (1999) 2832–2835 [astro-ph/9810076].

[171] K. Perez, K. C. Y. Ng, J. F. Beacom, C. Hersh, S. Horiuchi and R. Krivonos, *Almost closing the MSM sterile neutrino dark matter window with NuSTAR*, Phys. Rev. **D95** (2017), no. 12 123002 [arXiv:1609.0066].

[172] E. Bulbul, M. Markevitch, A. Foster, R. K. Smith, M. Loewenstein and S. W. Randall, *Detection of An Unidentified Emission Line in the Stacked X-ray spectrum of Galaxy Clusters*, Astrophys. J. **789** (2014) 13 [arXiv:1402.2301].

[173] A. Boyarsky, O. Ruchayskiy, D. Iakubovskyi and J. Franse, *Unidentified Line in X-Ray Spectra of the Andromeda Galaxy and Perseus Galaxy Cluster*, Phys. Rev. Lett. **113** (2014) 251301 [arXiv:1402.4119].

[174] O. Ruchayskiy and A. Ivashko, *Experimental bounds on sterile neutrino mixing angles*, JHEP **06** (2012) 100 [arXiv:1112.3319].

[175] R. E. Shrock, *New Tests For, and Bounds On, Neutrino Masses and Lepton Mixing*, Phys. Lett. **B96** (1980) 159–164.

[176] R. E. Shrock, *General Theory of Weak Leptonic and Semileptonic Decays. 1. Leptonic Pseudoscalar Meson Decays, with Associated Tests For, and Bounds on, Neutrino Masses and Lepton Mixing*, Phys. Rev. **D24** (1981) 1232.

[177] R. E. Shrock, *General Theory of Weak Processes Involving Neutrinos. 2. Pure Leptonic Decays*, Phys. Rev. **D24** (1981) 1275.

[178] P. Langacker and D. London, *Mixing Between Ordinary and Exotic Fermions*, Phys.Rev. **D38** (1988) 886.

[179] S. M. Bilenky and C. Giunti, *Seesaw type mixing and muon-neutrino —> tau-neutrino oscillations*, Phys.Lett. **B300** (1993) 137–140 [hep-ph/9211269].

[180] E. Nardi, E. Roulet and D. Tommasini, *Limits on neutrino mixing with new heavy particles*, Phys.Lett. **B327** (1994) 319–326 [hep-ph/9402224].

[181] D. Tommasini, G. Barenboim, J. Bernabeu and C. Jarlskog, *Nondecoupling of heavy neutrinos and lepton flavor violation*, Nucl.Phys. **B444** (1995) 451–467 [hep-ph/9503228].

[182] S. Antusch, C. Biggio, E. Fernandez-Martinez, M. Gavela and J. Lopez-Pavon, *Unitarity of the Leptonic Mixing Matrix*, JHEP **0610** (2006) 084 [hep-ph/0607020].

[183] S. Antusch, J. P. Baumann and E. Fernandez-Martinez, *Non-Standard Neutrino Interactions with Matter from Physics Beyond the Standard Model*, Nucl.Phys. **B810** (2009) 369–388 [arXiv:0807.1003].

[184] C. Biggio, *The Contribution of fermionic seesaws to the anomalous magnetic moment of leptons*, Phys. Lett. **B668** (2008) 378–384 [arXiv:0806.2558].

[185] R. Alonso, M. Dhen, M. Gavela and T. Hambye, *Muon conversion to electron in nuclei in type-I seesaw models*, JHEP **1301** (2013) 118 [arXiv:1209.2679].

[186] E. Akhmedov, A. Kartavtsev, M. Lindner, L. Michaels and J. Smirnov, *Improving Electro-Weak Fits with TeV-scale Sterile Neutrinos*, JHEP **05** (2013) 081 [arXiv:1302.1872].

[187] S. Antusch and O. Fischer, *Non-unitarity of the leptonic mixing matrix: Present bounds and future sensitivities*, JHEP **1410** (2014) 94 [arXiv:1407.6607].

[188] E. Fernandez-Martinez, J. Hernandez-Garcia, J. Lopez-Pavon and M. Lucente, *Loop level constraints on Seesaw neutrino mixing*, JHEP **10** (2015) 130 [arXiv:1508.0305].

[189] A. Abada and T. Toma, *Electric Dipole Moments of Charged Leptons with Sterile Fermions*, JHEP **02** (2016) 174 [arXiv:1511.0326].

[190] A. Abada and T. Toma, *Electron electric dipole moment in Inverse Seesaw models*, JHEP **08** (2016) 079 [arXiv:1605.0764].

[191] **MINOS** Collaboration, P. Adamson et. al., *Active to sterile neutrino mixing limits from neutral-current interactions in MINOS*, Phys. Rev. Lett. **107** (2011) 011802 [arXiv:1104.3922].

[192] **Super-Kamiokande** Collaboration, K. Abe et. al., *Limits on sterile neutrino mixing using atmospheric neutrinos in Super-Kamiokande*, Phys. Rev. **D91** (2015) 052019 [arXiv:1410.2008].

[193] **MiniBooNE, SciBooNE** Collaboration, G. Cheng et. al., *Dual baseline search for muon antineutrino disappearance at* $0.1\text{eV}^2 < \Delta m^2 < 100\text{eV}^2$, Phys. Rev. **D86** (2012) 052009 [arXiv:1208.0322].

[194] F. Dydak et. al., *A Search for Muon-neutrino Oscillations in the Delta m**2 Range 0.3-eV**2 to 90-eV**2*, Phys. Lett. **134B** (1984) 281.

[195] S. Choubey, *Signature of sterile species in atmospheric neutrino data at neutrino telescopes*, JHEP **12** (2007) 014 [arXiv:0709.1937].

[196] A. Esmaili, F. Halzen and O. L. G. Peres, *Constraining Sterile Neutrinos with AMANDA and IceCube Atmospheric Neutrino Data*, JCAP **1211** (2012) 041 [arXiv:1206.6903].

[197] A. Esmaili, F. Halzen and O. L. G. Peres, *Exploring* $\nu_\tau - \nu_s$ *mixing with cascade events in DeepCore*, JCAP **1307** (2013) 048 [arXiv:1303.3294].

[198] J. M. Conrad, C. M. Ignarra, G. Karagiorgi, M. H. Shaevitz and J. Spitz, *Sterile Neutrino Fits to Short Baseline Neutrino Oscillation Measurements*, Adv. High Energy Phys. **2013** (2013) 163897 [arXiv:1207.4765].

[199] A. Esmaili and A. Yu. Smirnov, *Restricting the LSND and MiniBooNE sterile neutrinos with the IceCube atmospheric neutrino data*, JHEP **12** (2013) 014 [arXiv:1307.6824].

[200] G. H. Collin, C. A. Argüelles, J. M. Conrad and M. H. Shaevitz, *First Constraints on the Complete Neutrino Mixing Matrix with a Sterile Neutrino*, Phys. Rev. Lett. **117** (2016), no. 22 221801 [arXiv:1607.0001].

[201] M. Dentler, Á. Hernández-Cabezudo, J. Kopp, M. Maltoni and T. Schwetz, *Sterile neutrinos or flux uncertainties? — Status of the reactor anti-neutrino anomaly*, JHEP **11** (2017) 099 [arXiv:1709.0429].

[202] J. F. Cherry and I. M. Shoemaker, *A Sterile Neutrino Origin for the Upward Directed Cosmic Ray Showers Detected by ANITA*, [arXiv:1802.0161].

[203] **ANITA** Collaboration, P. W. Gorham et. al., *Characteristics of Four Upward-pointing Cosmic-ray-like Events Observed with ANITA*, Phys. Rev. Lett. **117** (2016), no. 7 071101 [arXiv:1603.0521].

[204] A. C. Vincent, E. F. Martinez, P. Hernández, M. Lattanzi and O. Mena, *Revisiting cosmological bounds on sterile neutrinos*, JCAP **1504** (2015), no. 04 006 [arXiv:1408.1956].

[205] L. Vecchi, *Light sterile neutrinos from a late phase transition*, Phys. Rev. **D94** (2016), no. 11 113015 [arXiv:1607.0416].

[206] **IceCube** Collaboration, M. G. Aartsen et. al., *Search for sterile neutrino mixing using three years of IceCube DeepCore data*, Phys. Rev. **D95** (2017), no. 11 112002 [arXiv:1702.0516].

[207] **CHORUS** Collaboration, E. Eskut et. al., *Final results on nu(mu) —> nu(tau) oscillation from the CHORUS experiment*, Nucl. Phys. **B793** (2008) 326–343 [arXiv:0710.3361].

[208] **NOMAD** Collaboration, P. Astier et. al., *Final NOMAD results on muon-neutrino —> tau-neutrino and electron-neutrino —> tau-neutrino oscillations including a new search for tau-neutrino appearance using hadronic tau decays*, Nucl. Phys. **B611** (2001) 3–39 [hep-ex/0106102].

[209] Z.-z. Xing, *Correlation between the Charged Current Interactions of Light and Heavy Majorana Neutrinos*, Phys. Lett. **B660** (2008) 515–521 [arXiv:0709.2220].

[210] Z.-z. Xing, *A full parametrization of the 6 X 6 flavor mixing matrix in the presence of three light or heavy sterile neutrinos*, Phys. Rev. **D85** (2012) 013008 [arXiv:1110.0083].

[211] F. J. Escrihuela, D. V. Forero, O. G. Miranda, M. Tortola and J. W. F. Valle, *On the description of nonunitary neutrino mixing*, Phys. Rev. **D92** (2015), no. 5 053009 [arXiv:1503.0887]. [Erratum: Phys. Rev.D93,no.11,119905(2016)].

[212] Y.-F. Li and S. Luo, *Neutrino Oscillation Probabilities in Matter with Direct and Indirect Unitarity Violation in the Lepton Mixing Matrix*, Phys. Rev. **D93** (2016), no. 3 033008 [arXiv:1508.0005].

[213] M. Blennow, P. Coloma, E. Fernandez-Martinez, J. Hernandez-Garcia and J. Lopez-Pavon, *Non-Unitarity, sterile neutrinos, and Non-Standard neutrino Interactions*, JHEP **04** (2017) 153 [arXiv:1609.0863].

[214] C. S. Fong, H. Minakata and H. Nunokawa, *A framework for testing leptonic unitarity by neutrino oscillation experiments*, JHEP **02** (2017) 114 [arXiv:1609.0862].

[215] C. A. Argüelles Delgado, J. Salvado and C. N. Weaver, *A Simple Quantum Integro-Differential Solver (SQuIDS)*, Comput. Phys. Commun. **196** (2015) 569–591 [arXiv:1412.3832].

[216] C. A. Argüelles Delgado, J. Salvado and C. N. Weaver, *ν-SQuIDS*, .

[217] A. Fedynitch, R. Engel, T. K. Gaisser, F. Riehn and T. Stanev, *Calculation of conventional and prompt lepton fluxes at very high energy*, EPJ Web Conf. **99** (2015) 08001 [arXiv:1503.0054].

[218] T. K. Gaisser, T. Stanev and S. Tilav, *Cosmic Ray Energy Spectrum from Measurements of Air Showers*, Front. Phys.(Beijing) **8** (2013) 748–758 [arXiv:1303.3565].

[219] S. Ostapchenko, *Monte Carlo treatment of hadronic interactions in enhanced Pomeron scheme: I. QGSJET-II model*, Phys. Rev. **D83** (2011) 014018 [arXiv:1010.1869].

[220] S. V. Ter-Antonyan and L. S. Haroyan, *About EAS size spectra and primary energy spectra in the knee region*, [hep-ex/0003006].

[221] J. R. Hoerandel, *On the knee in the energy spectrum of cosmic rays*, Astropart. Phys. **19** (2003) 193–220 [astro-ph/0210453].

[222] V. I. Zatsepin and N. V. Sokolskaya, *Three component model of cosmic ray spectra from 100-gev up to 100-pev*, Astron. Astrophys. **458** (2006) 1–5 [astro-ph/0601475].

[223] **PAMELA** Collaboration, O. Adriani et. al., *PAMELA Measurements of Cosmic-ray Proton and Helium Spectra*, Science **332** (2011) 69–72 [arXiv:1103.4055].

[224] R. S. Fletcher, T. K. Gaisser, P. Lipari and T. Stanev, *SIBYLL: An Event generator for simulation of high-energy cosmic ray cascades*, Phys. Rev. **D50** (1994) 5710–5731.

[225] A. M. Dziewonski and D. L. Anderson, *Preliminary reference earth model*, Phys. Earth Planet. Interiors **25** (1981) 297–356.

[226] S. S. Wilks, *The Large-Sample Distribution of the Likelihood Ratio for Testing Composite Hypotheses*, Annals Math. Statist. **9** (1938), no. 1 60–62.

[227] M. Tortola, *Status of three-neutrino oscillation parameters*, Fortsch. Phys. **61** (2013) 427–440.

[228] D. V. Forero, M. Tortola and J. W. F. Valle, *Neutrino oscillations refitted*, Phys. Rev. **D90** (2014), no. 9 093006 [arXiv:1405.7540].

[229] M. C. Gonzalez-Garcia, M. Maltoni and T. Schwetz, *Updated fit to three neutrino mixing: status of leptonic CP violation*, JHEP **11** (2014) 052 [arXiv:1409.5439].

[230] M. C. Gonzalez-Garcia, M. Maltoni and T. Schwetz, *Global Analyses of Neutrino Oscillation Experiments*, Nucl. Phys. **B908** (2016) 199–217 [arXiv:1512.0685].

[231] F. Capozzi, E. Lisi, A. Marrone, D. Montanino and A. Palazzo, *Neutrino masses and mixings: Status of known and unknown 3ν parameters*, Nucl. Phys. **B908** (2016) 218–234 [arXiv:1601.0777].

[232] P. Ramond, *The Family Group in Grand Unified Theories*, in International Symposium on Fundamentals of Quantum Theory and Quantum Field Theory Palm Coast, Florida, February 25-March 2, 1979, pp. 265–280, 1979. [hep-ph/9809459].

[233] E. K. Akhmedov, M. Lindner, E. Schnapka and J. W. F. Valle, *Dynamical left-right symmetry breaking*, Phys. Rev. **D53** (1996) 2752–2780 [hep-ph/9509255].

[234] M. Klasen, F. Lyonnet and F. S. Queiroz, *NLO+NLL collider bounds, Dirac fermion and scalar dark matter in the $B-L$ model*, Eur. Phys. J. **C77** (2017), no. 5 348 [arXiv:1607.0646].

[235] W. Wang and Z.-L. Han, *Radiative linear seesaw model, dark matter, and $U(1)_{B-L}$*, Phys. Rev. **D92** (2015) 095001 [arXiv:1508.0070].

[236] N. Okada and S. Okada, *Z'_{BL} portal dark matter and LHC Run-2 results*, Phys. Rev. **D93** (2016), no. 7 075003 [arXiv:1601.0752].

[237] N. Okada and S. Okada, *Z'-portal right-handed neutrino dark matter in the minimal U(1)$_X$ extended Standard Model*, Phys. Rev. **D95** (2017), no. 3 035025 [arXiv:1611.0267].

[238] P. Bandyopadhyay, E. J. Chun and R. Mandal, *Implications of right-handed neutrinos in $B-L$ extended standard model with scalar dark matter*, [arXiv:1707.0087].

[239] Y. Cai and W. Chao, *The Higgs Seesaw Induced Neutrino Masses and Dark Matter*, Phys. Lett. **B749** (2015) 458–463 [arXiv:1408.6064].

[240] F. Bazzocchi, *Minimal Dynamical Inverse See Saw*, Phys. Rev. **D83** (2011) 093009 [arXiv:1011.6299].

[241] S. Khalil, *TeV-scale gauged B-L symmetry with inverse seesaw mechanism*, Phys. Rev. **D82** (2010) 077702 [arXiv:1004.0013].

[242] L. Basso, O. Fischer and J. J. van der Bij, *Natural Z model with an inverse seesaw mechanism and leptonic dark matter*, Phys. Rev. **D87** (2013), no. 3 035015 [arXiv:1207.3250].

[243] E. Ma and R. Srivastava, *Dirac or inverse seesaw neutrino masses with $B-L$ gauge symmetry and S_3 flavor symmetry*, Phys. Lett. **B741** (2015) 217–222 [arXiv:1411.5042].

[244] E. Ma and R. Srivastava, *Dirac or inverse seesaw neutrino masses from gauged $B-L$ symmetry*, Mod. Phys. Lett. **A30** (2015), no. 26 1530020 [arXiv:1504.0011].

[245] M. Escudero, N. Rius and V. Sanz, *Sterile neutrino portal to Dark Matter I: The $U(1)_{B-L}$ case*, JHEP **02** (2017) 045 [arXiv:1606.0125].

[246] M. Escudero, N. Rius and V. Sanz, *Sterile Neutrino portal to Dark Matter II: Exact Dark symmetry*, [arXiv:1607.0237].

[247] A. Abada, G. Arcadi and M. Lucente, *Dark Matter in the minimal Inverse Seesaw mechanism*, JCAP **1410** (2014) 001 [arXiv:1406.6556].

[248] N. Rojas, R. A. Lineros and F. Gonzalez-Canales, *Majoron dark matter from a spontaneous inverse seesaw model*, [arXiv:1703.0341].

[249] G. Bertone, D. Hooper and J. Silk, *Particle dark matter: Evidence, candidates and constraints*, Phys. Rept. **405** (2005) 279–390 [hep-ph/0404175].

[250] J. Silk et. al., Particle Dark Matter: Observations, Models and Searches. Cambridge Univ. Press, Cambridge, 2010.

[251] D. Wyler and L. Wolfenstein, *Massless Neutrinos in Left-Right Symmetric Models*, Nucl. Phys. **B218** (1983) 205–214.

[252] J. W. F. Valle, *Neutrinoless Double Beta Decay With Quasi Dirac Neutrinos*, Phys. Rev. **D27** (1983) 1672–1674.

[253] J. W. F. Valle and M. Singer, *Lepton Number Violation With Quasi Dirac Neutrinos*, Phys. Rev. **D28** (1983) 540.

[254] J. A. Casas, J. R. Espinosa and I. Hidalgo, *Implications for new physics from fine-tuning arguments. 1. Application to SUSY and seesaw cases*, JHEP **11** (2004) 057 [hep-ph/0410298].

[255] F. Vissani, *Do experiments suggest a hierarchy problem?*, Phys. Rev. **D57** (1998) 7027–7030 [hep-ph/9709409].

[256] F. Bazzocchi, D. G. Cerdeno, C. Munoz and J. W. F. Valle, *Calculable inverse-seesaw neutrino masses in supersymmetry*, Phys. Rev. **D81** (2010) 051701 [arXiv:0907.1262].

[257] R. N. Mohapatra and R. E. Marshak, *Local B-L Symmetry of Electroweak Interactions, Majorana Neutrinos and Neutron Oscillations*, Phys. Rev. Lett. **44** (1980) 1316–1319. [Erratum: Phys. Rev. Lett.44,1643(1980)].

[258] R. E. Marshak and R. N. Mohapatra, *Quark - Lepton Symmetry and B-L as the U(1) Generator of the Electroweak Symmetry Group*, Phys. Lett. **B91** (1980) 222–224.

[259] J. C. Pati and A. Salam, *Lepton Number as the Fourth Color*, Phys. Rev. **D10** (1974) 275–289. [Erratum: Phys. Rev.D11,703(1975)].

[260] H. Georgi, *The State of the Art—Gauge Theories*, AIP Conf. Proc. **23** (1975) 575–582.

[261] H. Fritzsch and P. Minkowski, *Unified Interactions of Leptons and Hadrons*, Annals Phys. **93** (1975) 193–266.

[262] A. Abada and M. Lucente, *Looking for the minimal inverse seesaw realisation*, Nucl. Phys. **B885** (2014) 651–678 [arXiv:1401.1507].

[263] M. Drewes et. al., *A White Paper on keV Sterile Neutrino Dark Matter*, JCAP **1701** (2017), no. 01 025 [arXiv:1602.0481].

[264] T. P. Cheng and L.-F. Li, *Neutrino Masses, Mixings and Oscillations in $SU(2) \times U(1)$ Models of Electroweak Interactions*, Phys. Rev. **D22** (1980) 2860.

[265] T. Robens and T. Stefaniak, *LHC Benchmark Scenarios for the Real Higgs Singlet Extension of the Standard Model*, Eur. Phys. J. **C76** (2016), no. 5 268 [arXiv:1601.0788].

[266] **ATLAS, CMS** Collaboration, G. Aad et. al., *Measurements of the Higgs boson production and decay rates and constraints on its couplings from a combined ATLAS and CMS analysis of the LHC pp collision data at $\sqrt{s} = 7$ and 8 TeV*, JHEP **08** (2016) 045 [arXiv:1606.0226].

[267] F. Staub, *SARAH 3.2: Dirac Gauginos, UFO output, and more*, Comput. Phys. Commun. **184** (2013) 1792–1809 [arXiv:1207.0906].

[268] F. Staub, *SARAH 4 : A tool for (not only SUSY) model builders*, Comput. Phys. Commun. **185** (2014) 1773–1790 [arXiv:1309.7223].

[269] F. Staub, *Exploring new models in all detail with SARAH*, Adv. High Energy Phys. **2015** (2015) 840780 [arXiv:1503.0420].

[270] A. Vicente, *Computer tools in particle physics*, [arXiv:1507.0634].

[271] W. Porod, *SPheno, a program for calculating supersymmetric spectra, SUSY particle decays and SUSY particle production at e+ e- colliders*, Comput. Phys. Commun. **153** (2003) 275–315 [hep-ph/0301101].

[272] W. Porod and F. Staub, *SPheno 3.1: Extensions including flavour, CP-phases and models beyond the MSSM*, Comput. Phys. Commun. **183** (2012) 2458–2469 [arXiv:1104.1573].

[273] A. Belyaev, N. D. Christensen and A. Pukhov, *CalcHEP 3.4 for collider physics within and beyond the Standard Model*, Comput. Phys. Commun. **184** (2013) 1729–1769 [arXiv:1207.6082].

[274] G. Bélanger, F. Boudjema, A. Pukhov and A. Semenov, *micrOMEGAs4.1: two dark matter candidates*, Comput. Phys. Commun. **192** (2015) 322–329 [arXiv:1407.6129].

[275] A. Alves, A. Berlin, S. Profumo and F. S. Queiroz, *Dirac-fermionic dark matter in $U(1)_X$ models*, JHEP **10** (2015) 076 [arXiv:1506.0676].

[276] M. Lindner, A. Merle and V. Niro, *Enhancing Dark Matter Annihilation into Neutrinos*, Phys. Rev. **D82** (2010) 123529 [arXiv:1005.3116].

[277] E. W. Kolb and M. S. Turner, *The Early Universe*, Front. Phys. **69** (1990) 1–547.

[278] **Particle Data Group** Collaboration, C. Patrignani et. al., *Review of Particle Physics*, Chin. Phys. **C40** (2016), no. 10 100001.

[279] K. Cheung, P.-Y. Tseng, Y.-L. S. Tsai and T.-C. Yuan, *Global Constraints on Effective Dark Matter Interactions: Relic Density, Direct Detection, Indirect Detection and Collider*, JCAP **1205** (2012) 001 [arXiv:1201.3402].

[280] **LUX** Collaboration, D. S. Akerib et. al., *Results from a search for dark matter in the complete LUX exposure*, Phys. Rev. Lett. **118** (2017), no. 2 021303 [arXiv:1608.0764].

[281] **XENON** Collaboration, E. Aprile et. al., *First Dark Matter Search Results from the XENON1T Experiment*, [arXiv:1705.0665].

[282] **XENON** Collaboration, E. Aprile et. al., *Physics reach of the XENON1T dark matter experiment*, JCAP **1604** (2016), no. 04 027 [arXiv:1512.0750].

[283] **LZ** Collaboration, D. S. Akerib et. al., *LUX-ZEPLIN (LZ) Conceptual Design Report*, [arXiv:1509.0291].

[284] T. Basse, O. E. Bjaelde, J. Hamann, S. Hannestad and Y. Y. Y. Wong, *Dark energy properties from large future galaxy surveys*, JCAP **1405** (2014) 021 [arXiv:1304.2321].

[285] L. Amendola et. al., *Cosmology and Fundamental Physics with the Euclid Satellite*, [arXiv:1606.0018].

[286] **CMS** Collaboration, V. Khachatryan et. al., *Search for narrow resonances in dilepton mass spectra in proton-proton collisions at $\sqrt{s}$ = 13 TeV and combination with 8 TeV data*, Phys. Lett. **B768** (2017) 57–80 [arXiv:1609.0539].

[287] **ATLAS** Collaboration, T. A. collaboration, *Search for new high-mass resonances in the dilepton final state using proton-proton collisions at $\sqrt{s}$ = 13 TeV with the ATLAS detector*, .

[288] A. D. Martin, W. J. Stirling, R. S. Thorne and G. Watt, *Parton distributions for the LHC*, Eur. Phys. J. **C63** (2009) 189–285 [arXiv:0901.0002].

[289] P. S. B. Dev and R. N. Mohapatra, *TeV Scale Inverse Seesaw in SO(10) and Leptonic Non-Unitarity Effects*, Phys. Rev. **D81** (2010) 013001 [arXiv:0910.3924].

[290] S. Blanchet, P. S. B. Dev and R. N. Mohapatra, *Leptogenesis with TeV Scale Inverse Seesaw in SO(10)*, Phys. Rev. **D82** (2010) 115025 [arXiv:1010.1471].

[291] A. Abada, G. Arcadi, V. Domcke and M. Lucente, *Lepton number violation as a key to low-scale leptogenesis*, JCAP **1511** (2015), no. 11 041 [arXiv:1507.0621].

[292] P. Hernández, M. Kekic, J. López-Pavón, J. Racker and N. Rius, *Leptogenesis in GeV scale seesaw models*, JHEP **10** (2015) 067 [arXiv:1508.0367].

[293] D. V. Forero, S. Morisi, M. Tortola and J. W. F. Valle, *Lepton flavor violation and non-unitary lepton mixing in low-scale type-I seesaw*, JHEP **09** (2011) 142 [arXiv:1107.6009].

[294] W. Abdallah, A. Awad, S. Khalil and H. Okada, *Muon Anomalous Magnetic Moment and mu -> e gamma in B-L Model with Inverse Seesaw*, Eur. Phys. J. **C72** (2012) 2108 [arXiv:1105.1047].

[295] S. M. Boucenna, S. Morisi and J. W. F. Valle, *The low-scale approach to neutrino masses*, Adv. High Energy Phys. **2014** (2014) 831598 [arXiv:1404.3751].

[296] A. Abada, V. De Romeri and A. M. Teixeira, *Effect of steriles states on lepton magnetic moments and neutrinoless double beta decay*, JHEP **09** (2014) 074 [arXiv:1406.6978].

[297] A. Abada, V. De Romeri, S. Monteil, J. Orloff and A. M. Teixeira, *Indirect searches for sterile neutrinos at a high-luminosity Z-factory*, JHEP **04** (2015) 051 [arXiv:1412.6322].

[298] E. Arganda, M. J. Herrero, X. Marcano and C. Weiland, *Imprints of massive inverse seesaw model neutrinos in lepton flavor violating Higgs boson decays*, Phys. Rev. **D91** (2015), no. 1 015001 [arXiv:1405.4300].

[299] A. Abada, V. De Romeri and A. M. Teixeira, *Impact of sterile neutrinos on nuclear-assisted cLFV processes*, JHEP **02** (2016) 083 [arXiv:1510.0665].

[300] A. Abada, D. Bečirević, M. Lucente and O. Sumensari, *Lepton flavor violating decays of vector quarkonia and of the Z boson*, Phys. Rev. **D91** (2015), no. 11 113013 [arXiv:1503.0415].

[301] V. De Romeri, M. J. Herrero, X. Marcano and F. Scarcella, *Lepton flavor violating Z decays: A promising window to low scale seesaw neutrinos*, Phys. Rev. **D95** (2017), no. 7 075028 [arXiv:1607.0525].

[302] A. Abada, V. De Romeri, J. Orloff and A. M. Teixeira, *In-flight cLFV conversion: $e-\mu$, $e-\tau$ and $\mu-\tau$ in minimal extensions of the Standard Model with sterile fermions*, Eur. Phys. J. **C77** (2017), no. 5 304 [arXiv:1612.0554].

[303] P. Fileviez Perez, T. Han, G.-y. Huang, T. Li and K. Wang, *Neutrino Masses and the CERN LHC: Testing Type II Seesaw*, Phys. Rev. **D78** (2008) 015018 [arXiv:0805.3536].

[304] P. Fileviez Perez, T. Han, G.-Y. Huang, T. Li and K. Wang, *Testing a Neutrino Mass Generation Mechanism at the LHC*, Phys. Rev. **D78** (2008) 071301 [arXiv:0803.3450].

[305] E. Dudas and C. A. Savoy, *Multiple seesaw at low-energy*, Acta Phys. Polon. **B33** (2002) 2547–2558 [hep-ph/0205264].

[306] Z.-z. Xing and S. Zhou, *Multiple seesaw mechanisms of neutrino masses at the TeV scale*, Phys. Lett. **B679** (2009) 249–254 [arXiv:0906.1757].

[307] C. Bonilla, J. C. Romao and J. W. F. Valle, *Electroweak breaking and neutrino mass: 'invisible' Higgs decays at the LHC (type II seesaw)*, New J. Phys. **18** (2016), no. 3 033033 [arXiv:1511.0735].

[308] H. Ishida, S. Matsuzaki, S. Okawa and Y. Omura, *Scale generation via dynamically induced multiple seesaw mechanisms*, Phys. Rev. **D95** (2017), no. 7 075033 [arXiv:1701.0059].

[309] P.-H. Gu and R. N. Mohapatra, *Leptogenesis with TeV Scale W_R*, [arXiv:1712.0042].

[310] K. Choi, H. Kim and S. Yun, *Natural inflation with multiple sub-Planckian axions*, Phys. Rev. **D90** (2014) 023545 [arXiv:1404.6209].

[311] K. Choi and S. H. Im, *Realizing the relaxion from multiple axions and its UV completion with high scale supersymmetry*, JHEP **01** (2016) 149 [arXiv:1511.0013].

[312] D. E. Kaplan and R. Rattazzi, *Large field excursions and approximate discrete symmetries from a clockwork axion*, Phys. Rev. **D93** (2016), no. 8 085007 [arXiv:1511.0182].

[313] G. F. Giudice and M. McCullough, *A Clockwork Theory*, JHEP **02** (2017) 036 [arXiv:1610.0796].

[314] Y. Chikashige, R. N. Mohapatra and R. D. Peccei, *Are There Real Goldstone Bosons Associated with Broken Lepton Number?*, Phys. Lett. **98B** (1981) 265–268.

[315] Y. Chikashige, R. N. Mohapatra and R. D. Peccei, *Spontaneously Broken Lepton Number and Cosmological Constraints on the Neutrino Mass Spectrum*, Phys. Rev. Lett. **45** (1980) 1926.

[316] J. Schechter and J. W. F. Valle, *Neutrino Decay and Spontaneous Violation of Lepton Number*, Phys. Rev. **D25** (1982) 774.

[317] J. D. Clarke, R. Foot and R. R. Volkas, *Phenomenology of a very light scalar (100 MeV $< m_h <$ 10 GeV) mixing with the SM Higgs*, JHEP **02** (2014) 123 [arXiv:1310.8042].

[318] **KamLAND-Zen** Collaboration, A. Gando et. al., *Limits on Majoron-emitting double-beta decays of Xe-136 in the KamLAND-Zen experiment*, Phys. Rev. **C86** (2012) 021601 [arXiv:1205.6372].

[319] **Particle Data Group** Collaboration, C. Patrignani et. al., *Review of Particle Physics*, Chin. Phys. **C40** (2016), no. 10 100001.

[320] R. E. Shrock and M. Suzuki, *Invisible Decays of Higgs Bosons*, Phys. Lett. **110B** (1982) 250.

[321] B. A. Dobrescu and K. T. Matchev, *Light axion within the next-to-minimal supersymmetric standard model*, JHEP **09** (2000) 031 [hep-ph/0008192].

[322] **CMS** Collaboration, V. Khachatryan et. al., *Search for Higgs boson off-shell production in proton-proton collisions at 7 and 8 TeV and derivation of constraints on its total decay width*, JHEP **09** (2016) 051 [arXiv:1605.0232].

[323] **CMS Collaboration** Collaboration, *Combined measurements of the Higgs boson's couplings at $\sqrt{s} = 13$ TeV*, Tech. Rep. CMS-PAS-HIG-17-031, CERN, Geneva, 2018.

[324] A. Alloul, N. D. Christensen, C. Degrande, C. Duhr and B. Fuks, *FeynRules 2.0 - A complete toolbox for tree-level phenomenology*, Comput. Phys. Commun. **185** (2014) 2250–2300 [arXiv:1310.1921].

[325] J. Alwall, R. Frederix, S. Frixione, V. Hirschi, F. Maltoni, O. Mattelaer, H. S. Shao, T. Stelzer, P. Torrielli and M. Zaro, *The automated computation of tree-level and next-to-leading order differential cross sections, and their matching to parton shower simulations*, JHEP **07** (2014) 079 [arXiv:1405.0301].

[326] A. G. Akeroyd and M. Aoki, *Single and pair production of doubly charged Higgs bosons at hadron colliders*, Phys. Rev. **D72** (2005) 035011 [hep-ph/0506176].

[327] **CMS** Collaboration, A. M. Sirunyan et. al., *Search for heavy neutral leptons in events with three charged leptons in proton-proton collisions at $\sqrt{s} = 13$ TeV*, [arXiv:1802.0296].

[328] M. Cacciari, G. P. Salam and G. Soyez, *FastJet User Manual*, Eur. Phys. J. **C72** (2012) 1896 [arXiv:1111.6097].

[329] A. L. Read, *Presentation of search results: The CL(s) technique*, J. Phys. **G28** (2002) 2693–2704. [,11(2002)].

[330] D. N. Dinh, A. Ibarra, E. Molinaro and S. T. Petcov, *The $\mu - e$ Conversion in Nuclei, $\mu \to e\gamma, \mu \to 3e$ Decays and TeV Scale See-Saw Scenarios of Neutrino Mass Generation*, JHEP **08** (2012) 125 [arXiv:1205.4671]. [Erratum: JHEP09,023(2013)].

[331] E. Ma and U. Sarkar, *Neutrino masses and leptogenesis with heavy Higgs triplets*, Phys. Rev. Lett. **80** (1998) 5716–5719 [hep-ph/9802445].

[332] K. S. Babu, I. Gogoladze and S. Khan, *Radiative Electroweak Symmetry Breaking in Standard Model Extensions*, Phys. Rev. **D95** (2017), no. 9 095013 [arXiv:1612.0518].